DOE/NV/03624--0869

An Aerial Survey of the 200 East and 200 West Areas of the Hanford Nuclear Reservation

DISCLAIMER

DOE/NV/03624--0869

An Aerial Survey of the 200 East and 200 West Areas of the Hanford Nuclear Reservation

October 2016

National Security Technologies, LLC

Remote Sensing Laboratory

Las Vegas, Nevada

Survey Dates: September 18 -26, 2015

This page intentionally left blank.

Executive Summary

The U.S. Department of Energy (DOE) National Nuclear Security Administration (NNSA) Aerial Measuring System (AMS), based at the Remote Sensing Laboratory (RSL) in Las Vegas, Nevada, performed an aerial survey of the 200 West and 200 East Areas of the DOE Hanford Site during September 2015. The survey was performed using the RSL Bell 412 helicopter equipped with twelve 2"x4"x16" thallium-activated sodium iodide (NaI) logs with their spectra summed to form a single detector and a mechanically-cooled high-purity germanium (HPGe) detector. Both detectors collected gamma ray spectra from naturally-occurring radioactive materials and from anthropogenic radioactive materials present due to activities at the site. Data was collected over the site during the 30 hours of survey flight time, resulting in approximately 100,000 one-second spectra collected by both the NaI array and the HPGe detector. These data have been analyzed to map the distribution of anthropogenic radioactivity and identify the isotopes responsible for that activity.

This page intentionally left blank.

Table of Contents

Executive Summary iii
Table of Figures vii
List of Tables ix
Acronyms and Abbreviations xi
1.1. Introduction 1
2. Survey Area 2
3. Survey Method 4
3.1. Aerial Survey Equipment 4
3.2. Aerial Survey Technique 7
3.3. Aerial Data Collection 8
3.4. Ground Data Collection 10
4. Data Analysis 11
4.1. Gross Count Method 11
4.2. Man-Made Gross Count Method 12
4.3. Gamma Spectral Analysis 14
4.4. Spectral Distortions 15
5. Isotope Extraction Algorithms 15
5.1. The 2-Window Algorithm 15
5.2. The 3-Window Algorithm 16
5.3. Gaussian Extraction 17
5.4. Cesium-Specific Isotope Extraction Algorithm 17
6. Data Quality Control and Assurance 17
6.1. Daily Preflight Checks 18
6.2. Test Line and Water Line 20
7. Survey Results 24
7.1. Gross Count Rates and Exposure Rates 24
7.2. Anthropogenic Algorithm 29
7.3. Isotope Extractions 31
7.3.1. Isotopic Sensitivities 31

7.3.2. Americium-241 Extraction 31
7.3.3. Cs-137 Extraction 32
7.3.4. Co-60 Extraction 32
7.3.5. Pu-239 Extraction 32
7.4. KUT Extractions 37
7.4.1. Potassium 37
7.4.2. Uranium 37
7.4.3. Thorium 37
7.5. Regions of Interest 41
7.5.1. ROI 01 41
7.5.2. ROI 02 41
7.5.3. ROI 23 42
8. Ground Measurements 48
8.1. PIC Ground Measurements 48
8.2. HPGe Ground Measurements 49
9. Distributed Source Localization 51
10. Comparison With Previous Surveys 54
10.1. 1996 Survey 54
10.2. 2009 Survey 54
11. References 60
Appendix A. Survey Parameters 61
Appendix B. Spectra From Regions of Interest 62

Table of Figures

Figure 1. Map of survey areas on the Hanford Site. 3
Figure 2. Typical spectrum of natural radioactive background. 4
Figure 3. RSX-3 detector. 5
Figure 4. Components of the RSI data acquisition system. 6
Figure 5. AMS Bell 412 helicopter with externally mounted detector pods. 7
Figure 6. Cartoon showing some of the features of an aerial radiological survey. 9
Figure 7. Instrumentation used for ground measurements. 10
Figure 8. Two-window method for extracting excess count rates due to man-made isotopes. 13
Figure 9. Daily preflight background checks expressed as total gross count rate. 19
Figure 10. Daily preflight source checks expressed as total net count rate. 20
Figure 11. Locations of the test line and water line. 21
Figure 12. Average gross count rates along the water line. 22
Figure 13. Average gross count rates along the test line. 23
Figure 14. Net count rates along the test line. 23
Figure 15. Map showing flight lines, mobile drive route, and location of ground measurements. 25
Figure 16. Map showing gross count rates over the survey area. 26
Figure 17. Map showing background-corrected gross count rates in the 200 West area. 27
Figure 18. Map showing background-corrected gross count rates in the 200 East area. 28
Figure 19. Map showing excess count rates due to anthropogenic isotopes. 30
Figure 20. Map showing areas of excess count rate due to Am-241. 33
Figure 21. Map showing areas of excess count rate due to Cs-137. 34
Figure 22. Map showing areas of excess count rate due to Co-60. 35
Figure 23. Pu-239 extraction map produced using the HPGe data. 36
Figure 24. Potassium concentrations calculated using the IAEA stripping coefficient method. 38
Figure 25. Uranium concentrations calculated using the IAEA stripping coefficient method. 39
Figure 26. Thorium concentrations calculated using the IAEA stripping coefficient method. 40

Figure 27. HPGe spectrum from ROI 01 42
Figure 28. HPGe spectrum taken over ROI 02. 43
Figure 29. HPGe spectrum from ROI 23. 43
Figure 30. Major regions of interest in the 200 West Area. 44
Figure 31. Major regions of interest in the 200 East Area. 45
Figure 32. Minor regions of interest in the 200 West Area. 46
Figure 33. Minor regions of interest in the 200 East Area. 47
Figure 34. Ground-level PIC exposure rate measurements plotted with corresponding aerial measurements. 49
Figure 35. Comparative study of isotopic extractions in ROI 1 using the NaI data (top row) and HPGe data (bottom row). 53
Figure 36. Comparison of data from the 2015 survey with data from the 1996 survey. 55
Figure 37. Comparison of the overlap area from the 2009 and 2015 surveys. Contours are color-coded by exposure rate. 56
Figure 38. Comparison between the 2009 survey and 2015 survey over the 'coyote dens'. 57
Figure 39. Anthropogenic count rates in the 200 West area from the 1996 survey. 58
Figure 40. Spectrum 31 from the 1996 Hanford survey report. 59
Figure 41. Spectrum 27 from the 1996 Hanford survey report. 59

List of Tables

Table 1. Previous AMS surveys at the Hanford Nuclear Reservation. 1

Table 2. Isotopic conversion coefficients for the AMS 12-log NaI detector system at an aircraft altitude of 50 ft AGL. 31

Table 3. Ground measurements taken on the Hanford site. 48

Table 4. Soil concentrations of Am-241 extracted from HPGe in situ measurements taken 1 m off the ground. 50

Table 5. Soil concentrations of Cs-137 extracted from HPGe in situ measurements taken 1 m off the ground. 50

Table 6. Soil concentrations of Co-60 (using the 1173 keV peak) extracted from HPGe in situ measurements taken 1 m off the ground. 51

Table 7. Soil concentrations of Co-60 (using the 1332 keV peak) extracted from HPGe in situ measurements taken 1 m off the ground. 51

This page intentionally left blank.

Acronyms and Abbreviations

ADS	Advanced Digital Spectrometer
AGL	above ground level
Am-241	americium-241
AMS	Aerial Measuring System
BCCA	Burial Cribs Controlled Area
cm	centimeter
cps	counts per second
Cs-137	cesium-137
DGPS	Differential Global Positioning System
DOE	U.S. Department of Energy
GC	gross count
GIS	Geographic Information Systems
HNR	Hanford Nuclear Reservation
HPGe	high purity germanium
keV	kiloelectron volt
K-40	potassium-40
KUT	potassium, uranium, and thorium
MMGC	man-made gross count
NaI(Tl)	thallium-activated sodium-iodine
NNSA	National Nuclear Security Administration
pCi/g	picocurie per gram
PIC	pressurized ion chamber
PMT	photomultiplier tube
ROI	region of interest
RSI	Radiation Solutions, Inc
RSL–N	Remote Sensing Laboratory–Nellis
µR	microRoentgen

This page intentionally left blank.

1.1. Introduction

The U.S. Department of Energy (DOE) National Nuclear Security Administration (NNSA) Aerial Measuring System (AMS), based at the Remote Sensing Laboratory (RSL) in Las Vegas, Nevada, performed an aerial survey of the 200 West and 200 East Areas of the Hanford Nuclear Reservation (HNR) during September 2015. This survey was the latest in a series of AMS surveys at HNR.

Previous AMS surveys are listed in Table 1. The 1996 survey (Colton D. P., 1996) covered essentially the entire site. The 2009 survey (Lyons, 2009) covered the BC crib areas and included ground surveys utilizing the Kiwi and Kubuto systems. Because of the large extent of overlapping coverage, the 1996 survey was chosen for comparison with this survey. This comparison is outlined in Section 10 of this report.

The survey covered in this report was executed during September 18 – 26, 2015. The RSL Bel 412 helicopter required 22 flights and a total of 30 flight hours to complete the survey, not including transit time and test and water lines. Flights were conducted every day during the survey period, with the exception of one rest day.

Table 1. Previous AMS surveys at the Hanford Nuclear Reservation.

Abridged Title of Survey Report	Survey Locations	Survey Dates	Aircraft Type
Hanford Plant Area, Washington, and Oregon (ARMS II)	Bedrock 100 square miles	June 24 – July 23, 1959	Fixed Wing
Aerial Radiological Survey of US ERDA's Hanford Reservation (ARMS)	Site Wide Survey 1500 km	May 1973 – April 1974	Fixed Wing and Helicopter
Aerial Radiological Survey of DOE's Hanford Site	Areas 200 East, 200 North, BC Crib, 200 West, Columbia River Shores and Islands, 100 Areas, and Areas 300 and 400	May 1, 1978 – June 8, 1978	Helicopter
Washington Public Power Supply System (WPPSS) Nuclear Project	270 square kilometers centered on WPPSS	July 14 – 20 1982	Helicopter

Table 1. (Continued) Previous AMS surveys at the Hanford Nuclear reservation.

Abridged Title of Survey Report	Survey Locations	Survey Dates	Aircraft Type
An Aerial Radiological Survey of the Hanford Site and Surrounding Area	630 square miles including east of the site and along the banks of the Columbia River down to McNary Dam near Umatilla	July 5, 1988 – August 26, 1988	Helicopter
An Aerial Radiological Survey of the Hanford Reservation	560 square miles. Additional flights were flown along the banks of the Columbia River extending from Priest Rapids Dam in the northwest to Kennewick in the southeast.	February 29, 1996 – March 21, 1996	Helicopter
An Aerial Radiological Survey of the Hanford BC Controlled Area and West Lake Area	BCCA, Zones A, B, C, West Lake and Gable Mountain Pond areas	September 22 – 30, 2009	Helicopter

2. Survey Area

The Hanford Nuclear Reservation (HNR) lies within the Pasco Basin of the Columbia Plateau in south central Washington State and covers an area of approximately 1,450-square-kilometers (560-square-miles). This area is a semi-arid, shrub-steppe region with an average annual rainfall of 16 cm (6.3-inches). The Columbia River flows through the northern part of the reservation and forms part of the site's eastern boundary. The Yakima River runs along the southern boundary and joins the Columbia River below the city of Richland, Washington, located at the site's southeastern boundary. Rattlesnake Mountain, Yakima Ridge, and Umtanum Ridge form the southwestern and western boundaries. The Saddle Mountains form the northern boundary. The nearest population center is the Tri-Cities area (Richland, Pasco and Kennewick, Washington), located directly downstream from the site.

Since the facility began operation in 1944, activities at the HNR have centered on the nine graphite-moderated plutonium production reactors located along the southern bank of the Columbia River. All nine of the reactors have been shut down. Located in the center of the reservation are two large chemical separation areas (200 East and 200 West), where plutonium and uranium were extracted from irradiated uranium fuel elements. Large

quantities of liquid and solid radioactive wastes are stored in underground tank farms and burial sites located within and around the 200-Areas.

The focus of this survey was the 200 West and 200 East areas, shown in Figure 1. Coverage of the entire area with a flight line spacing of 100 ft required about 30 hours of flight time, not including transit time to the area and flights over the test and water lines.

AMS performed a helicopter survey of the Burial Cribs Controlled Area (BCCA) in September 2009. The purpose of that survey was to update the previous radiological surveys of the BCCA. During the 2009 survey an altitude of 15 meters (50 feet) above ground level (AGL) and parallel line spacing of 23 meters (75 feet) were chosen to maximize sensitivity to man-made radiation and to reduce the effective footprint of the helicopter radiation acquisition system. The BCCA deposition footprint was more complex than mapped after previous aerial surveys, primarily in 1996, due to the enhanced spatial resolution and sensitivity of the 2009 survey. The survey results confirmed that the soil contamination levels in Zone A exceeded the project's clean-up levels.

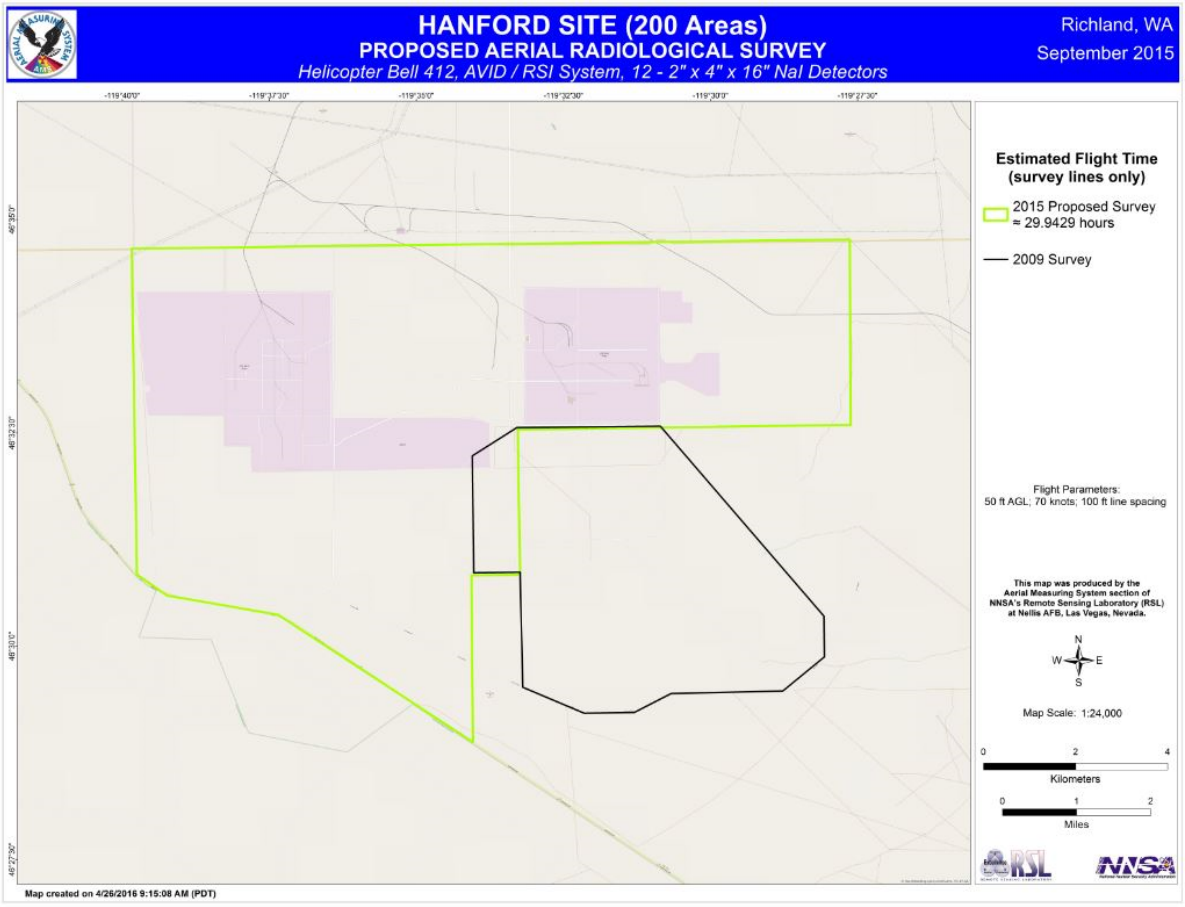

Figure 1. Map of survey areas on the Hanford Site. Also shown is the boundary of the 2009 AMS survey.

3. Survey Method

Aerial radiological surveys are designed to measure spectra of gamma ray energies originating from terrestrial radioactive sources, e.g., naturally-occurring radioisotopes in rocks and soils and anthropogenic sources deposited intentionally or unintentionally on the ground. Data are collected with a detector made up of an array of thallium-activated sodium iodide crystals [NaI(Tl)] which, when coupled to photomultiplier tubes (PMT), produce electrical signals proportional to the energies of the gamma rays that strike the detector. For a more detailed discussion of gamma detectors see, for example, (Knoll, 2010). Charting all of the gamma energies collected by the detector in a given amount of time (the count rate) as the number of gammas per some energy interval, a spectrum of gamma energies is produced (Figure 2). However, since the detector responds to all gamma rays regardless of their source, contributions to the spectra from non-terrestrial sources (e.g., cosmic rays and atmospheric radon) must be subtracted from the raw data. A properly calibrated detector can convert count rates into exposure rates at ground level, and information about specific radioisotopes can be extracted from the spectra. The remainder of this section details the data collection techniques used during this survey.

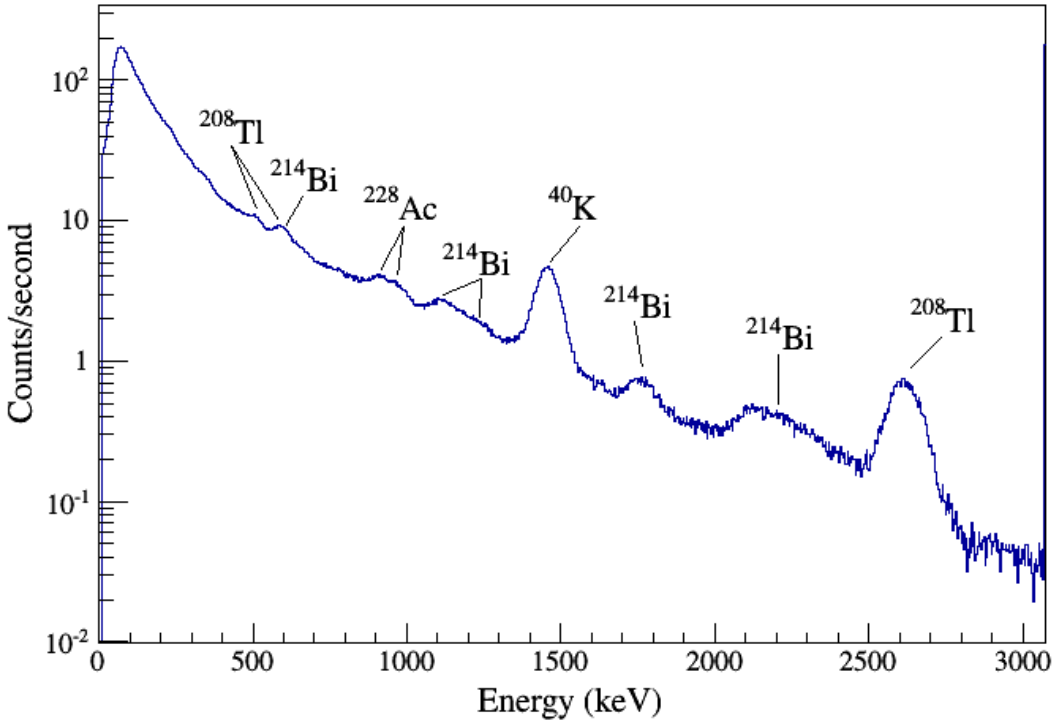

Figure 2. Typical spectrum of natural radioactive background. The spectrum was created from data collected by the AMS NaI(Tl) detectors at nominal survey altitude. Annotated peaks are commonly observed signatures of various decay products from radioactive potassium, uranium and thorium.

3.1. Aerial Survey Equipment

The radiation detectors used by AMS were manufactured by Radiation Solutions, Inc. (RSI). The active material is NaI(Tl) fabricated as 2"x4"x16" rectangular “logs”. A total of twelve logs were used in the detector system,

with each log coupled to a PMT to convert the light pulses generated by gamma rays in the logs to electrical pulses. The electrical pulses are digitized and counted to produce a spectrum of gamma energies collected during each one-second integration time. These one-second spectra can be added together (summed) to improve counting statistics over selected areas.

The twelve NaI(Tl) logs are packaged in carbon fiber boxes with three logs to a box (Figure 3) along with their associated PMTs. Each PMT sends its pulses to an Advanced Digital Spectrometer (ADS), which processes the electrical signals into digital signals. The logs are oriented so that a 4"x16" face points downward to maximize the detection surface area exposed to the ground. The carbon fiber boxes are mounted in two aluminum pods with two boxes in each pods. The pods are mounted on the exterior of a helicopter with one pod on either side of the aircraft. Electronics and power supplies are distributed in the pods and in the cabin of the helicopter.

Once per second, gamma-spectral data from each of the three ADS modules are sent to an RS-701 console which manages each detector's data stream and dynamically adjusts detector gain to compensate for spectral drift. The digital output from the four RSX-3/RS-701 units is aggregated by an RS-501 console which stores the data and allows it to be monitored real-time in the aircraft via an Ethernet connection to a laptop computer. The RS-501 unit also provides power distribution and houses a Trimble differential GPS receiver. The laptop computer controls the configuration, startup, and shutdown of the data acquisition system via the RS-501 using RSI's RadAssist software (Figure 4).

Figure 3. RSX-3 detector. The three 2" × 4" × 16" NaI(Tl) scintillators, three photomultiplier tubes, and three ADS modules can be seen.

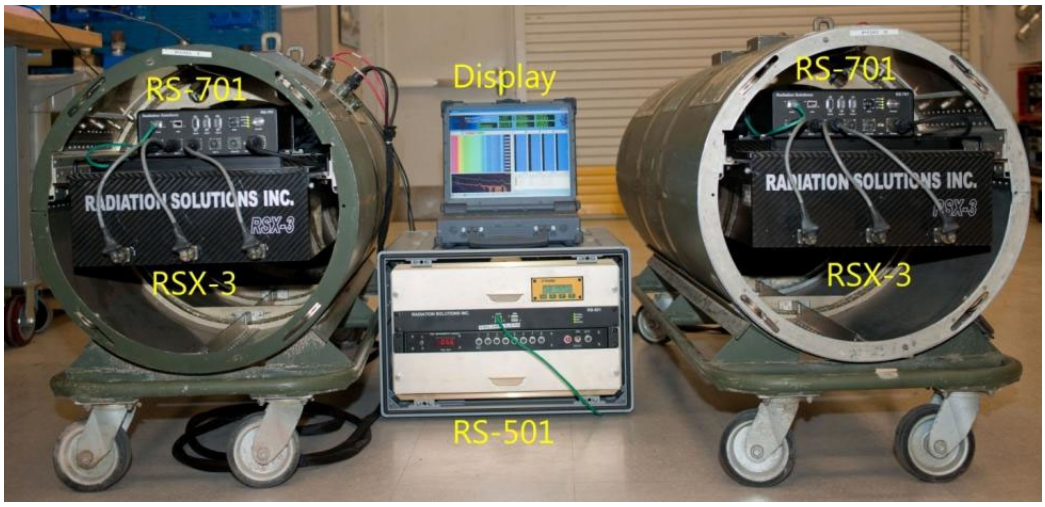

Figure 4. Components of the RSI data acquisition system.

The detectors are sensitive to gamma rays with energies from 20 – 3000 keV. These gamma rays originate from the decay of radioactive isotopes and nuclear reactions produced by cosmic rays. Since the decay of a given radioisotope produces gamma rays with characteristic energies, peaks in the spectra can be used to identify the radioisotopes contributing to the spectra. Because soil, rocks, and other materials block gamma rays, the detection system is sensitive to gamma rays originating from the surface or within a few centimeters of the surface of the ground. That is, significant shielding (ground cover or buildings) will reduce the number of gamma rays seen by the detectors.

The detectors are omnidirectional; they accept gamma rays incident from any direction without distinction. However, because of air attenuation, signals from nearer sources are stronger than signals from more distant sources. Thus, while sources more or less directly under the aircraft dominate the signal, it is possible to see an influence from sources further away. As a rule of thumb, about 60% of the signal received in the detectors is from a circle, centered directly under the aircraft, with a radius equal to the height of the aircraft above ground level. This percentage is energy dependent, with higher energy gammas contributing more from further away than lower energy gammas. Additionally, since the aircraft is moving and a spectrum is produced for each second of flight, this circle, known as the detector footprint, is elongated in the direction of flight. The collected spectrum is thus an average of the signal seen over the area of the footprint.

The aircraft used to perform the survey is a Bell 412, a twin engine utility helicopter that has been manufactured by Bell Helicopter since 1981 (Figure 5). With a standard fuel capacity of 330 gallons, the helicopter is capable of flying for up to 3.7 hours, with a maximum range of 356 nautical miles and a cruising speed of 122 knots. However, with the AMS radiation survey configuration of 12 detectors, four crew members (two pilots, a mission scientist and an equipment operator), the DOE Bell 412 is capable of only 2.5 hours of flight time with a survey speed of 70 knots (120 feet/sec) at survey altitude of 50 ft AGL.

Figure 5. AMS Bell 412 helicopter with externally mounted detector pods.

Other equipment was used during the survey to take radiation measurements on the ground. These measurements were used to check the calibration of the aerial detectors and spot-check aerial results. A GE Reuter-Stokes pressurized ionization chamber (PIC) was used to measure exposure rates at selected locations within the survey area. Gamma ray spectra were collected at these locations using an Ortec mechanically-cooled high purity germanium (HPGe) detector. The HPGe detector has a better energy resolution than the NaI(Tl) detectors and was used to identify radioisotopes on the ground. An HPGe detector was also carried onboard the helicopter, but because count rates in this relatively small detector were much less than in the NaI(Tl) array, airborne HPGe spectra are in general useful only when there is a large ground source. Additionally, a single NaI(Tl) log was mounted in an HNR vehicle and driven around the site. This detector was not calibrated for exposure rate and was used to confirm the locations of high-activity areas found during the aerial survey.

3.2. Aerial Survey Technique

Aerial radiological surveys are performed to characterize the radiological landscape of the area surveyed. The general techniques for flying a survey and doing a basic analysis of the data collected are quite mature, and an introduction can be found in (Proctor, 1997). As computers have become faster, smaller, and with more data storage capacity, analyses can be performed that extract more information from contemporary surveys. Tradeoffs between survey cost, time, and data quality (notably spatial resolution) place some important limits on the data and how it can be interpreted.

Aerial surveys are flown in a series of parallel lines (flight lines) spaced to give 100% coverage of the survey area with the assumption that the detector footprint diameter

is twice the flight altitude AGL. Spatial resolution is therefore governed by flight altitude, and to improve resolution, flight altitude and speed are chosen as low as possible. For this survey, the flight altitude was 50 ft AGL, with a corresponding line spacing of 100 ft. Flight speed was 70 kts, which is the minimum speed the Bell 412 can fly while maintaining good flight characteristics (e.g., low vibration, good fuel economy). The speed of 70 kts (120 ft/s) also nearly matches the line spacing for 1 Hz data collection. Flight lines were flown east to west or west to east, with the direction of flight changing after turns at the ends of the lines.

Navigation along the flight lines is maintained by using a Trimble steering computer. The Trimble is programmed with the desired flight lines, and an integral GPS receiver monitors aircraft position relative to the programmed flight lines. This relative position is communicated to the pilots using an LED light bar mounted on the helicopter dashboard, and by watching the position of lit LEDs on the light bar, the pilots can maintain helicopter's position along the flight lines. Aircraft height AGL is measured with a radar altimeter which is also monitored by the pilots. The radar altimeter data is inserted into the data stream and recorded with the radiological data.

3.3. Aerial Data Collection

As the helicopter flies over the survey area, data are collected as a series of gamma ray energy spectra, with a spectrum collected and saved each second; that is, the spectra are collected at a rate of 1 Hz. The one-second spectra can be summed during post-processing to improve statistics, which can result in isotopic identifications with higher confidence levels. Saved with the spectra are the GPS location of the aircraft, the aircraft height AGL from the radar altimeter, and data indicating the state of health of the detector system.

The gamma ray spectra collected include contributions from terrestrial sources and non-terrestrial sources (e.g., airborne radon and cosmic rays). Because a few feet of water effectively shields gamma rays coming from terrestrial sources, the non-terrestrial component in the data can be estimated by collecting data over a body of water, such as a lake or wide river. For this survey, a section of the Columbia River was used to collect non-terrestrial background data. A so-called water line was flown at the beginning and end of each survey flight, and used to correct the survey data.

The survey itself is flown as a series of parallel lines, offset from each other with a line spacing equal to twice the flight altitude AGL (Figure 6). Wide turns are made at the end of each line to allow time for the helicopter to resume level flight before starting the next line.

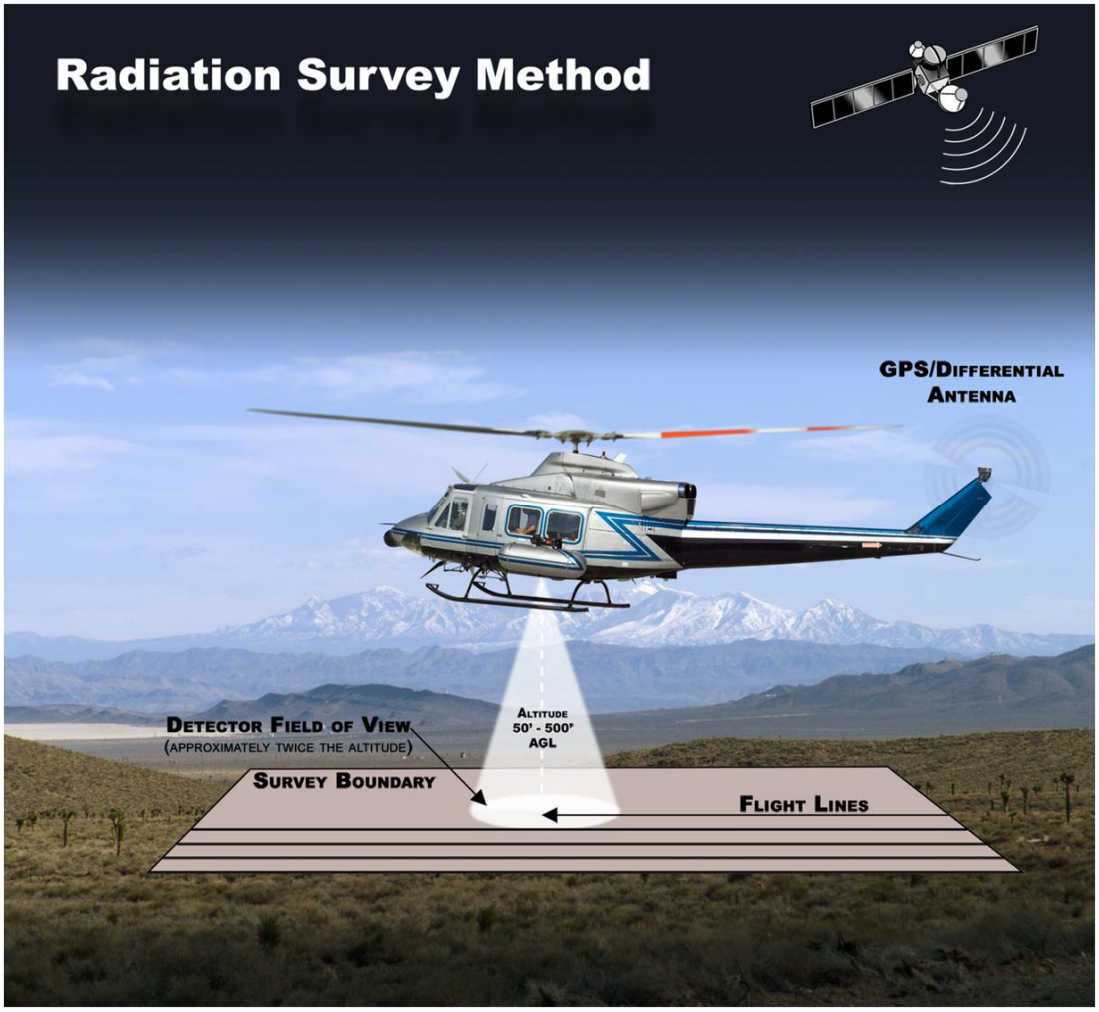

Figure 6. Cartoon showing some of the features of an aerial radiological survey. The aircraft flies at a constant altitude in a series of parallel flight lines. Aircraft position is determined by GPS.

Location information from the GPS receiver is used to georeference the aerial data, which allows for the correlation of the aerial data with features on the ground. Spectra are collected during each one-second integration, after which the spectra are saved along with the GPS location of the aircraft at the end of the integration period. Because each spectrum is an average taken over the length of flight line covered by the aircraft during a one-second interval, the location of this data needs to be moved in post-processing to the center of the section of flight line it represents. Failure to do this results in a "herringbone" pattern in the data, caused by the data being artificially shifted forward by about one half of second and the aircraft flying in opposite directions on adjacent flight lines.

Aircraft altitude above ground level is measured with a radar altimeter attached to the aircraft. Air currents (wind gusts, updrafts, and downdrafts) cause the aircraft altitude to vary. For straight flight over level ground this variation is normally about 10%. Because air attenuates the gamma rays reaching the detectors, as the aircraft altitude varies, the fraction of gamma rays from the ground also varies, with a lower percentage reaching the

detectors as aircraft altitude increases. Because gamma count rates vary in a predictable way with altitude, the recorded radar altimeter height is used to correct the data, effectively removing changes in count rates not caused by changes in radiation on the ground.

Spectra from the HPGe detector on board the aircraft is also collected and stored every second. As with the NaI(Tl) spectra, the HPGe spectra can be summed to improve statistics and isotopic identification.

3.4. Ground Data Collection

The NaI(Tl) detectors aboard the aircraft are calibrated to convert count rates measured during flight to exposure rates at 3 ft above the ground. This calibration was carried out at the Lake Mohave Calibration Range south of Las Vegas, NV (Colton & Hendricks, 1999). However, differences in elevation above sea level and weather at the survey area made it necessary to check this calibration with data collected on the ground locally. While not a true calibration, the local ground measurements were used verify that detector calibration and functionality (e.g., sensitivity) did not changed significantly during the survey.

Ground measurements were made with a GE Reuter-Stokes pressurized ionization chamber (PIC) and an Ortec mechanically-cooled HPGe detector (Figure 7). The PIC was calibrated by an outside laboratory for exposure rate, and the HPGe was calibrated by RSL for activity concentrations, assuming several different isotopic distributions in the soil (surface, exponentially decreasing down from the surface, and uniform).

Ground measurements can be grouped into two categories: those made along the test line (flown at the beginning and end of each survey flight) and those made in the survey area. Test line ground

Figure 7. Instrumentation used for ground measurements. The mechanically-cooled high-purity germanium detector is on the left and the pressurized ion chamber is on the right.

measurements are used to verify the exposure rate calibration of the detector, and measurements in the survey area are used as a ground truth check of the aerial data. Care must be used when comparing ground and aerial data, however, because of the difference in height above ground level of the detectors. Ground measurements are taken at a height of 1 m, and sample an area only several meters across. Aerial data taken at a height of 50 ft AGL samples an area greater than 100 ft across.

4. Data Analysis

Data collected during the survey were subjected to several corrections and quality assurance tests to ensure the resulting maps represented the terrestrial radiation environment as accurately as possible. This section outlines the correction and analysis methods used during data processing. Section 6 presents the data quality and control measures taken.

4.1. Gross Count Method

To obtain a gross count (GC) contour, the count data that were collected by the AMS equipment were first integrated between 20 and 3,000 keV:

$$C_G = \sum_{E=20}^{3000} c(E) \qquad (1)$$

Where

C_G = gross count rate (counts per second [cps]),

E = photon energy (keV), and

$c(E)$ = count rate in the energy spectrum at energy E (cps).

The gross count rates obtained are corrected for detector dead time[1]. Since GC contours are meant only to depict net terrestrial radiation levels, counts from cosmic radiation and airborne radon must be subtracted using the water line data. To convert a terrestrial count rate to ground-level exposure rate E_G, a conversion factor S_f must be applied:

$$E_G = \frac{C_G}{S_f} \qquad (2)$$

The conversion from gross count to an exposure rate is based on the assumption that the source is spread uniformly over the width of the detector footprint, or field of view. Because of this assumption, the exposure rate is underestimated over sources that are small with respect to the size of the footprint. For example, an intense point source of radiation can produce measured count rates at the detector equivalent to those from a much less intense large-area source.

GC data include contributions from natural sources of radiation. Consequently, these data include variations in terrestrial background radiation levels. Contours resulting from these variations in natural radiation often match specific surface features, such as tree lines, boundaries of cultivated land, and bodies of water, because of different attenuation characteristics of different materials. Exposure rate contours offer a sensitive means of identifying anomalous, potentially anthropogenic changes in the radiation environment, in addition to detailing variations in the natural background radiation emissions.

[1] While detector electronics are processing a signal pulse, no other signals are accepted. This is referred to as dead time; conversely, the time that the electronics can accept a signal is called live time. See (Knoll, 2010) for a more complete discussion.

4.2. Man-Made Gross Count Method

The man-made gross count (MMGC) method is used to differentiate between anthropogenic radiation and naturally occurring radiation in a survey. The MMGC method also referred to here as the MMGC filter, relies on the fact that most gamma-ray emissions from long-lived, anthropogenic sources of radioactivity occur in the energy region below about 1,400 keV. In areas where only natural sources of gamma radiation are present, the ratio of the counts appearing below 1,400 keV to those appearing above 1,400 keV remains relatively constant. This relationship is true even if natural background radiation levels vary by a factor of 10 across the survey area. If this ratio changes spatially, it is most likely because of a contribution from anthropogenic gamma radiation.

The MMGC algorithm is a means of identifying regions in the survey area where the shape of the energy spectrum deviates significantly from the shape of the background, or reference spectrum. The MMGC algorithm is very sensitive to small changes in the abundance of anthropogenic isotopes, while being very insensitive to large changes in the abundance of natural isotopes.

The MMGC algorithm is very general and is sensitive to changes in the low-energy portion of the spectrum. It does not identify the cause of the change. The changes can be caused by:

- Man-made isotopes in the survey region
- Scattered gamma rays from natural radionuclides
- Changes in the isotope ratios from where the ratio of low-energy to high energy spectral windows was measured.

Figure 8 shows two typical NaI gamma-ray spectra. Superimposed on a background spectrum is a spectrum obtained with Co-60 present. Counts from an anthropogenic radioisotope, such as Co-60, fall almost entirely in the low-energy region below about 1,400 keV. This condition is true for most anthropogenic radioisotopes of concern, which causes the ratio of counts in the low-energy range to counts in the high-energy range to change.

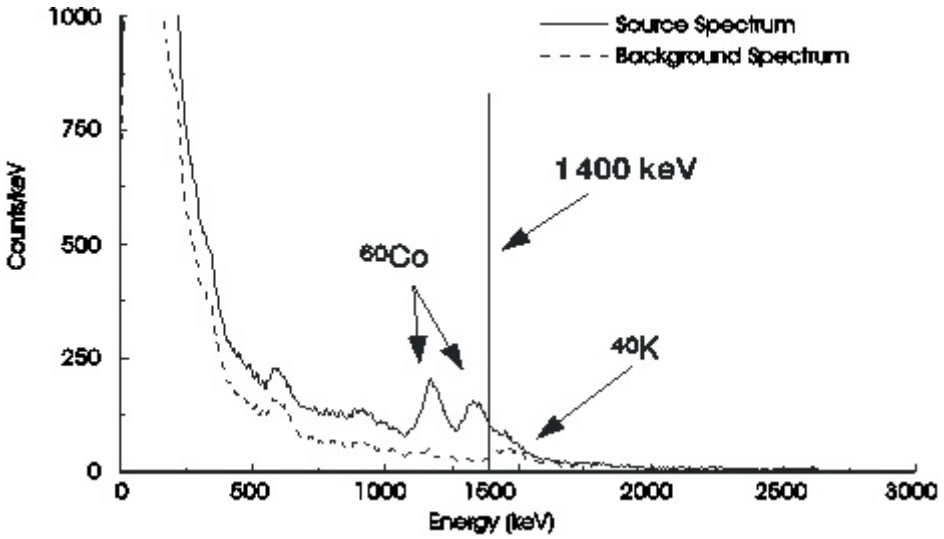

Figure 8. Two-window method for extracting excess count rates due to man-made isotopes. The presence of man-made peaks in the lower half of the spectrum distorts the ratio of low-energy counts to high-energy counts.

The normal ratio of counts in the low-energy region to counts in the high-energy region for a survey area is calculated from data obtained in an area that contains only natural sources of radioactivity. These counts are integrated over each energy region. To match the energy limits of the discrete channels of the acquired spectra, the low-energy region extends from 20 to 1,364 keV. The high-energy limits are then 1,364 to 3,000 keV. This ratio can be computed using Equation 3:

$$K_{MM} = \frac{\sum_{E=38}^{1394} c_{ref}(E)}{\sum_{E=1394}^{3026} c_{ref}(E)} \qquad (3)$$

The subscript "ref" denotes that the counts in each channel, $c(E)$, are obtained from a reference area of natural background radiation. This ratio is applied to each second of data from the survey area:

$$C_{MM} = \left[\sum_{E=38}^{1394} c(E)\right] - K_{MM}\left[\sum_{E=1394}^{3026} c(E)\right] \qquad (4)$$

where

C_{MM} = Anthropogenic (man-made) count rate (cps).

The MMGC algorithm allows data to be analyzed in such a way that variations in the count rate due to changes in natural background levels are filtered out. In regions with only natural background radiation, the MMGC algorithm will yield count rates that fluctuate statistically around zero. Variations in count rate due to anthropogenic or industrially enhanced radioisotopes then appear as isolated contours.

The increase in sensitivity obtained with the MMGC analysis over that of the GC method is significant. However, the MMGC filter is also sensitive to changes in the relative composition of natural background radiation. For example, areas exhibiting excess concentrations of natural potassium, uranium, and/or thorium, the ratio of the low-energy to high-energy gamma rays may be different, even though the gamma rays are emitted by naturally occurring radioisotopes. In such cases, the MMGC

algorithm may generate a set of "false positive" anomalies on the MMGC contour map. A background-subtracted gamma energy spectrum in this case will only show natural radioisotopes or a smoothly varying background with no discernable peaks.

4.3. Gamma Spectral Analysis

The MMGC algorithm is very general and is sensitive to any change in the low-energy portion of the spectrum. It does not exactly identify the causes of the change—whether (1) a true anthropogenic isotope is present in this region, (2) the increased low-energy gamma rays are caused by naturally occurring isotopes whose gamma rays underwent more inelastic scatterings before reaching the detectors (for example, a change from a grassy meadow to a dense wooded area), or (3) the isotopic composition of the spectrum in this region of the survey is significantly different from where K_{MM} was determined (for example, granite versus limestone). Once a region appears in the anthropogenic contours, the energy spectrum is searched for individual isotopes. An analysis of the gamma-ray spectrum is used to identify the isotopes that are present in the spectrum and caused the MMGC deviation.

Generally, the large background field (from the naturally occurring isotopes) is not of interest—only the portion of the spectrum attributable to the anthropogenic isotopes is. Unfortunately, the number of counts at any given energy in a single one-second measurement is so small as to make the identification of a particular isotope very difficult. To increase the number of counts in the spectrum being analyzed (and thus produce better statistics), the spectra from neighboring measurements are combined to produce a single spectrum showing the radiation measured over some larger area.

To determine net spectra at an identified anomaly, each area of interest is divided into "peak" and "background" regions. The contour levels used to define these regions are usually MMGC levels. The peak and background boundaries may be defined by other means (e.g., GC contour levels). The peak region of the spectrum consists of the spectra contained in the area bounded by the chosen contour level. The background region consists of the spectra contained outside the chosen contour level. This partitioning generally guarantees that the background spectrum is representative of the geology near the anomaly, but there will be some contribution of anthropogenic radioactivity in the background region.

This technique produces a net spectrum that has very little contribution from the naturally occurring radioisotopes in the region and makes identification of the remaining isotopes relatively easy. This technique has one major drawback, in that it does not necessarily produce a true indication of the activity of the isotopes seen in the net spectrum. That is, comparing the intensity of an isotope in one net spectrum with the intensity of that same isotope in another spectrum may not be meaningful.

Numerous techniques can be used to scale background spectra when creating a net gamma-ray spectrum. One technique used involves computing the ratio of the live times of the peak and background regions and using the results to normalize the data. This technique therefore creates a net spectrum by subtracting the background spectrum, normalized by the ratio of the peak live time to the background live time, from the peak spectrum:

$$c_{Net}(E) = c_{Peak}(E) - \frac{T_{Peak}}{T_{Bkg}} c_{Bkg}(E) \qquad (5)$$

Where:

$c_{Net}(E)$ = counts in the net energy spectrum at the energy E (cps)

$c_{Peak}(E)$ = counts in the peak energy spectrum at the energy E (cps)

T_{Peak} = total spectrum live time composed of all peak-region spectra (s)

T_{Bkg} = total spectrum live time from all background-region spectra (s), and

$c_{Bkg}(E)$ = counts in the background energy spectrum at energy E (cps).

This method of normalization is relatively straightforward to implement. If there is an excess of naturally occurring radioisotopes, the net spectrum will preserve the high-energy photopeaks of these isotopes.

4.4. Spectral Distortions

If the survey contains areas of very high activity, the count rate in the detectors may become high enough to distort the spectra. This distortion results from having insufficient time between the electrical pulses generated by the amplifiers on the photomultiplier tubes. When these pulses reach the data collector, one pulse is superimposed on the tail of another pulse, and the data collector determines a voltage for this combined pulse that is no longer characteristic of the individual pulses. At moderate count rates, this distortion may appear as a broadening of the photopeaks and possibly as a shift in a photopeak's apparent energy. At very high count rates, these effects become more severe, and it may be nearly impossible to recognize any photopeak pattern in the spectra. Additionally, the NaI detector array may saturate resulting in the data collection software recording no NaI data. In these cases, the HPGe data was used to augment the NaI data.

5. Isotope Extraction Algorithms

The windowing algorithms employed in the search for particular isotopes are very similar to the MMGC algorithm. The major difference is that instead of using the full gamma ray energy spectrum, they use only a few small portions of it. Two such algorithms are the 2-window algorithm and the 3-window algorithm. Fits to individual peaks to determine counts rates from specific gamma rays energies are also used.

5.1. The 2-Window Algorithm

The 2-window algorithm is the simplest of several window algorithms in use. It employs a narrow window centered on the energy of the specific photopeak of the isotope of concern. The algorithm assumes that the background counts in the photopeak window are proportional to the counts recorded in a background window located at higher energies. The background window may abut the photopeak window or may be separated from it in the energy spectrum. Note that the form of the equation for C_2 is identical in form to the equation for MMGC previously defined:

$$C_2 = \left[\sum_{E=E_1}^{E_2} c(E)\right] - K_2\left[\sum_{E=E_3}^{E_4} c(E)\right] \qquad (6)$$

with

$$K_2 = \frac{\sum_{E=E_1}^{E_2} c_{ref}(E)}{\sum_{E=E_3}^{E_4} c_{ref}(E)} \qquad (7)$$

where

C_2 = count rate from the 2-window algorithm (cps),

$c(E)$ = count rate in the gamma-ray energy spectrum at the energy E (cps),

E_n = limiting energies of the windows ($E_1 < E_2 \leq E_3 < E_4$) (keV),

K_2 = ratio of the counts in the photopeak window to the counts in the background window in the reference region of the survey area,

$c_{ref}(E)$ = count rate in the reference gamma-ray energy spectrum at energy E (cps),

The proportionality factor, K_2, is determined in a region of the survey area that does not contain any of the specific isotopes of concern so that the photopeak window contains only background counts and, therefore, can be simply related to the number of counts in the background window. If the principal source of background gamma rays in the photopeak window is from scattered gamma rays from photopeaks at higher energies, this is a good assumption. If there are other isotopes with photopeaks in or near the photopeak and background windows, this algorithm fails.

5.2. The 3-Window Algorithm

If a reference region free of the isotope of interest cannot be found, or if the compositions of other isotopes change drastically between the reference region and the rest of the survey area, then a simple multiplicative factor will not relate the counts in the photopeak window to the counts in the background window. To solve this problem, the 3-window algorithm [Equation (8)] employs a background window on each side of the photopeak window. (The two background windows generally abut the photopeak window in energy.) This algorithm assumes that for any spectrum, the number of background counts in the photopeak window is linearly related to the counts in the two background windows.

$$C_3 = \left[\sum_{E=E_2}^{E_3} c(E)\right] - K_3\left[\left(\sum_{E=E_1}^{E_2} c(E)\right) + \left(\sum_{E=E_3}^{E_4} c(E)\right)\right] \tag{8}$$

with

$$K_3 = \frac{\sum_{E=E_2}^{E_3} c_{ref}(E)}{\sum_{E=E_1}^{E_2} c_{ref}(E) + \sum_{E=E_3}^{E_4} c_{ref}(E)} \tag{9}$$

where

C_3 = count rate from the 3-window algorithm,

E_n = limiting energies of the windows ($E_1 < E_2 < E_3 < E_4$),

K_3 = ratio of the counts in the primary window to the counts in the two background windows in a reference region of the survey area.

The 3-window algorithm is also very useful in extracting low-energy photopeak counts where

the shape of the Compton-scattering contributions in the spectrum from other isotopes is changing significantly.

5.3. Gaussian Extraction

As an alternative to a window-based extraction, a Gaussian extraction may be used. This technique uses the fact the energy-dependent distribution of count rates centered on the energy of a characteristic isotopic peak has a Gaussian (also called normal) distribution. With this method, an attempt is made to fit a Gaussian function to an isotopic peak above an assumed background shape. If there is no excess above background, the technique returns zero counts, although because of normal statistical fluctuations a negative fit may result.

The functional form of the distribution is

$$f(E, E_m, \sigma^2, A, B) = Ae^{-\frac{(E-E_m)^2}{2\sigma^2}} + B(E) \quad (10)$$

where

E = gamma ray energy,

E_m = mean energy of peak,

σ^2 = variance of distribution,

A = amplitude of peak (cps), and

B = background distribution (cps).

In practice, the fit is performed over a narrow range of energies to simplify the background term, which in its simplest form would be linear. The mean energy E_m and variance σ^2 can be fixed or allowed to vary over a range of energies. The goal of the fit is to extract the number of counts in a target peak, which can be calculated from the amplitude A and the variance σ^2.

Unlike the windowing methods, the Gaussian method does not depend on the availability of a target isotope-free area to tune the extraction. That is, a constant like the K of the windowing methods does not need to be determined; however, the Gaussian fit is insensitive to downscattered photons from the target isotope.

5.4. Cesium-Specific Isotope Extraction Algorithm

The Cs-137 isotope has a primary a photopeak at 662 keV. The variable natural background also contributes to that photopeak. A spectrum-based algorithm can remove the variable background contribution in a second-by-second operation. The resulting data has a statistical distribution of counts centered on a net value of zero in regions where only natural background contributions are present. If a statistically significant source is present, its activity will show up as an excursion above the statistical bounds associated with the natural background activity.

The form and function of the Cs-137 extraction algorithm is set for the specific extraction of the Cs-137 source contribution. The source energy window (region of interest or ROI) is set to 594 through 730 keV. The background energy windows are set to 526 through 594 keV for background 1 and 730 through 798 keV for background 2. The three-window algorithm is very useful in extracting photopeak counts where the shape of the Compton-scatter contributions from other isotopes is highly variable.

6. Data Quality Control and Assurance

Performing measurements of any kind always requires the utmost attention to the details of the measurement, including factors such as the state of health of the equipment, the environment where the measurements are taken, and any unusual events that may affect the data. Operating sensitive radiation

detection equipment outside of a laboratory setting, i.e., in the field, puts an addition burden on data quality control simply because there are so many variables outside the control of the technicians and scientists. For example, one of the largest causes of data variations is the diurnal variations of radon concentration in the atmosphere. Additional corrections need to be made for cosmic rays adding to the detected radiation and variations in flight altitude of the aircraft. These variations put an additional burden on data quality control because they must be distinguishable from hardware variations that may be correctable. This section describes the data quality control and quality assurance procedures followed during data collection and analysis.

6.1. Daily Preflight Checks

Before each day's flights, an equipment check was performed using both normally occurring background at the FBO and a Cs-137 check source. Normally occurring background at most locations is almost entirely due to naturally-occurring radioactive materials (NORM) and cosmic rays. NORM includes the radioactive isotopes of potassium, uranium, and thorium (KUT) present essentially everywhere on Earth, and the daughter products of these isotopes, including radon in the atmosphere. The radon component is time and weather dependent. There is a normal diurnal cycle (atmospheric radon concentration is normally highest in the morning) and precipitation will wash radon progeny out of the air. The cosmic contribution is largely constant for a given elevation above sea level and latitude. Data collected during each preflight check was analyzed for quality and consistency, and results were examined before each day's flights.

Figure 9 shows the background count rate collected with the helicopter on the ground at the FBO. These backgrounds were collected at roughly the same time each morning, and show the variability in radon and radon progeny concentrations. Figure 10 shows net count rates collected with a radioactive Cs-137 check source during the morning preflight checks. The morning background count rates have been subtracted from the source data. Net rates remained statistically the same for the entire survey period, demonstrating the stability of the detection system.

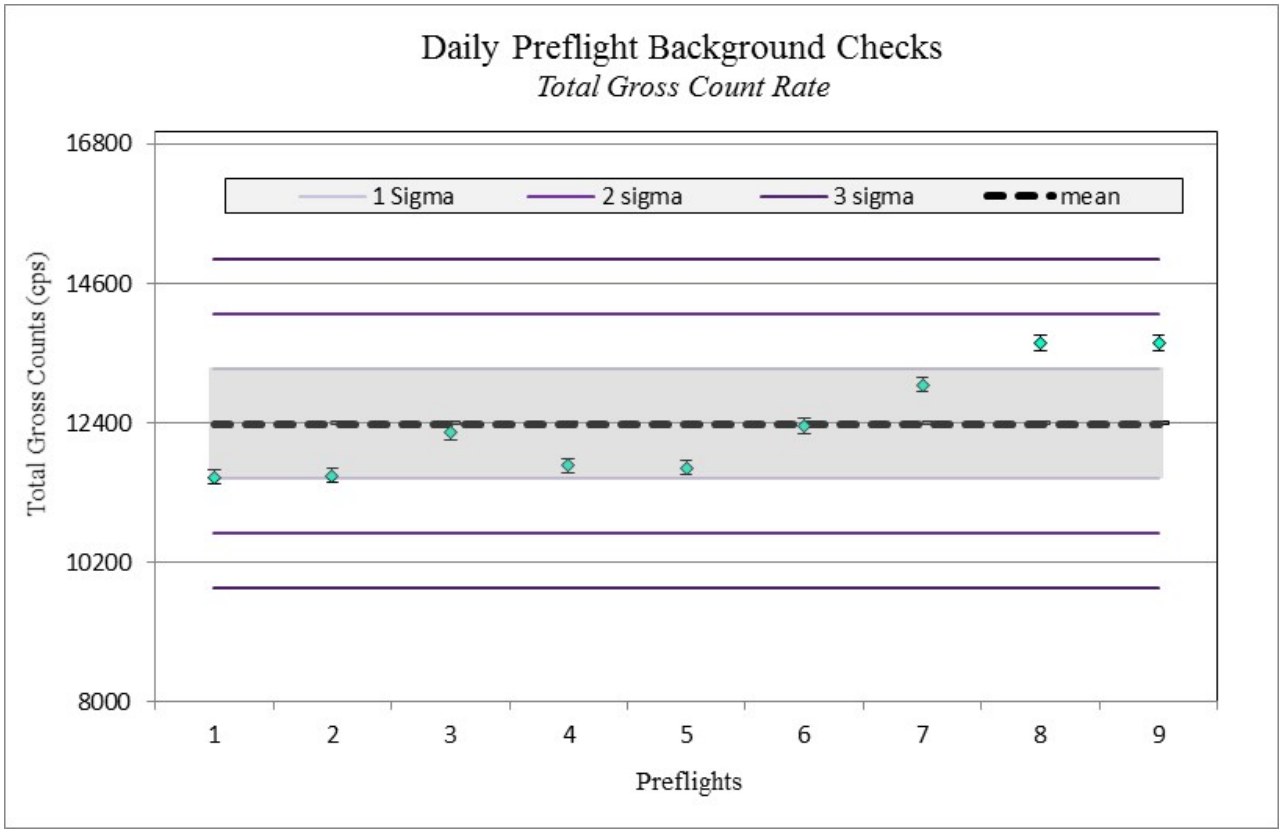

Figure 9. Daily preflight background checks expressed as total gross count rate. The variations seen are largely due to changes in atmospheric radon.

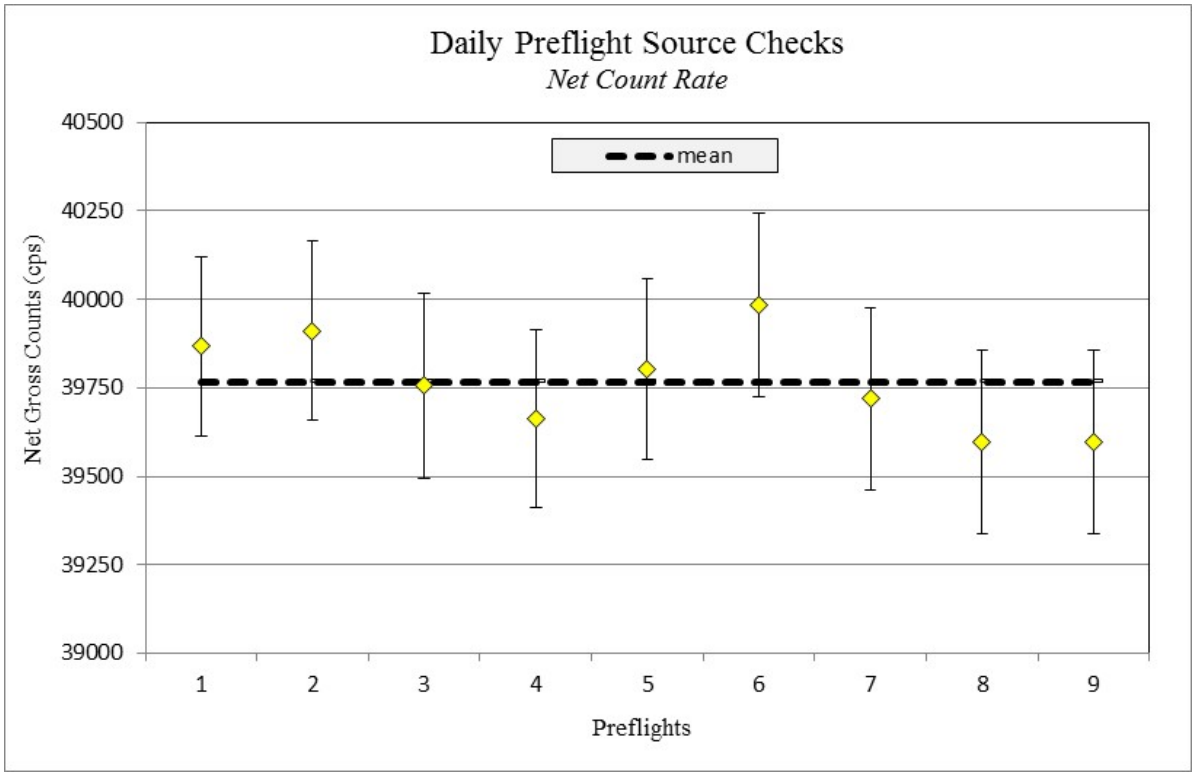

Figure 10. Daily preflight source checks expressed as total net count rate.

6.2. Test Line and Water Line

At the beginning and end of each flight, a water line and a test line were flown at survey altitude. The purposes of these lines are to obtain a non-terrestrial background and to monitor system performance at survey altitude and speed. The non-terrestrial backgrounds are subtracted from the gross count rates when ground-level exposure rates are calculated (see Section 4.1).

Figure 11 shows the locations of the test and water lines. The water line was chosen over a section of the Columbia River wide enough so that the portion of the detector footprint not over water was minimized (survey altitude was 50 ft AGL and the helicopter was at least 700 ft from either bank). The test line was chosen to be representative of uncontaminated NORM background and to be easily accessible for ground measurements. The ground measurements are used as an additional check on detector calibration.

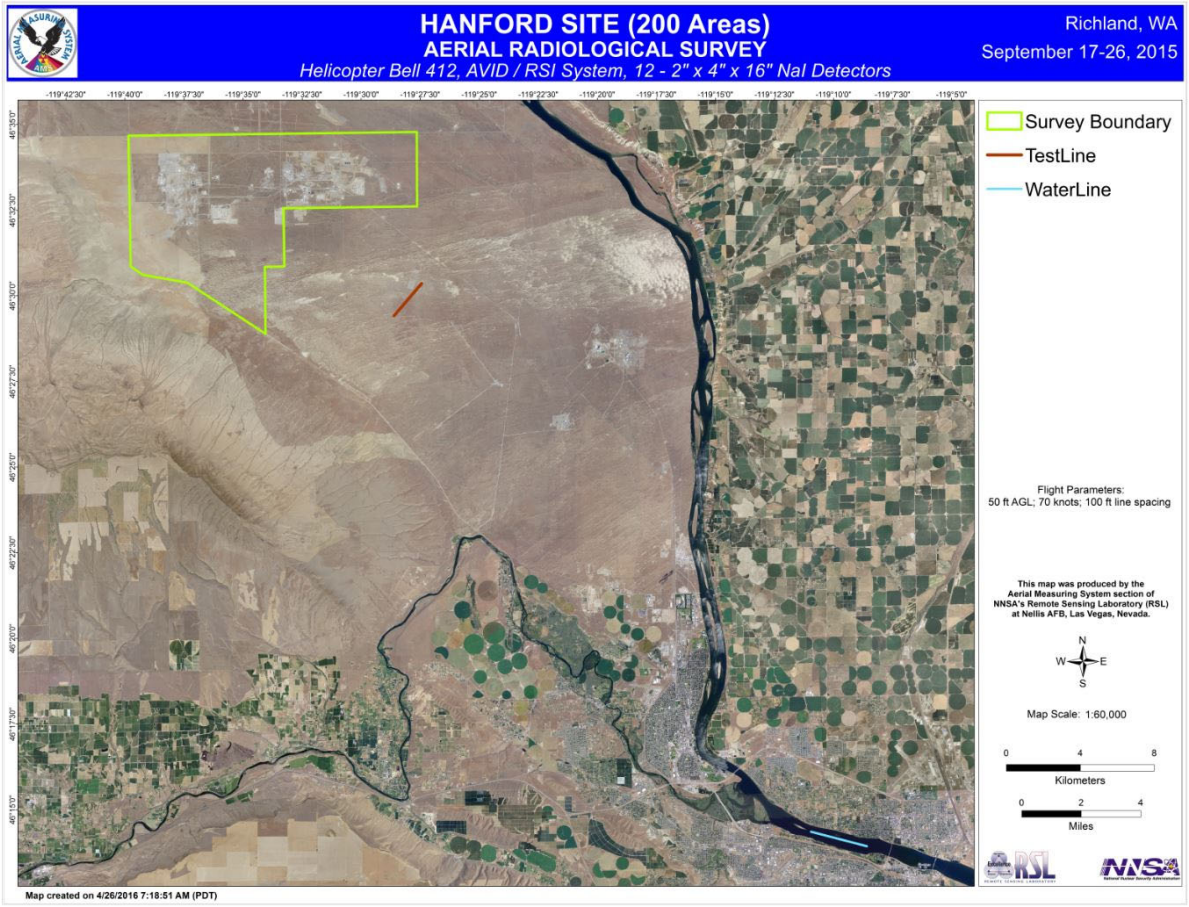

Figure 11. Locations of the test line and water line. These lines were flown at survey altitude at the beginning and end of each survey flight.

Figure 12 shows the total count rates along the water line, averaged over the length of the line. Data were collected with the helicopter at the survey altitude of 50 ft AGL. Diurnal variation of radon concentration can be seen in this plot, most obviously during the latter half of the survey. Differences in day-to-day radon concentrations can generally be attributed to weather changes over the course of the survey. Calm weather can increase the variation seen over the course of a day because radon can collect near ground level during the cool night hours. After sunrise, ground warming dissipates accumulated radon. The water lines are used to correct survey data for non-terrestrial contributions, and in general count rates taken at the beginning and end of each flight are averaged together to obtain the correction for the flight.

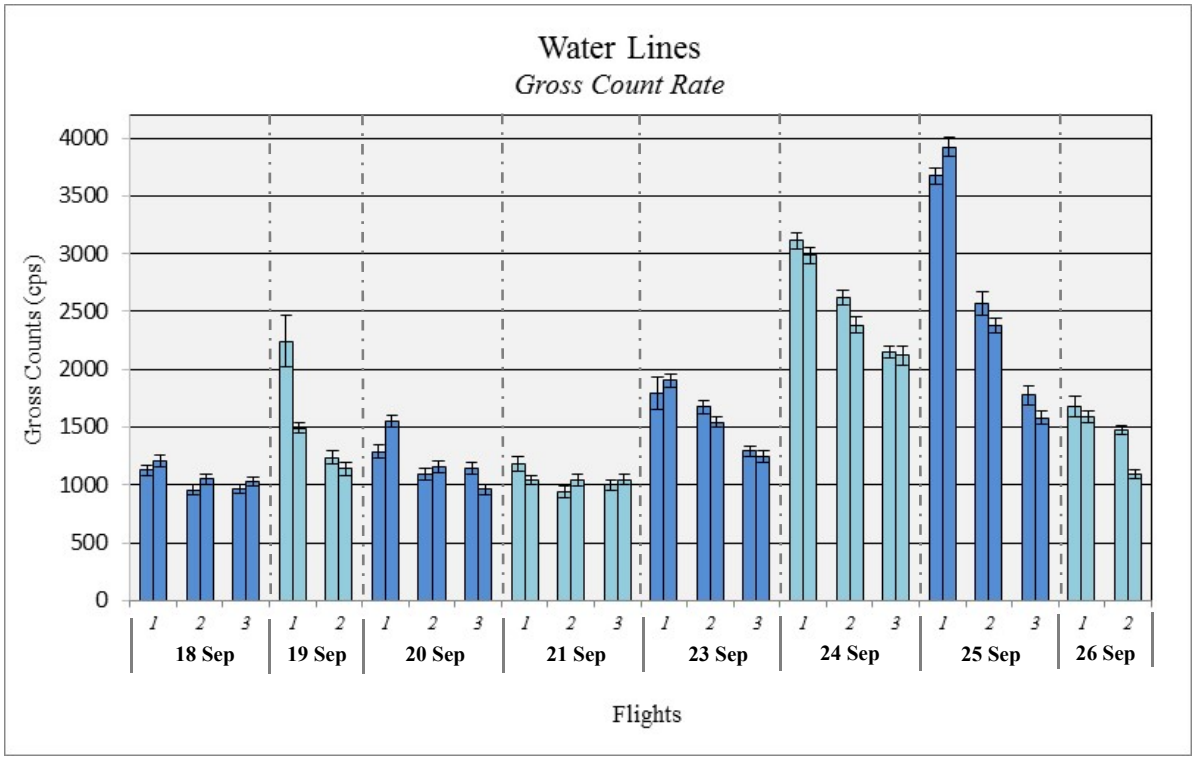

Figure 12. Average gross count rates along the water line.

Figure 13 shows the gross count rates collected at the beginning and end of each survey flight along the test line. The data were collected with the helicopter flying at the survey altitude of 50 ft AGL and survey speed of 70 kts. These count rates have not been corrected for non-terrestrial contributions. Diurnal variations in the water line data are also seen (radon contributions are generally higher early in the day). Figure 14 shows the net count rates along the test line (gross count rate – corresponding water line rate). Large variations due to radon concentration have been mostly removed.

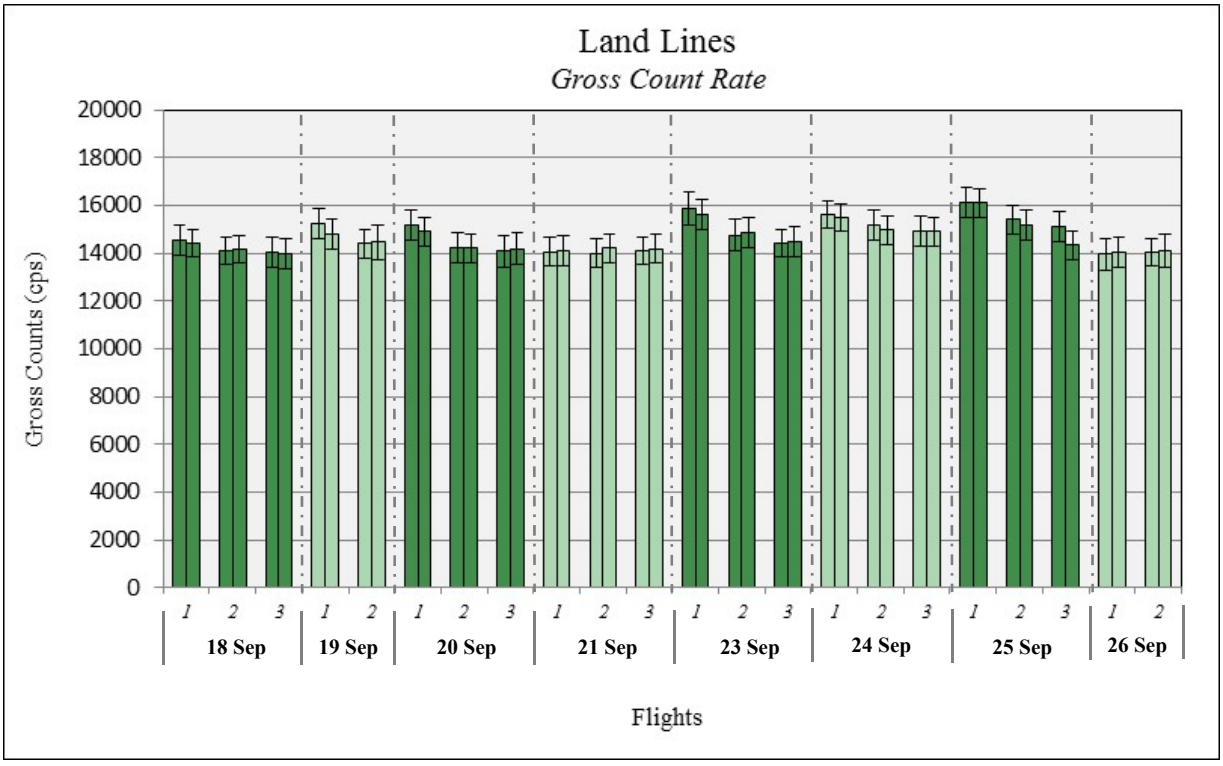

Figure 13. Average gross count rates along the test line.

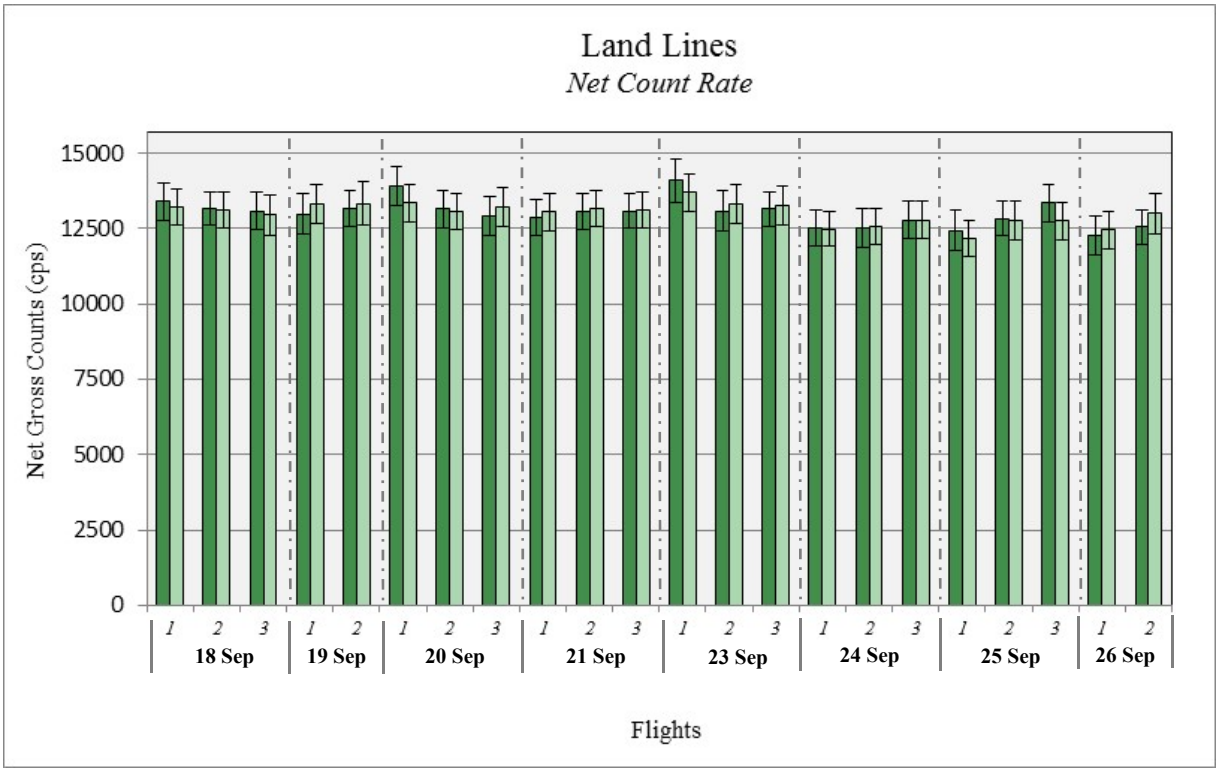

Figure 14. Net count rates along the test line.

7. Survey Results

The survey was completed in a period of ten days, including a surveillance flight (to identify aviation hazards) on the first day and a crew rest day. Figure 15 shows an overview of all flights, along with the route taken by the mobile drive and the locations of ground measurements (PIC and HPGe). In the southwest corner of the map is the test line, which was flown at survey altitude (50 ft AGL) at the beginning and end of each survey flight. There are three holes in the survey coverage; two of these are areas the helicopter was not permitted to fly over, and one was caused by the helicopter flying around a tower.

7.1. Gross Count Rates and Exposure Rates

Spectral data collected over the survey area is summed to obtain a gross count rate, which is converted to exposure rate as outline in section 4.1.

Figure 16 shows the result of this analysis. Several areas of high exposure rate are seen, up to 350 μR/h, which was expected for this survey. While this map is useful for locating these areas of relatively high exposure rate, several factors must be taken into account when attempting to read absolute exposure rates: the conversion factor used to convert count rates to exposure rates was derived using NORM background, the indicated exposure rates are averaged over the detection footprint of the helicopter, and in several areas the detectors on the helicopter saturated.

Figures 17 and 18 show zoomed in maps of the altitude and background-corrected count rates for the 200 West area and 200 East areas, respectively. Care must be taken in interpreting the highest count-rate areas shown (765,841 – 1,018,885 cps) because of detector saturation which can cause one or more NaI(Tl) logs to drop out (stop collecting data), resulting in low or no counts collected for that sample period.

Exposure rate is a function of photon flux and the energies of those photons. The cps to exposure rate conversion factor used in this report was derived using NORM background at the Lake Mohave Calibration Range (Colton & Hendricks, 1999). This calibration constant is valid for areas with similar spectral profiles. If the profile significantly changes, the calibration may under- or over-report the actual exposure rate.

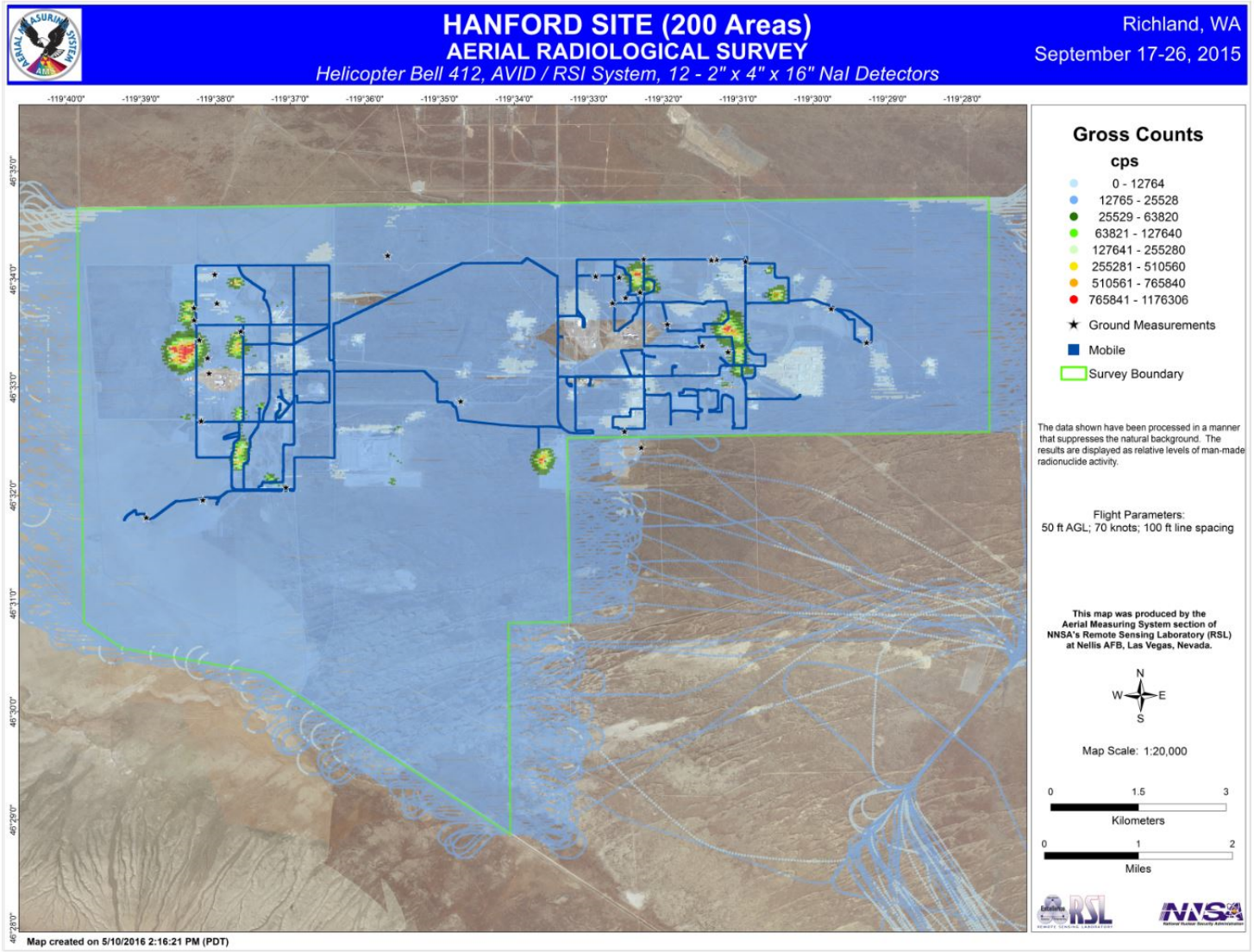

Figure 15. Map showing flight lines, mobile drive route, and location of ground measurements.

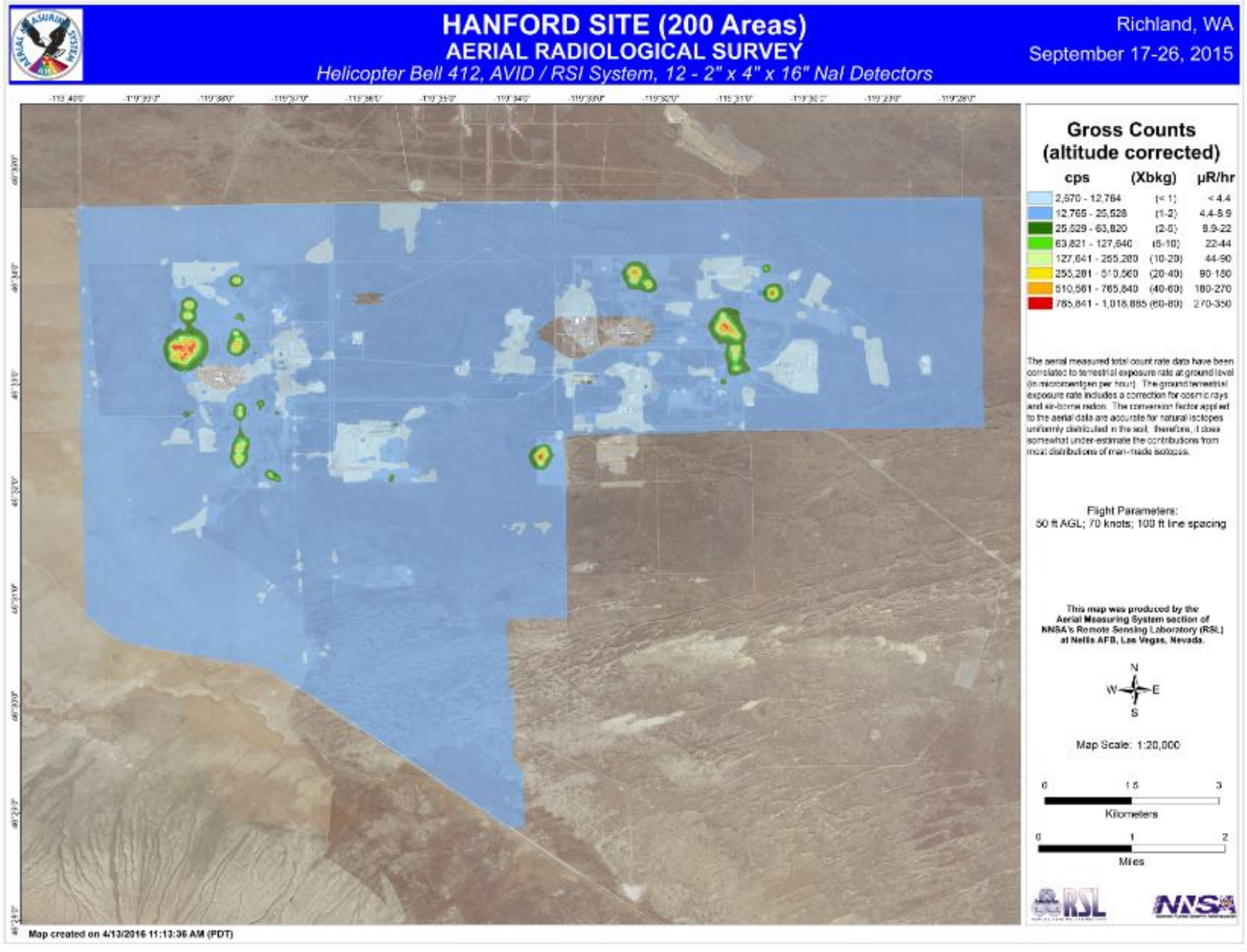

Figure 16. Map showing gross count rates over the survey area. Data have been corrected for non-terrestrial backgrounds and altitude variations. Scales are given in counts per second at survey altitude, number of standard deviations above background, and exposure rate at 1 m above ground level.

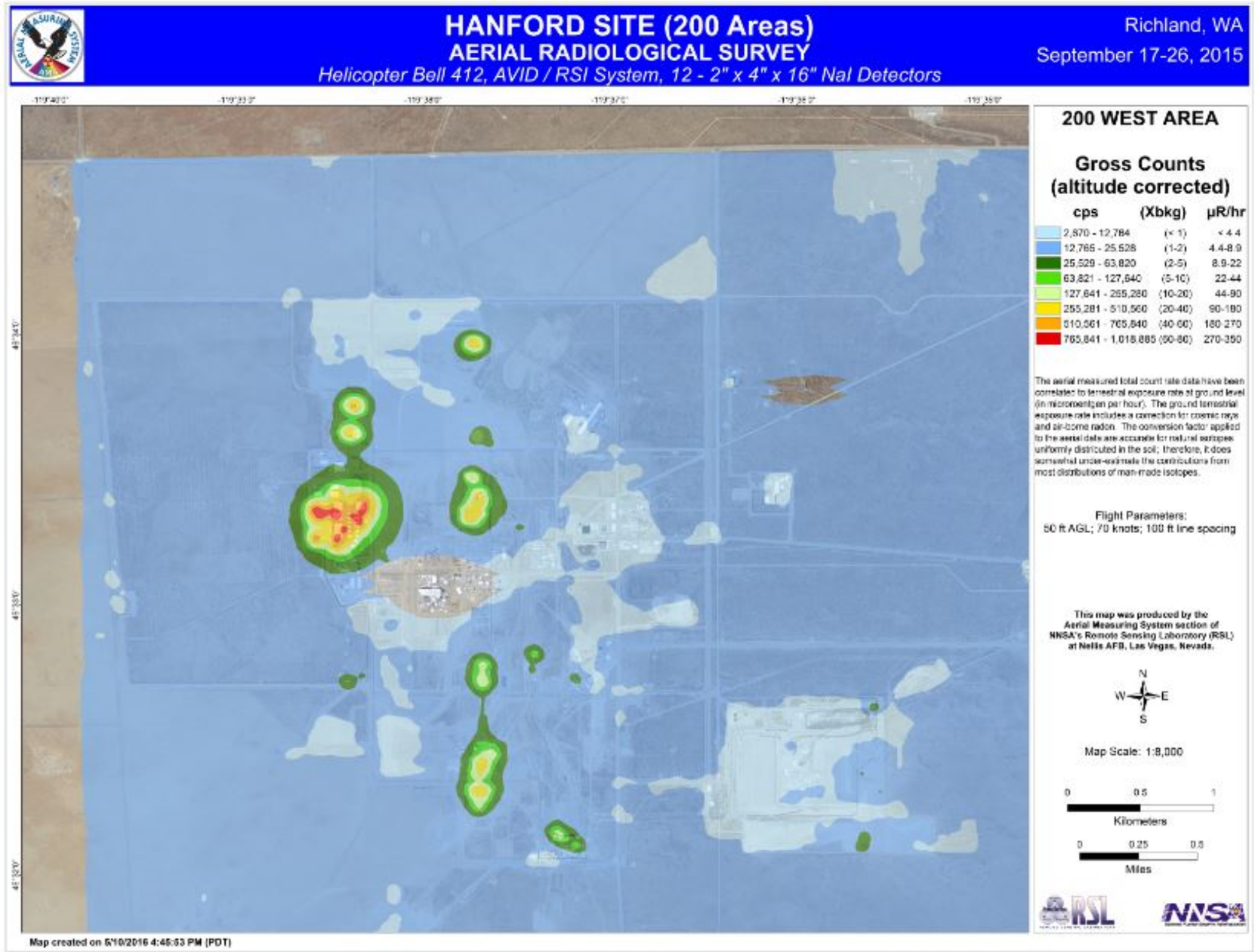

Figure 17. Map showing background-corrected gross count rates in the 200 West area.

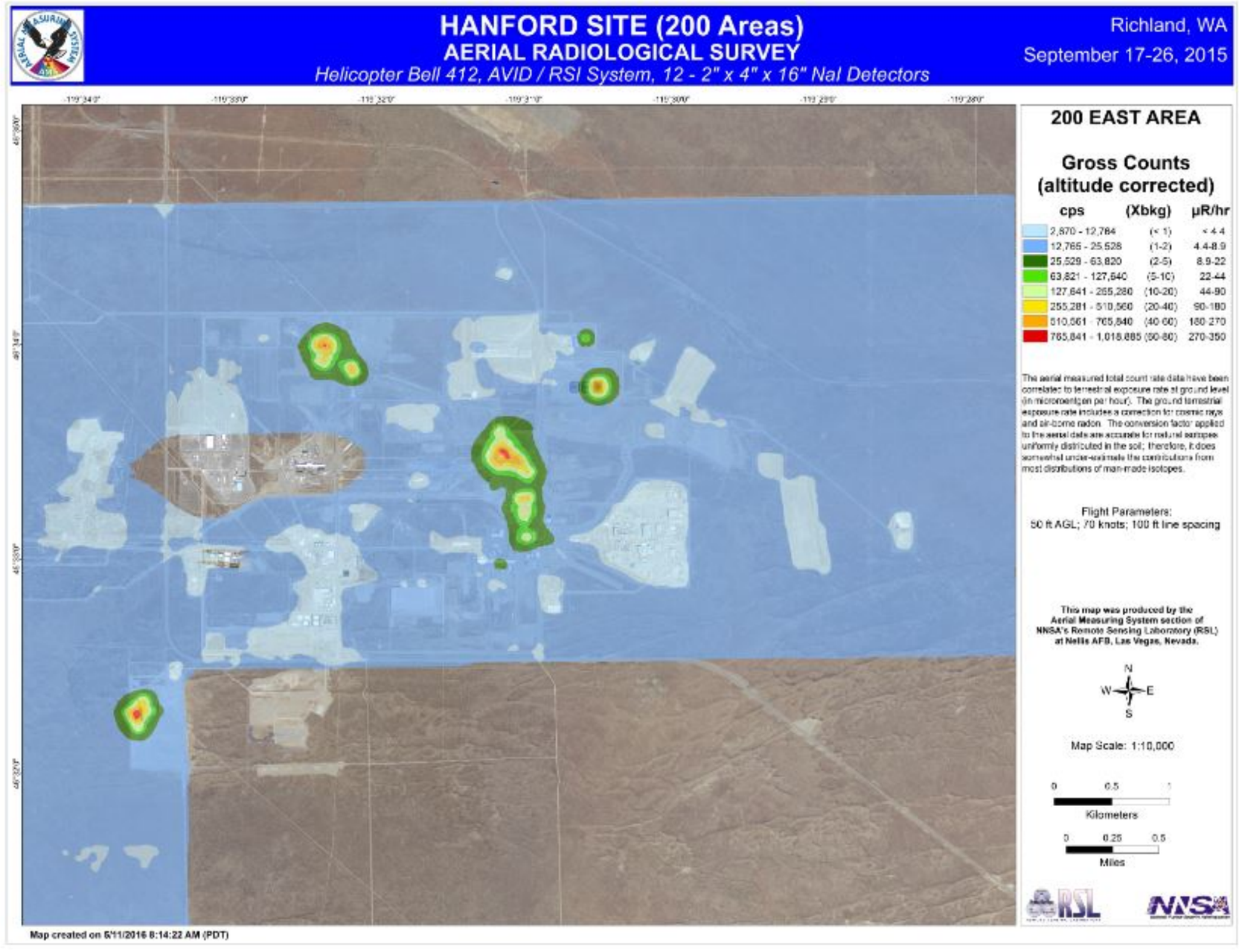

Figure 18. Map showing background-corrected gross count rates in the 200 East area.

As discussed in Section 3, as the helicopter flies above a section of ground, the detectors onboard are sensitive to photons coming from an area of the ground with a diameter roughly equal to twice the helicopter altitude AGL. About 60% of the signal collected by the detectors comes from this area, which can be taken as a general rule of thumb. The actual percentage of signal depends on photon energy, source distribution, and topology. Thus, for a flight altitude of 150 ft AGL, the detector footprint is 300 ft across. The footprint is not circular, however, because the helicopter travels about 120 ft each second, which is also the data integration time. Therefore, the reported count rates are averages from an elongated circle roughly 300 ft by 420 ft.

The highest count rates measured by the detectors are about 10^6 cps. Above this rate, the NaI detectors saturate and no data is recorded for that 1-second interval. The contour map in Figure 16 masks this effect to some degree; that is, the data holes are smoothed over by the contouring algorithm. Some lost information can be recovered by using the HPGe data that was collected concurrently with the NaI data. By plotting exposure rate as determined from the NaI data against the total count rate from the HPGe detector, an ersatz conversion factor may be obtained for the HPGe data. Using this technique, preliminary results indicate the highest exposure rates are below 1 mR/h. Because the HPGe uses the same integration time as the NaI (1 s) point source exposure rates may be higher.

7.2. Anthropogenic Algorithm

The anthropogenic algorithm described in Section 4.2 uses the NaI data to map areas associated with an excess of non-NORM isotopes. This technique is used as a general analysis method independent of specific isotopes. It thus has the advantage of not having the requirement of a piori knowledge of those isotopes. Figure 19 shows the result of this analysis. Because the algorithm suppresses variation in NORM background, it can reveal contaminated areas not seen in a simple gross count map. Four isotopes were explicitly looked for (Am-241, Cs-137, Co-60, and Pu-239) and the results of these investigations are presented in the following sections.

Near the eastern edge of the survey there is an area of slightly elevated anthropogenic count rate, which appears as a band in the north-south direction. There is a power line here, and the helicopter had to gain altitude to clear the lines. Because air attenuation is energy dependent, as the aircraft changes altitude the shape of collected spectra changes. The anthropogenic algorithm detects this change as the helicopter altitude changes over the power line.

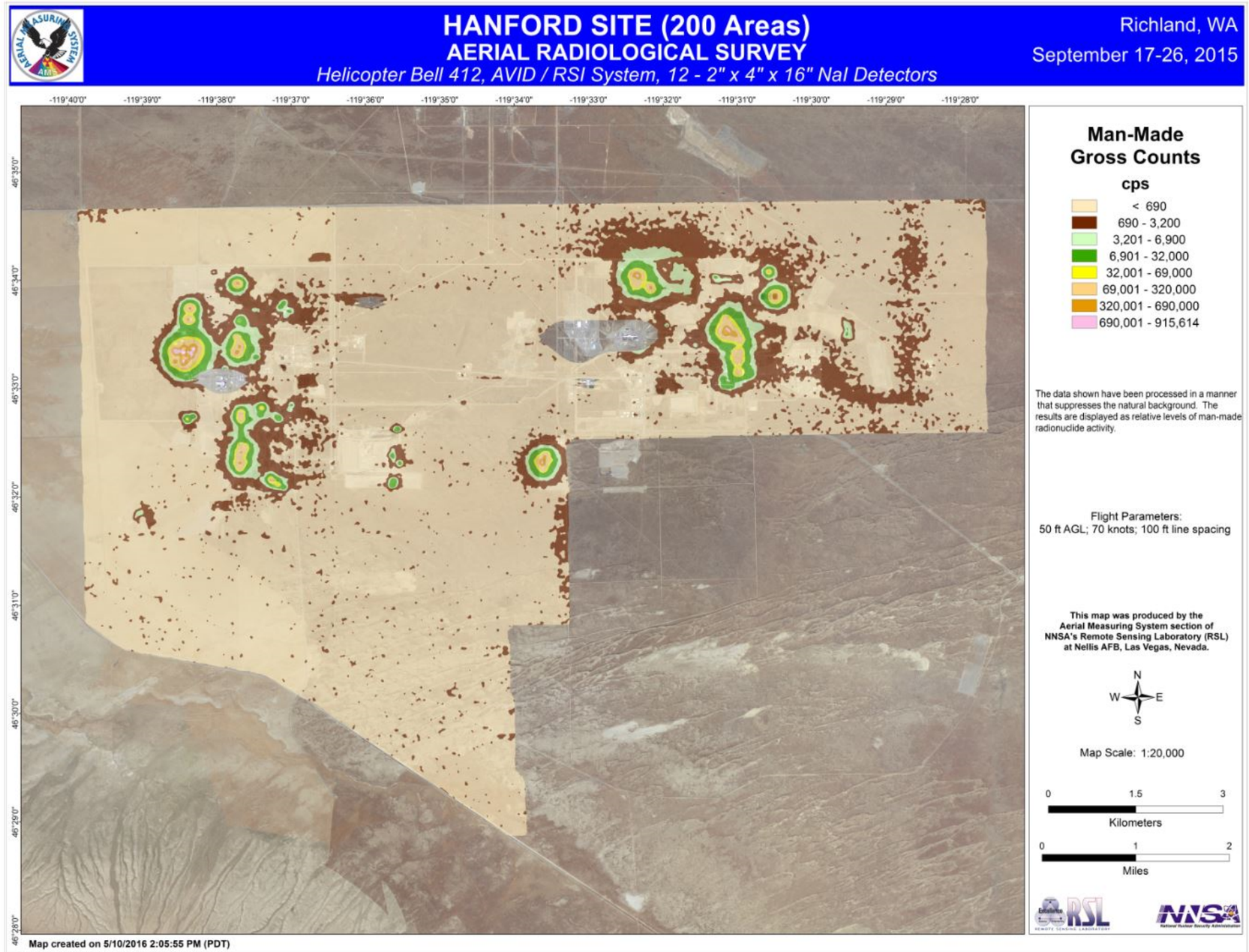

Figure 19. Map showing excess count rates due to anthropogenic isotopes. The map shows essentially the same features seen in Figure 16.

7.3. Isotope Extractions

The isotope extraction algorithms outlined in Section 5 were employed to identify areas with excess count rates attributable to the isotopes Am-241, Cs-137, Co-60, and Pu-239. The three-window algorithm is generally the preferred method because of its simplicity and ability to detect small enhancements in a spectrum. However, there are two caveats to this procedure: interference from other isotopes may affect the result obtained for the target isotope, and it extracts only count rates due to the target isotope, and does not indicate actual areal or volumetric activities. Also, because this method uses the NaI data exclusively, points where the detectors saturated will not have data to perform the extraction. These areas are identified in Section 7.5.

As an alternative to the three-window method, Gaussian fits of target peaks may be used. This is the preferred method if there is another interfering isotope, or if HPGe data is used, since peaks in a spectrum are better defined.

7.3.1. Isotopic Sensitivities

Concentrations of specific radioisotopes are derived from the extractions by using appropriate conversion coefficients, also known as isotopic sensitivities. Sensitivities for several isotopes have been calculated for the twelve-log NaI(Tl) detector system using known properties of gamma ray transport through soil and air, and the nominal detection efficiency of the NaI(Tl) detectors, both of which depend on gamma ray energy. The distribution of the radioisotope in the soil needs to be assumed, and two simple cases, uniform or exponential (i.e., decreasing with soil depth) distribution, have been used. The difference in sensitivities based on these two assumptions is dependent on gamma ray energy, with the difference decreasing as gamma energy increases.

Table 2 lists conversion coefficients calculated for several isotopes of interest at a flight altitude of 50 ft AGL. Because the actual isotopic distribution in the soil is unknown, is probably neither purely uniform nor exponential, and is likely spatially inconsistent, an average sensitivity was used to estimate isotopic abundances. The abundances are reported with the caveat that they have large uncertainties.

Table 2. Isotopic conversion coefficients for the AMS 12-log NaI detector system at an aircraft altitude of 50 ft AGL.

Isotope	Energy [keV]	Uniform Distribution [pCi/g/cps]	Exponential Distribution [pCi/g/cps]	Average [pCi/g/cps]
Am-241	59.5	0.0247	0.0151	0.020
Cs-137	661.6	0.00435	0.00369	0.004
Co-60	1332.5	0.00261	0.00233	0.0025

7.3.2. Americium-241 Extraction

The Am-241 extraction was preformed using the Gaussian technique because of interference from photons downscattered from the Cs-137 peak. The NaI(Tl) data were used for this extraction. The result is shown in Figure 20. Several areas of relatively high activity are seen, particularly in the 200 West area. Isolated

spots of slightly elevated count rate (52-156 cps) are seen throughout the survey area, and are most likely attributable to statistical fluctuations.

7.3.3. Cs-137 Extraction

The Cs-137 extraction is shown in Figure 21. The three-window technique was used for this extraction using the NaI(Tl) data. Relatively high areas are seen in both the 200 West and 200 East areas. Slightly elevated levels (32-150 cps) are seen to the east end north of many of the highly-elevated areas.

7.3.4. Co-60 Extraction

The three-window technique applied to the NaI(Tl) data was also used for the Co-60 extraction, and the result is shown in Figure 22. Only a few areas of elevated count rate are seen, most notably over the US Ecology site. Isolated points of slightly elevated count rate (29-130 cps) are seen, again most likely due to statistical fluctuations in the data.

7.3.5. Pu-239 Extraction

Because of the low levels of the relative soft Pu-239 gamma rays, characteristic peaks from this isotope were not observed in the NaI(Tl) data. However, in the higher resolution HPGe data these peaks could be found. Using the 413.7 keV peak in a Gaussian extraction at least one area of elevated Pu-239 activity can be found.

Figure 23 shows the result of this extraction. The area exhibiting the highest level of activity is in the 200 West area, in the same location where elevated levels of the other three isotopes were found. At this location there is an apparent depression in the activity in the middle of the elevated distribution. High dead times in this area (as high as above 50%) distort the HPGe spectrum and produce an anomalously low result.

The horizontal band of missing data is due to an equipment malfunction during one flight. Results are not presented as isotopic concentrations because the detector has not been modeled for a response to Pu-239.

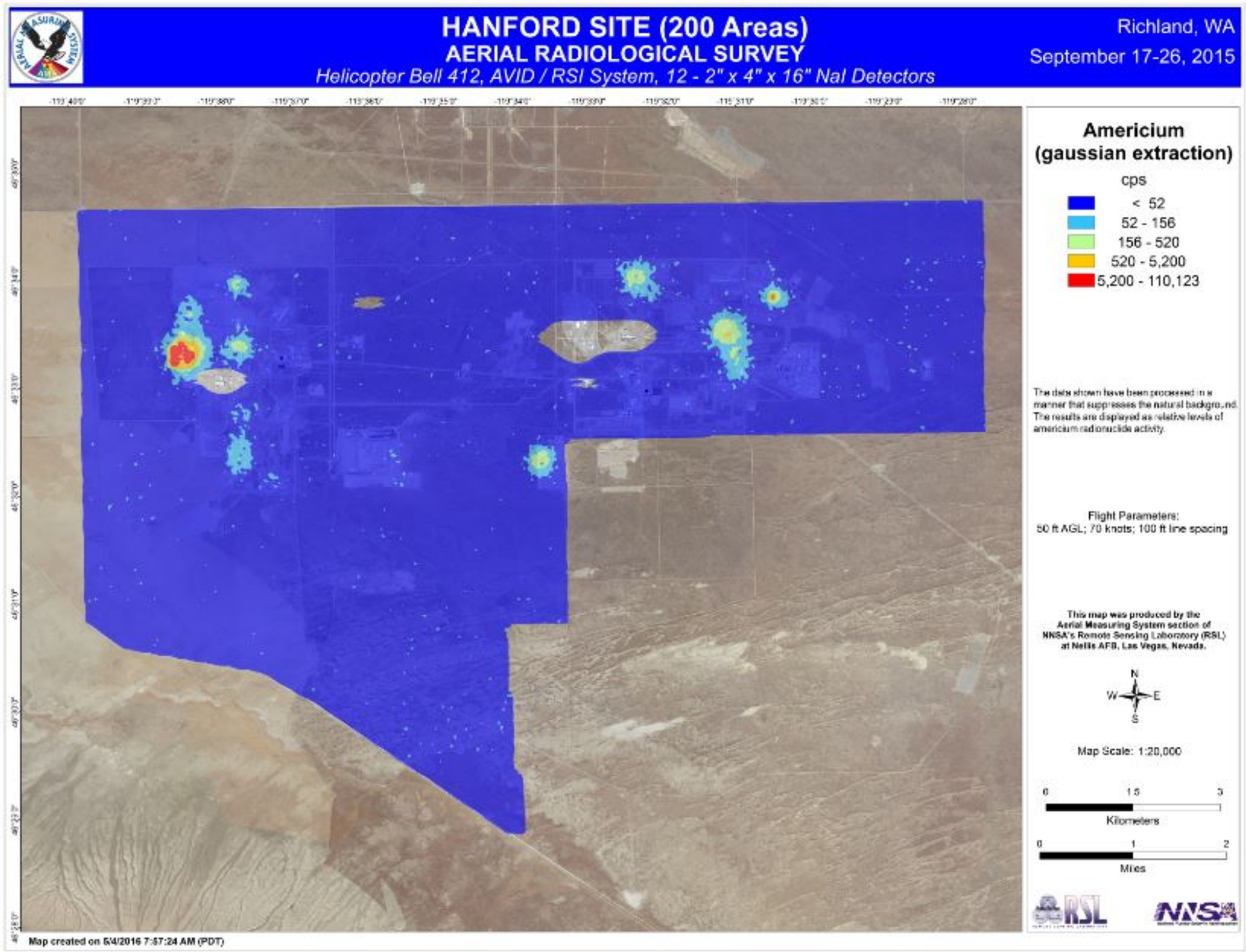

Figure 20. Map showing areas of excess count rate due to Am-241.

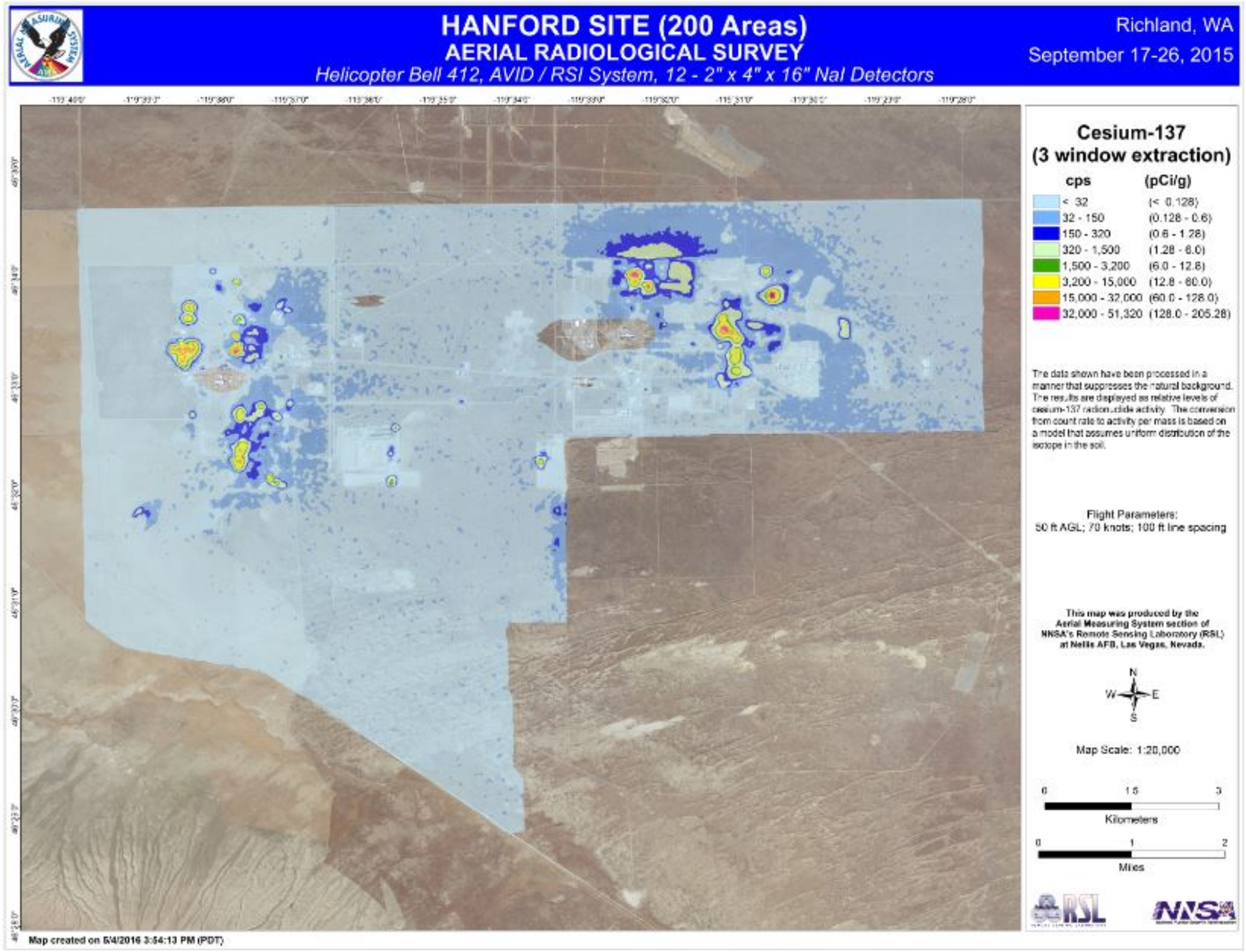

Figure 21. Map showing areas of excess count rate due to Cs-137.

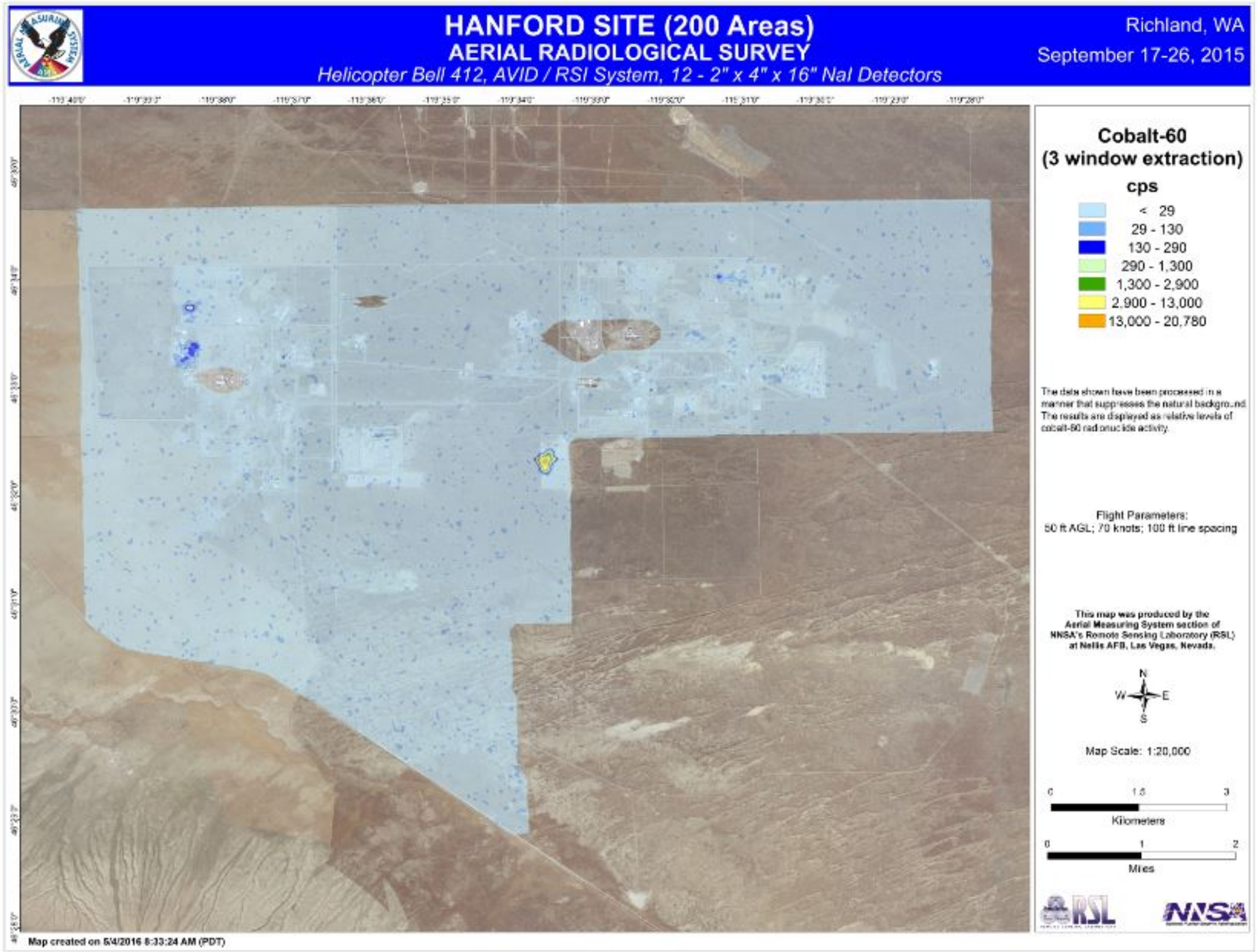

Figure 22. Map showing areas of excess count rate due to Co-60.

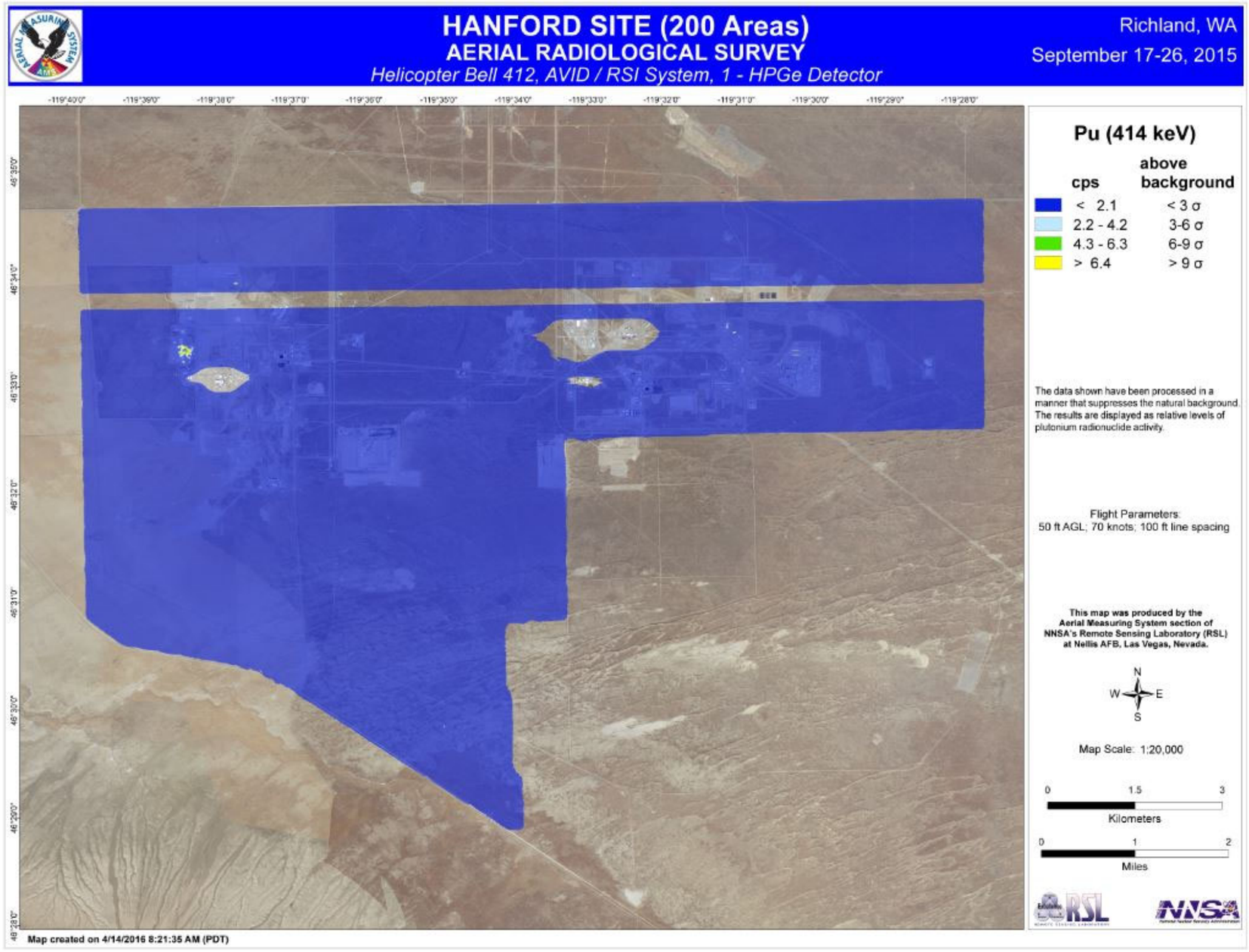

Figure 23. Pu-239 extraction map produced using the HPGe data. The most significant signal is over ROI 01. The horizontal band of missing data is due to an equipment malfunction during the survey.

7.4. KUT Extractions

Concentrations of the naturally-occurring radioactive isotopes of potassium, uranium, and thorium (KUT) can be extracted from the aerial data using the well-known technique of spectral stripping (IAEA, 2003). Stripping coefficients for the AMS NaI(Tl) system were derived from measurements taken at the Department of Energy calibration facility located at Walker Field in Grand Junction, Colorado, on the Large Area Calibration Pads.

The technique sums the total counts (peak and background) in energy windows centered on the 1462 keV K-40 peak, the 1765 keV Bi-214 peak, and the 2614 keV Tl-208 peak. The U-238 daughter Bi-214 is used as a surrogate for U-238, and the Th-232 daughter Tl-208 is used as a surrogate for Th-232. Because U-238 and Th-232 are measured using their daughters, an assumption of secular equilibrium is implicit in this method. Using the stripping coefficients, downscatter contributions in the lower energy peaks are accounted for when calculating isotopic concentrations. Because of air attenuation, count rates are corrected for aircraft height AGL.

This IAEA method was developed for aerial surveys over regions containing only naturally radioactive isotopes. If an anthropogenic isotope is present that significantly contributes to the monitored windows (e.g., the 1332 keV Co-60 peak) the method will give erroneous results. No corrections were made for interfering isotopes when doing this analysis. The USGS concentrations quoted in the following sections come from (US Geological Survey, 2104)

7.4.1. Potassium

Figure 24 shows potassium concentrations in weight per cent derived from the IAEA method. In general, the concentration is rather uniform over the survey area. A notable exception is over the US ecology plant, where high Co-60 levels create a large peak at 1332 keV that contributes positively to the K-40 window. USGS potassium concentrations in the Hanford Site area range from about 1.3 to 1.7 weight percent.

7.4.2. Uranium

The uranium IAEA extraction, shown in Figure 25, shows a few areas of elevated activity, particularly over the region in the 200 West area where elevated activity from several other isotopes is found. Because no spectral correction for airborne radon has been made, horizontal bands of relative high or low activity are seen, corresponding to different levels of radon during different flights. USGS uranium concentrations range from about 1.5 to above 2 ppm.

7.4.3. Thorium

The thorium extraction, seen in Figure 26, has an elevated region in the 200 West area. Additionally, slightly lower concentrations are seen in disturbed areas, including buildings and roads. USGS thorium levels are in the range of about 5 – 7 ppm.

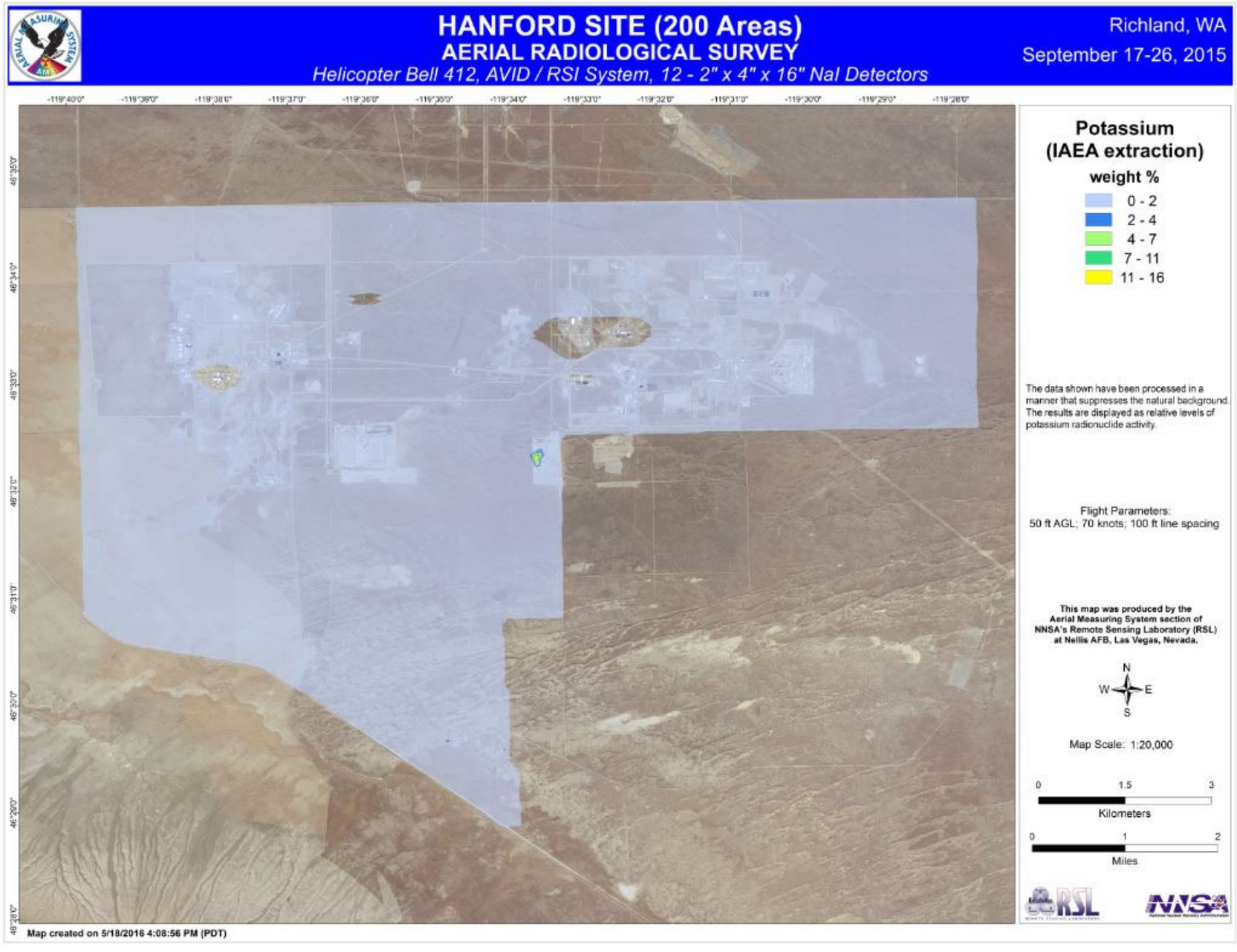

Figure 24. Potassium concentrations calculated using the IAEA stripping coefficient method. This method assumes uniform distribution of the isotope in the soil.

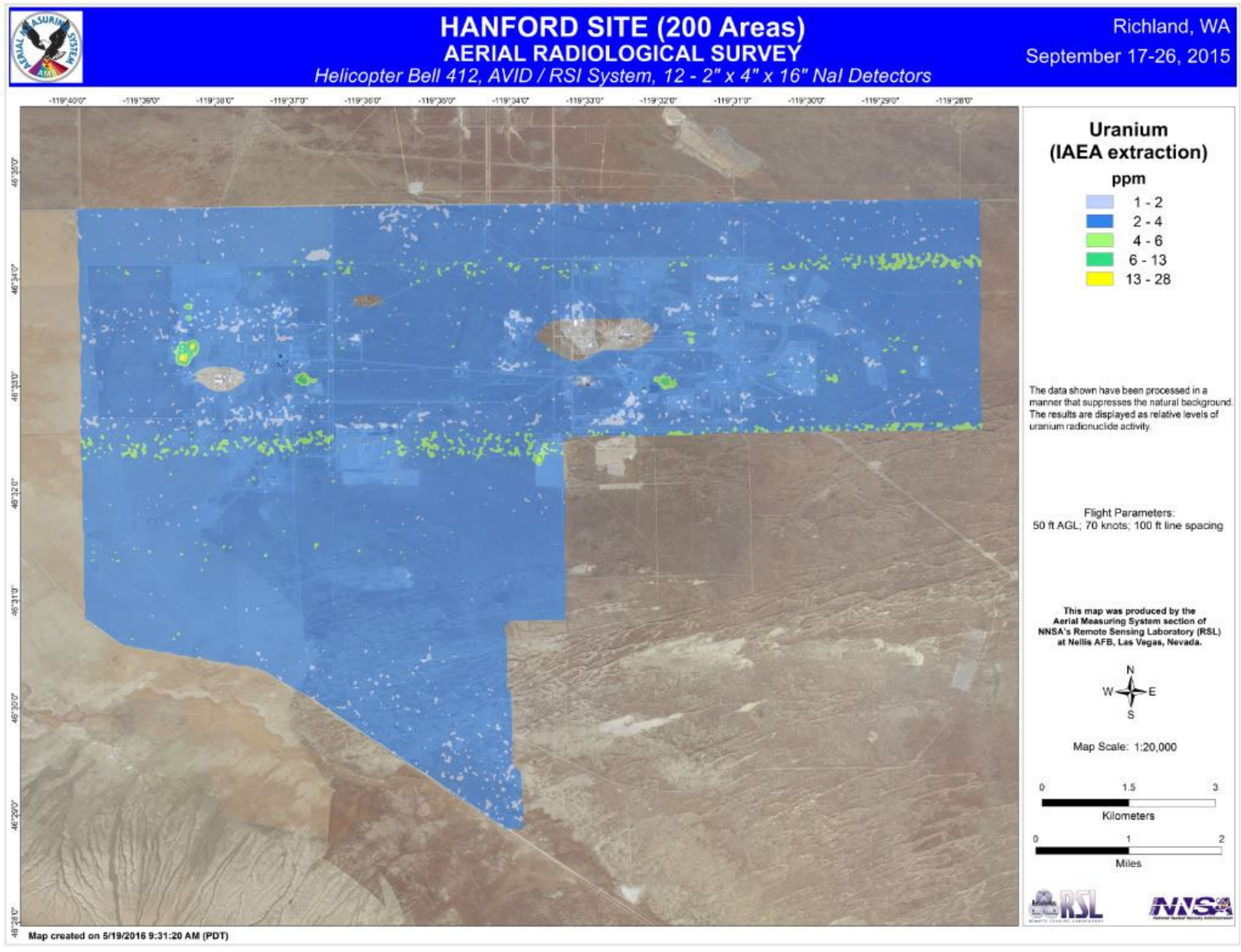

Figure 25. Uranium concentrations calculated using the IAEA stripping coefficient method. This method assumes uniform distribution of the isotope in the soil. The higher-concentration horizontal bands are data artifacts caused by relatively high atmospheric radon levels.

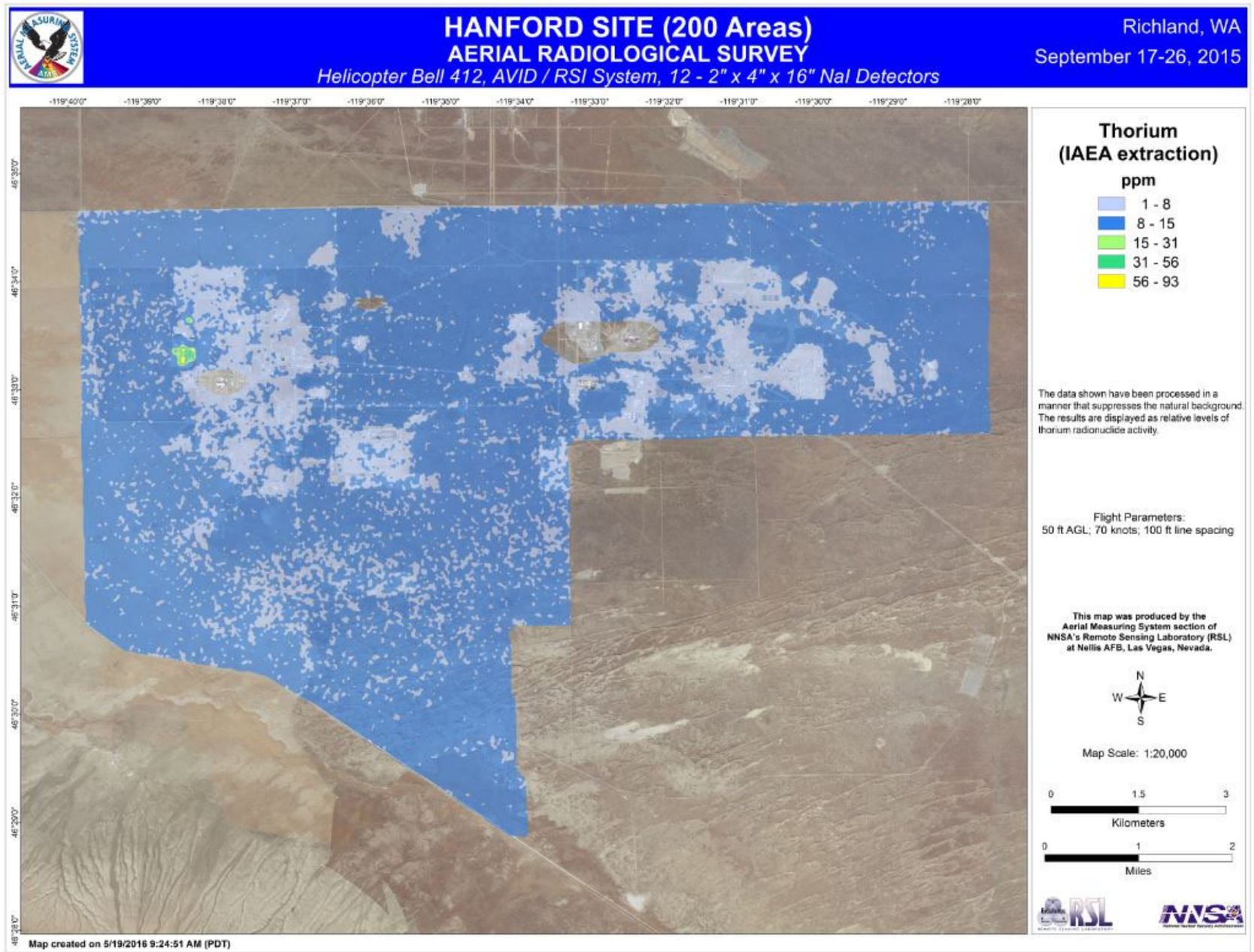

Figure 26. Thorium concentrations calculated using the IAEA stripping coefficient method. This method assumes uniform distribution of the isotope in the soil. There is a pattern of lower concentrations in areas where the topsoil has been disturbed.

7.5. Regions of Interest

The several methods of data analysis (gross count, anthropogenic, isotope extraction) are all designed to indicate areas of activity in excess of NORM activity. These are collectively termed areas of interest (ROI). A total of 68 regions of interest were identified in the survey area. Because these ROIs were identified by several analysis methods, there is occasional overlap. Also, a large ROI may be subdivided into smaller regions. ROIs identified in the anthropogenic extraction are shown in Figures 30 through 33.

For the preliminary investigation, spectral extractions were made from these areas from the NaI data. The spectra are presented in Appendix B, and have not had any corrections made to them, e.g., background subtraction or suppression of data drop-outs caused by detector saturation. NaI data dropouts are present in ROIs 1, 4, 7, 24, 25, and 31. Isotopes identified are, in addition to NORM, Cs-137, Am-241, and Co-60. Individual one-second spectra are available for each ROI, and further investigation of isotopic distribution within the ROIs can be done.

HPGe data collected from the helicopter flying over NORM background is generally too sparse to produces meaningful one-second spectra. Several of the ROIs, however, exhibit activities high enough for producing significantly higher quality spectra. These spectra can be used for more detailed examination of the spatial distributions of isotopes and examined for other isotopic signatures.

7.5.1. ROI 01

Gamma ray flux over ROI 01 was intense enough to saturate the NaI(Tl) detectors; that is, the count rate in the detector was too great for the electronics to adequately record events. The intensity was similarly responsible for high dead times in the HPGe detector, above 50% for some spectra. However, the summed spectrum has a dead time of 13%, which still allows for isotopic identification without excess spectral distortion.

The HPGe spectrum from ROI 01 is shown in Figure 27. The Am-241 59.5 keV and Cs-137 661.6 keV peaks are quite evident. A peak at 772.0 keV is also visible and attributable to Am-241. The small peaks just below 80 keV are due to x-rays originating in the detector itself. A thin layer of gold covers the HPGe crystal and serves as an electrode and thermal reflector. Gamma rays incident on this gold layer induce x-rays which are detected.

Two peaks consistent with Pu-239 can be identified at 375.0 and 413.7 keV. This region of the spectrum suffers from a great deal of downscatter from the Cs-137, which may be masking the lower-yield Pu-239 peaks. The 413.7 keV peak was used to perform a Gaussian extraction for Pu-239 on the entire survey.

Enhancements at 1173.2 and 1332.5 keV are present, consistent with the presence of Co-60. Remaining peaks were identified as NORM background.

7.5.2. ROI 02

The summed HPGe spectrum from ROI 02 is shown in Figure 28. This is a small region, and the spectrum has a live time of only 13 seconds. The only anthropogenic radioisotope seen in the spectrum is Cs-137. Note that in the NaI(Tl) spectrum from this ROI (Appendix B) there is also an indication of the 1332.5 and 1173.2 keV Co-60 peaks. The other identified peak at 1460.8 keV is from K-40, a component of NORM background.

7.5.3. ROI 23

The summed HPGe spectrum collected over ROI 23 is shown in Figure 29. This spectrum has a live time of 27 seconds, but a dead time of only 1%, which is indicative of a small number of gamma rays reaching the detector. The Cs-137 661.6 keV peak is still quite evident. The other identified peaks are from NORM background.

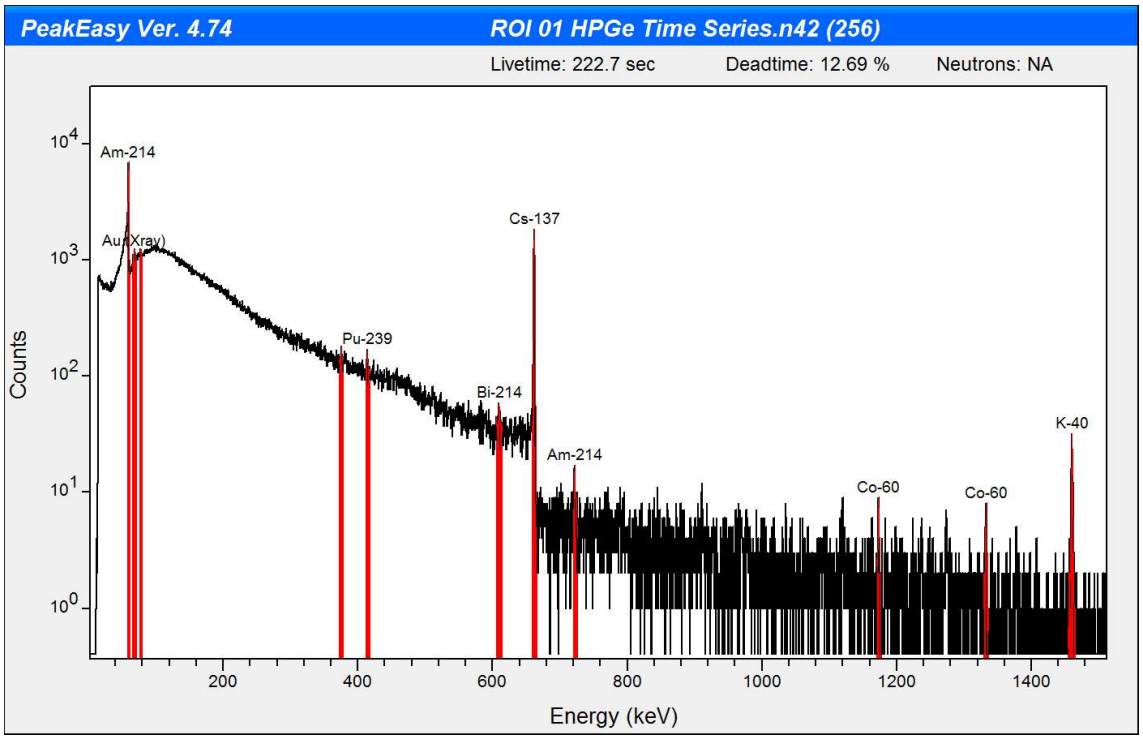

Figure 27. HPGe spectrum from ROI 01. Note the energy scale is shown only to 1500 keV. Identified anthropogenic isotopes are Am-241, Pu-239, Cs-137, and Co-60. The Au x-ray peaks are from the detector, and the Bi-214 and K-40 are NORM background.

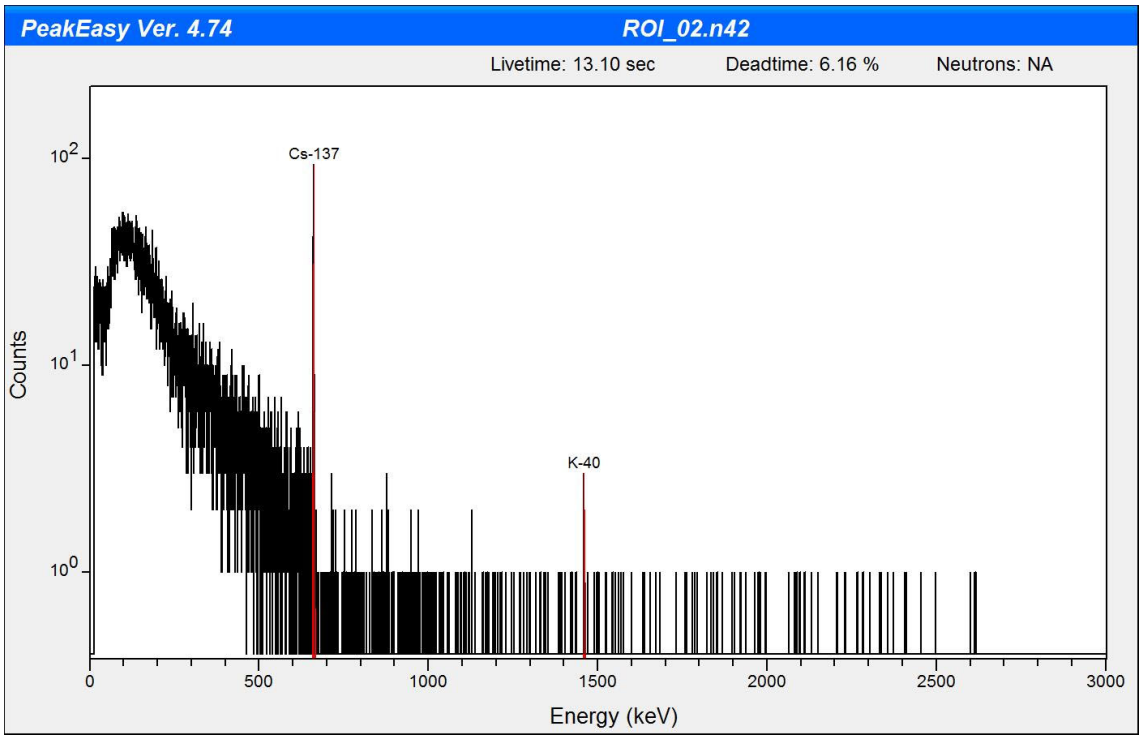

Figure 28. HPGe spectrum taken over ROI 02. The Cs-137 662 keV peak is prominent. No other anthropogenic radioisotopes are evident.

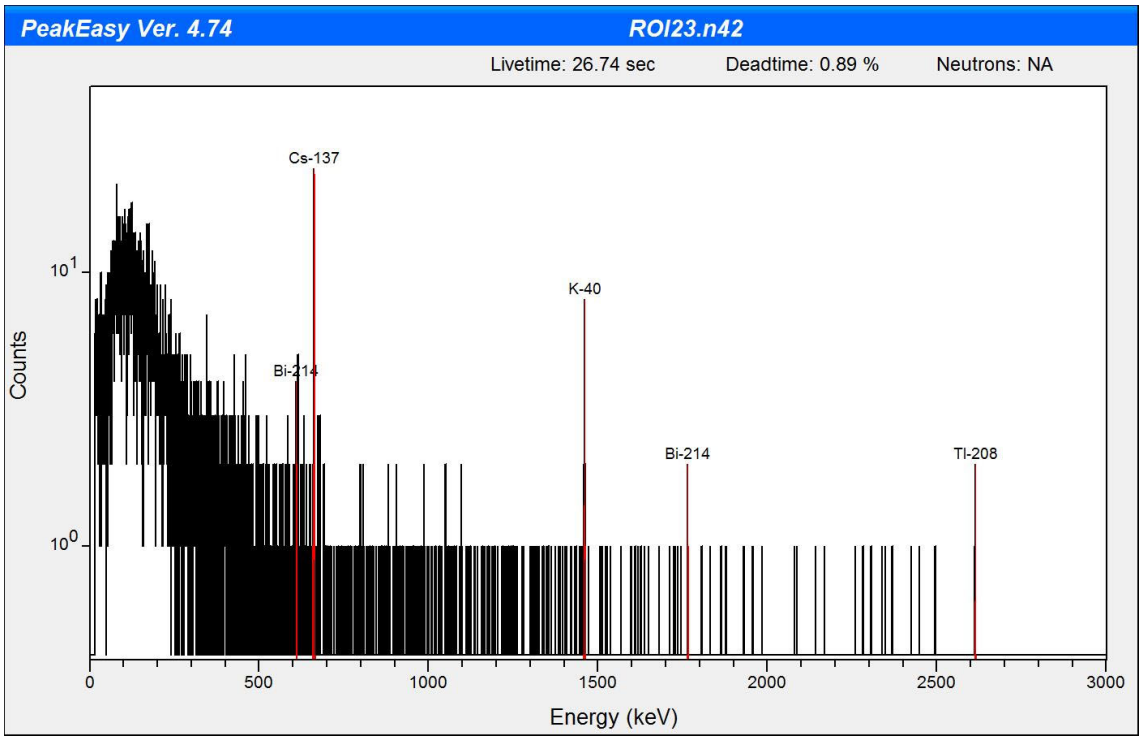

Figure 29. HPGe spectrum from ROI 23. The 662 keV Cs-137 peak is clearly evident. Other identified peaks are NORM background.

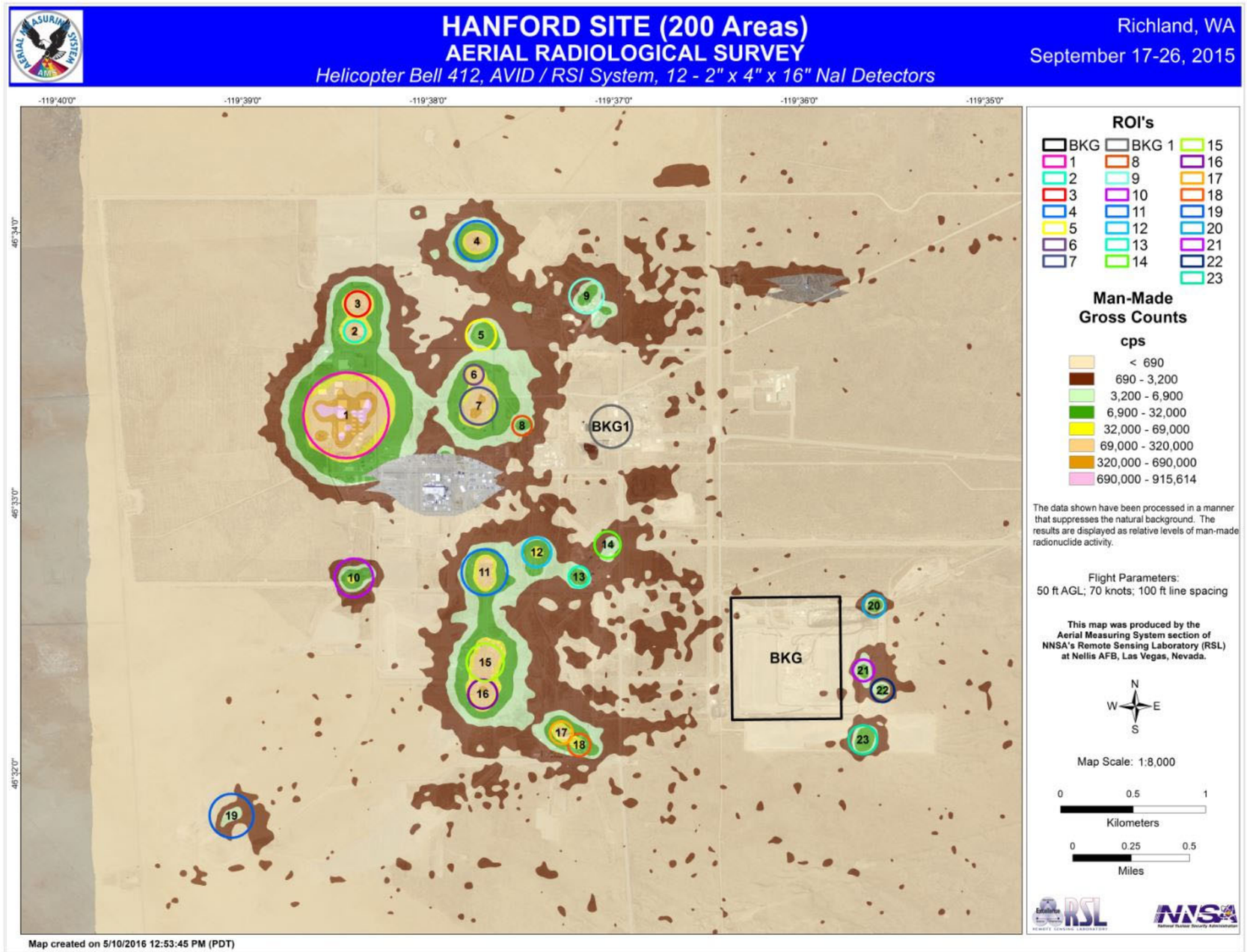

Figure 30. Major regions of interest in the 200 West Area.

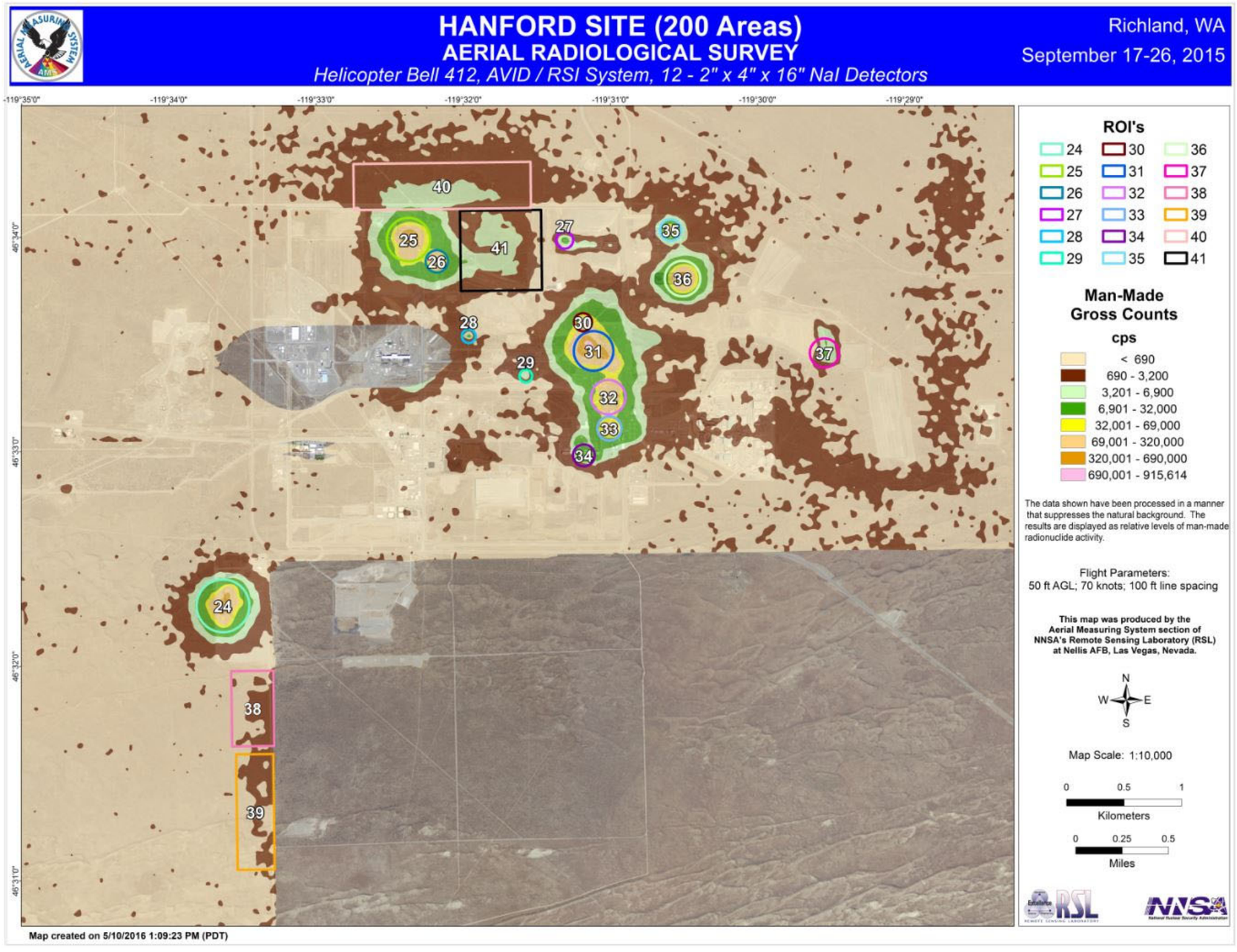

Figure 31. Major regions of interest in the 200 East Area.

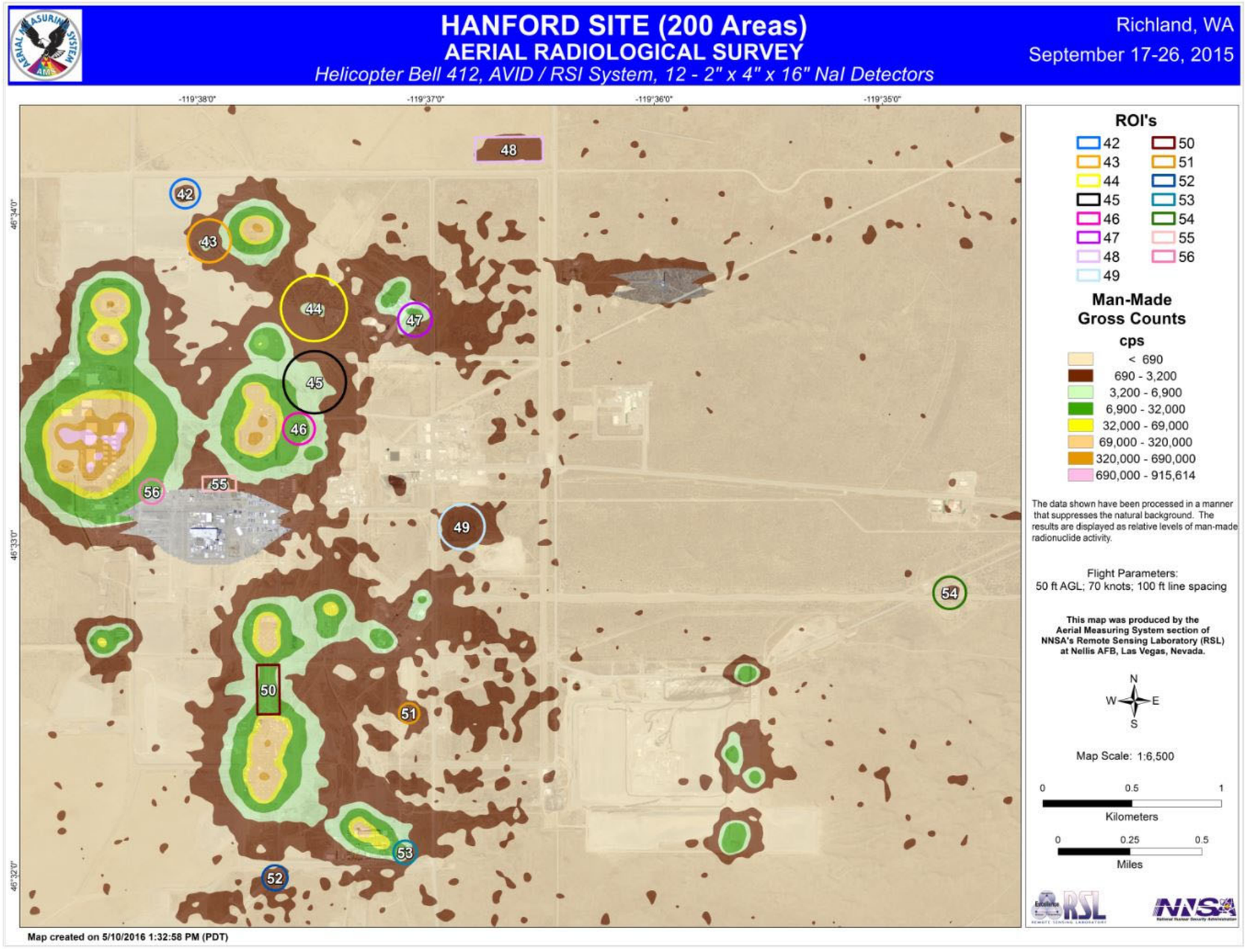

Figure 32. Minor regions of interest in the 200 West Area.

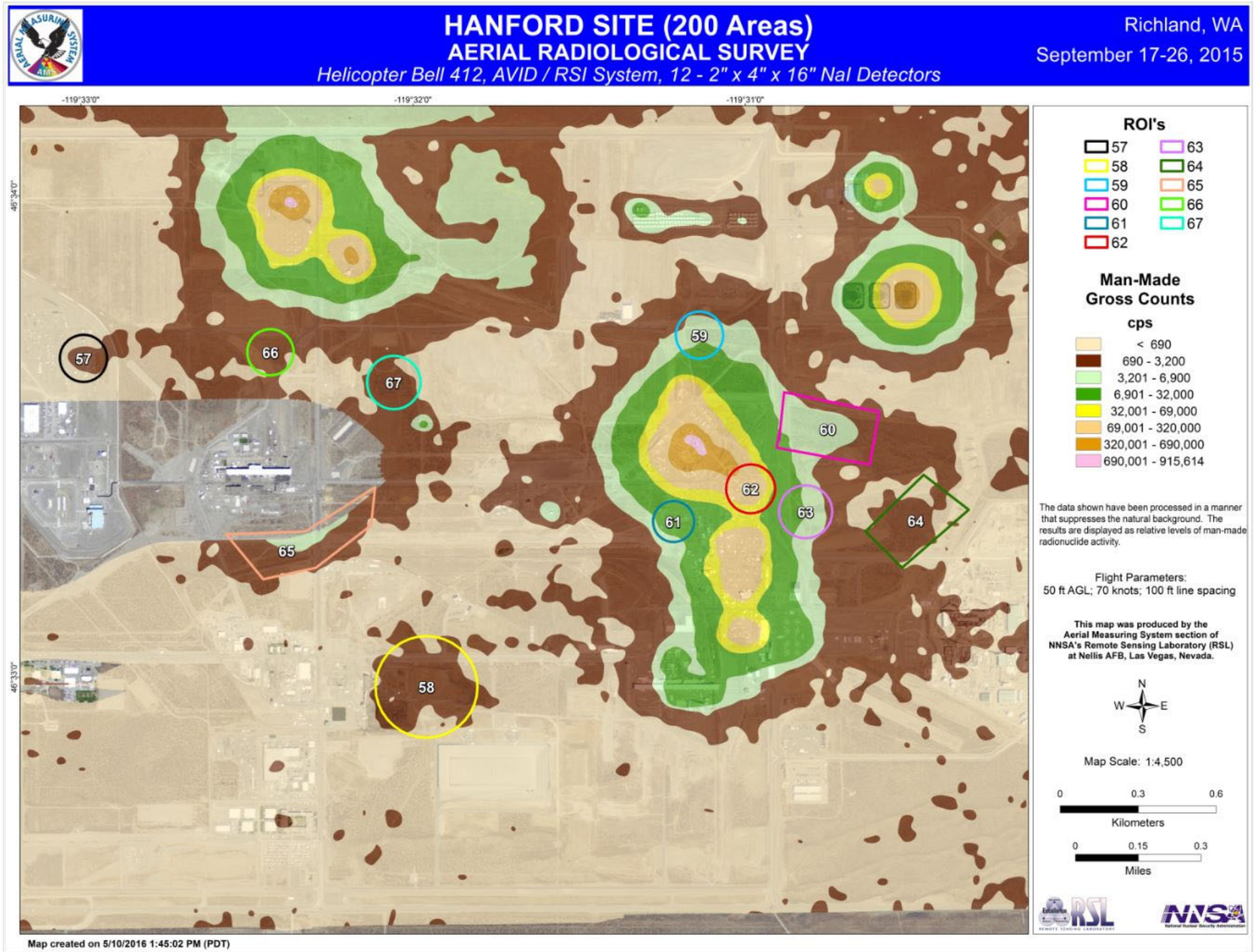

Figure 33. Minor regions of interest in the 200 East Area.

8. Ground Measurements

Ground measurements using a pressurized ionization chamber (PIC) and HPGe detector were made at several locations on the site. The PIC was a GE Reuter-Stokes model RS-131 and was positioned 1 m above ground level on a tripod. The HPGe was an Ortec mechanically-cooled HPGe, also positioned 1 m above ground level on a tripod.

8.1. PIC Ground Measurements

Ground measurements are summarized in Table 3. Measurements were taken for approximately 30 minutes at each site, and no corrections have been made for non-terrestrial contributions to the measured exposure rates. At one site (WS01) no PIC data was recorded due to equipment malfunction. The PIC data is compared to aerial data by finding the aerial data point closest in distance to a given PIC measurement location. Two PIC locations (ES11 and WS06) had no aerial data because they were located within no fly zones.

Table 3. Ground measurements taken on the Hanford site.

ID	Longitude	Latitude	PIC Exposure Rate [μR/h]	Nearest Aerial Point Data [μR/h]
ES01	-119.54292	46.54218	8.2 ± 0.3	4.5
ES02	-119.53817	46.56872	11.8 ± 0.3	6.6
ES03	-119.52194	46.56850	10.5 ± 0.2	4.3
ES04	-119.49651	46.56069	9.5 ± 0.3	4.2
ES05	-119.48869	46.55542	10.6 ± 0.3	4.2
ES06	-119.51548	46.56815	10.1 ± 0.2	4.0
ES07	-119.53908	46.56359	11.4 ± 0.3	8.5
ES08	-119.54371	46.56594	12.4 ± 0.3	6.6
ES09	-119.57938	46.54713	10.1 ± 0.2	4.8
ES10	-119.59530	46.56971	10.7 ± 0.3	4.9
ES11	-119.53923	46.53967	9.8 ± 0.4	No Fly Zone
ES12	-119.54525	46.56200	10.2 ± 0.3	4.8
ES13	-119.54232	46.56280	10.1 ± 0.2	5.1
ES14	-119.53308	46.55862	11.8 ± 0.3	6.5
ES15	-119.52535	46.55521	11.1 ± 0.3	5.7
ES16	-119.51964	46.55424	11.2 ± 0.3	7.0
ES17	-119.54893	46.56614	10.4 ± 0.3	4.9
ES18	-119.52309	46.56842	9.7 ± 0.2	4.6
WS01	-119.61857	46.53415	No Data	4.8
WS02	-119.63352	46.56266	9.4 ± 0.3	4.3
WS03	-119.63393	46.56712	9.4 ± 0.2	3.8
WS04	-119.63754	46.55705	17.2 ± 0.2	26.3
WS05	-119.63573	46.55424	11.4 ± 0.3	8.6
WS06	-119.63543	46.55188	9.9 ± 0.3	No Fly Zone

ID	Longitude	Latitude	PIC Exposure Rate [µR/h]	Nearest Aerial Point Data [µR/h]
WS07	-119.63863	46.56010	11.6 ± 0.1	9.8
WS08	-119.63862	46.56197	12.2 ± 0.1	12.9
WS09	-119.63714	46.53238	9.8 ± 0.3	4.1
WS10	-119.64979	46.52976	11 ± 0.3	5.2
WS11	-119.63732	46.54454	10.2 ± 0.3	4.4
WS12	-119.62826	46.55831	10.7 ± 0.3	6.7

Figure 34 shows the exposure rate data of Table 3 plotted as a function of ground measurement ID. Excluding data from IDs WS04, WS05, WS07, and WS08, the average difference is approximately 5 µR/h, about what would be expected from cosmic and radon contributions. The excluded locations are close to areas of high activity on the site, and show a smaller difference, or even a higher exposure rate than the ground data, due to the larger field of view of the airborne detectors.

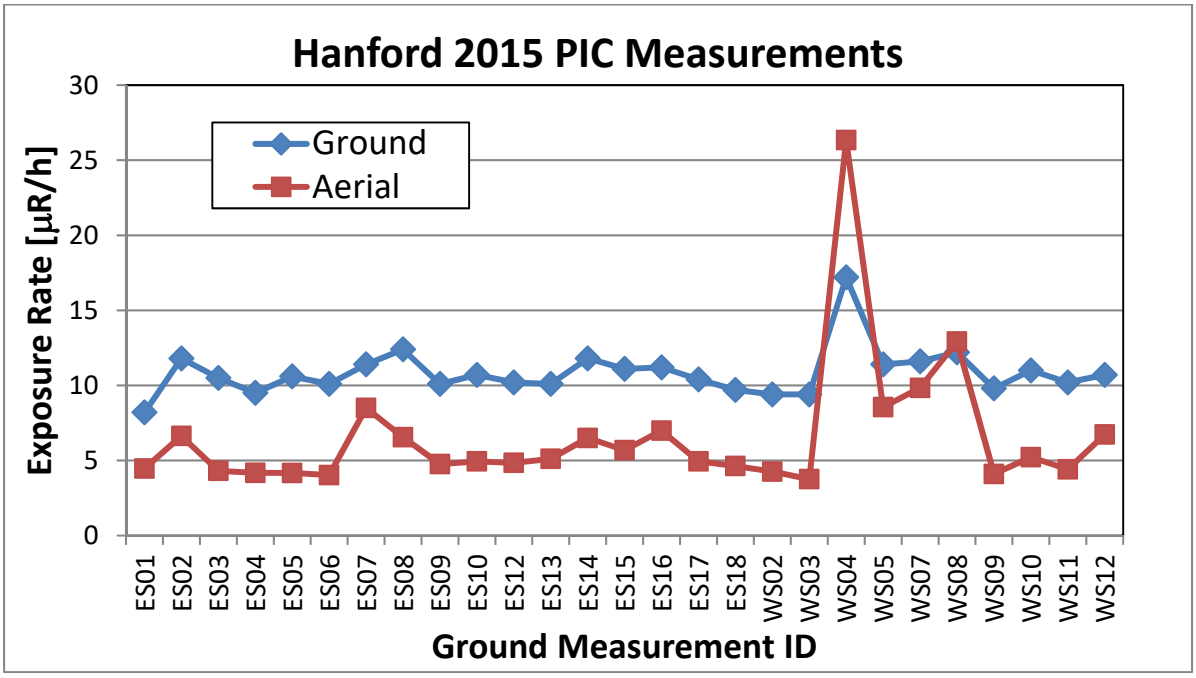

Figure 34. Ground-level PIC exposure rate measurements plotted with corresponding aerial measurements.

8.2. HPGe Ground Measurements

Spectra were collected with the HPGe detector at the same locations as the PIC measurements. To obtain adequate statistics, spectra were collected at each location for about 20 minutes. The spectra were examined for the existence of peaks from Am-241 (59.5 keV), Cs-137 (661.7 keV), and Co-60 (1173.2 and 1332.5 keV) peaks. If these peaks were found, they were fit with a Gaussian function and the numbers of counts in the peaks recorded and used to calculate the activity density in the soil beneath

the detector. The calculation requires an assumption about the isotopic distribution, either uniform or exponential.

Tables 4 through 7 show soil concentrations of these elements derived from the HPGe measurements. Location IDs that are not listed did not have measureable amounts of the isotopes.

Table 4. Soil concentrations of Am-241 extracted from HPGe in situ measurements taken 1 m off the ground.

HPGe Am-241				
ID	**Longitude**	**Latitude**	**Uniform Distribution [pCi/g]**	**Exponential Distribution [pCi/g]**
ES09	-119.57938	46.54713	2.19 ± 0.82	2.95 ± 1.10
WS06	-119.63543	46.55188	2.06 ± 0.72	2.78 ± 0.97
WS10	-119.64979	46.52976	1.34 ± 0.95	1.81 ± 1.29

Table 5. Soil concentrations of Cs-137 extracted from HPGe in situ measurements taken 1 m off the ground.

HPGe Cs-137				
ID	**Longitude**	**Latitude**	**Uniform Distribution [pCi/g]**	**Exponential Distribution [pCi/g]**
ES01	-119.54292	46.54218	0.30 ± 0.03	0.56 ± 0.06
ES02	-119.53817	46.56872	2.78 ± 0.07	5.24 ± 0.13
ES03	-119.52194	46.56850	0.46 ± 0.03	0.86 ± 0.06
ES04	-119.49651	46.56069	0.08 ± 0.02	0.16 ± 0.04
ES05	-119.48869	46.55542	0.33 ± 0.03	0.62 ± 0.06
ES06	-119.51548	46.56815	0.17 ± 0.03	0.32 ± 0.05
ES07	-119.53908	46.56359	2.12 ± 0.06	4.01 ± 0.12
ES08	-119.54371	46.56594	1.38 ± 0.05	2.61 ± 0.10
ES09	-119.57938	46.54713	0.16 ± 0.03	0.30 ± 0.05
ES10	-119.59530	46.56971	0.32 ± 0.03	0.61 ± 0.06
ES11	-119.53923	46.53967	0.15 ± 0.03	0.28 ± 0.05
ES12	-119.54525	46.56200	2.59 ± 0.07	4.89 ± 0.13
ES13	-119.54232	46.56280	0.12 ± 0.02	0.23 ± 0.04
ES14	-119.53308	46.55862	0.54 ± 0.04	1.03 ± 0.07
ES15	-119.52535	46.55521	0.38 ± 0.03	0.73 ± 0.06
ES16	-119.51964	46.55424	0.07 ± 0.02	0.13 ± 0.04
ES17	-119.54893	46.56614	0.23 ± 0.03	0.44 ± 0.05

HPGe Cs-137				
ES18	-119.52309	46.56842	0.24 ± 0.03	0.45 ± 0.05
WS03	-119.63393	46.56712	0.26 ± 0.03	0.48 ± 0.05
WS04	-119.63754	46.55705	1.35 ± 0.05	2.55 ± 0.10
WS05	-119.63573	46.55424	0.22 ± 0.03	0.41 ± 0.05
WS06	-119.63543	46.55188	0.28 ± 0.03	0.53 ± 0.05
WS07	-119.63863	46.56010	0.09 ± 0.02	0.18 ± 0.04
WS09	-119.63714	46.53238	0.14 ± 0.02	0.26 ± 0.05
WS10	-119.64979	46.52976	1.18 ± 0.05	2.24 ± 0.09
WS11	-119.63732	46.54454	0.03 ± 0.02	0.05 ± 0.03
WS12	-119.62826	46.55831	0.59 ± 0.04	1.11 ± 0.07

Table 6. Soil concentrations of Co-60 (using the 1173 keV peak) extracted from HPGe in situ measurements taken 1 m off the ground.

Co-60 HPGe 1173 keV Peak				
ID	**Longitude**	**Latitude**	**Uniform Distribution [pCi/g]**	**Exponential Distribution [pCi/g]**
ES11	-119.53923	46.53967	0.02 ± 0.01	0.05 ± 0.02
WS04	-119.63754	46.55705	0.04 ± 0.02	0.09 ± 0.03

Table 7. Soil concentrations of Co-60 (using the 1332 keV peak) extracted from HPGe in situ measurements taken 1 m off the ground.

Co-60 HPGe 1332 keV Peak				
ID	**Longitude**	**Latitude**	**Uniform Distribution [pCi/g]**	**Exponential Distribution [pCi/g]**
ES12	-119.54525	46.56200	0.01 ± 0.01	0.03 ± 0.03
WS04	-119.63754	46.55705	0.03 ± 0.01	0.07 ± 0.03
WS10	-119.64979	46.52976	0.02 ± 0.01	0.04 ± 0.02

9. Distributed Source Localization

The NaI detectors aboard the aircraft are uncollimated. This is an intentional configuration to maximize the sensitivity of the detector array. However, if the aircraft is flying over an area with a steep radiation gradient, the detector's ability to isolate the area directly under the aircraft can be compromised by that gradient; that is, the detector will see a larger (or smaller) exposure rate than actually exists under the aircraft. This effectively reduces the spatial resolution of the data. To compensate for this effect, the HPGe data can be utilized.

In general, while flying over only NORM or very low level anthropomorphic isotopes, a one-second spectrum from the HPGe detector will not contain usable spectral data. However, over several areas of the site exposure rates are high enough that individual HPGe spectra do yield usable information. Because the HPGe is mounted in the helicopter such that the most active face of the detector is pointed downward, its detection footprint is smaller than the NaI, which contributes to an effectively higher spatial resolution for the HPGe data. More importantly, the higher energy resolution of the HPGe allows for more accurate isolation of individual isotopes when performing spectral extractions.

Another effect that downgrades analysis of individual isotopes is interference from non-target isotopes. For example, a large Cs-137 concentration causes downscatter in a spectrum which degrades or even completely overwhelms any Am-241 signal. By choosing an appropriate area to calculate K_2 [as in Equation (6)] or K_3 [as in Equation (8)] and doing a two- or three-window extraction for Am-241 interference from Cs-137 downscatter can be accounted for. The result is a higher-resolution mapping of Am-241.

Figure 35 shows a comparative study using data collected over ROI 1. The top row shows gross count rate, Cs-137 extraction, and Am-241 extractions using the NaI data. The bottom row shows the same plots but using the HPGe data. The difference is most evident in the far right plots showing the Am-241 extractions. It is also important to realize that several raw data points are missing from the NaI data, a fact which is not evident in the top row since the contouring algorithm can fill in blank spots. Missing data is not a problem in the HPGe data, although results from individual points may be affected by large dead times.

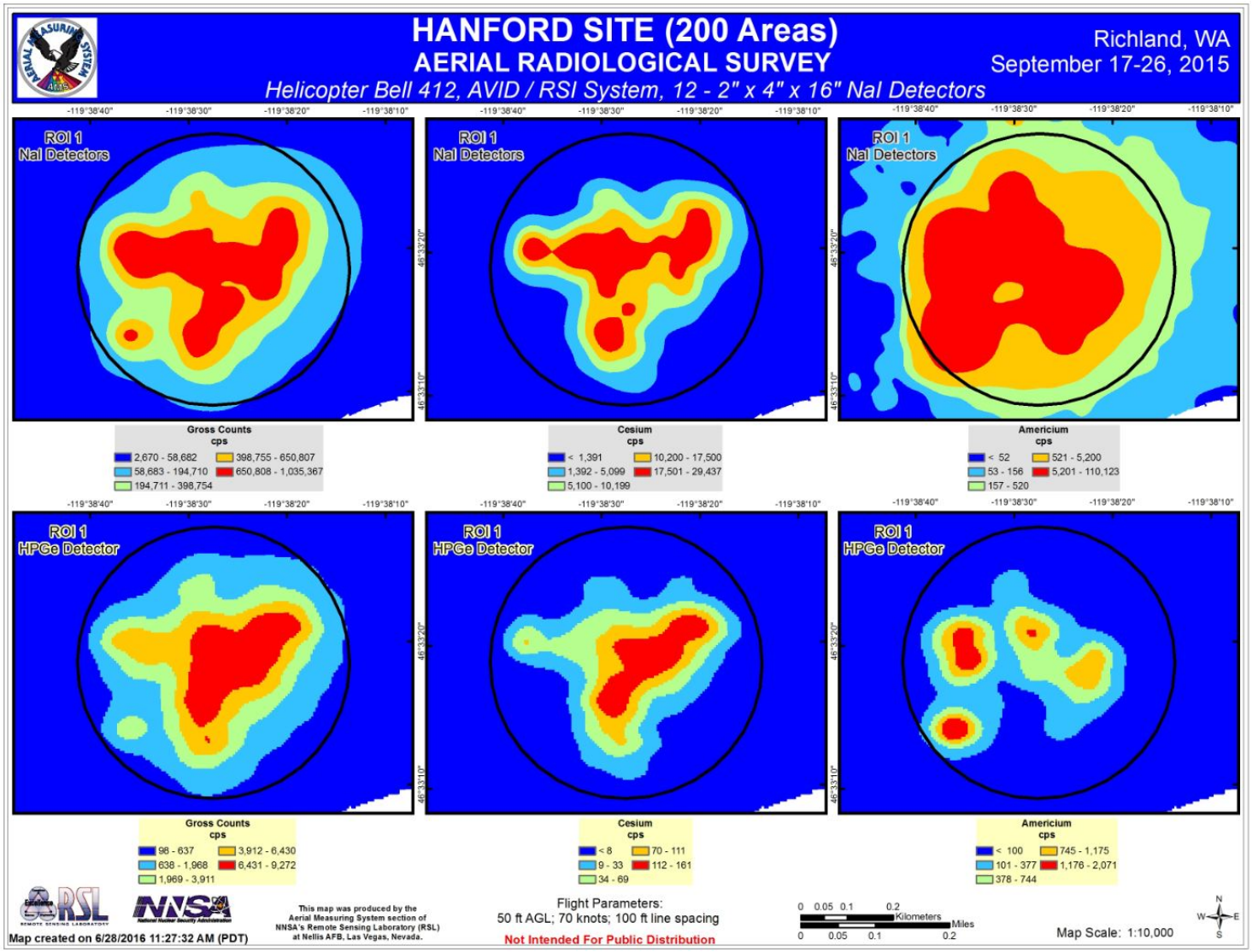

Figure 35. Comparative study of isotopic extractions in ROI 1 using the NaI data (top row) and HPGe data (bottom row).

10. Comparison With Previous Surveys

10.1. 1996 Survey

The current survey has been compared to the 1996 survey (Colton D. P., 1996) to locate areas which have change radiologically. The first and simplest comparison was to do a direct subtraction of the 1996 exposure rate map from the current exposure rate map. The result gives a general idea of areas that have significantly changed. Figure 36 is the 2015 – 1996 difference map, and shows several areas of change. In this map, blue indicates a negative difference (i.e., areas that have lower exposure rate values in 2015 than in 1996) and red indicates a positive difference (i.e., areas that have a higher exposure rate in 2015 than in 1996).

A more detailed comparison can be made by correlating 2015 ROIs with 1996 ROIs. For example, 2015 ROI 1 (Figure 30) corresponds to 1996 ROI 31 (Figure 39). The spectrum from the 1996 ROI 31 identifies Cs-137 and possible Co-60 (Figure 40). The spectrum from the 2015 ROI1 identifies Cs-137 and Am-241 (Appendix A). In the 2015 survey, two ROIs were identified north of ROI 1 (ROI 2 and ROI 3), both of which show Cs-137 and Co-60 in their spectra. These ROIs are absent in the 1996 survey. However, the 1996 survey shows an ROI north of the 1996 ROI 31 (1996 ROI 27) which is absent in the 2015 survey, and shows Cs-137 and Co-60 (Figure 41). Similar comparisons can be made over the entire survey area.

10.2. 2009 Survey

The present survey was designed to have an area of overlap with the 2009 survey (Lyons, 2009).The overlap area covers the US Ecology site, and was designed to have the eastern edge of the US Ecology site as its eastern boundary. Turns made by the helicopter immediately to the east of the overlap area were over areas identified as Zones A and B in the 2009 survey. These areas had relatively high concentrations of Cs-137 contamination, much of it attributed to the biological activity of wildlife. Some comparison can be made over these areas, but because the helicopter was turning (and changing altitude and attitude) these comparisons are qualitative at best.

A comparison between the 2009 survey and the planned 2015 survey area is shown in Figure 37. In the figure, contours are color-coded by exposure rate. The highest exposure rate is over the US Ecology facility in both surveys. The spatial extent of the high exposure rate area is larger in 2015, but this may be a function of activities occurring at the facility on the days of the surveys.

Figure 38 shows the comparison between the 2009 and 2015 surveys over Zones A and B, known as the ‘coyote dens’. In the figure, the Cs-137 activity from the 2009 survey is shown as colored contours. Superimposed over the contours are data from the 2015 survey, shown as breadcrumbs. The contours and breadcrumbs have been colorized to the same scale. A region of relatively high Cs-137 activity is seen in the 2009 data. The 2015 data maps onto the 2009 data, starting from background levels and increasing at the boundary of the high Cs-137 region. However, in the interior of this region, the 2015 levels drop and become consistent with background levels.

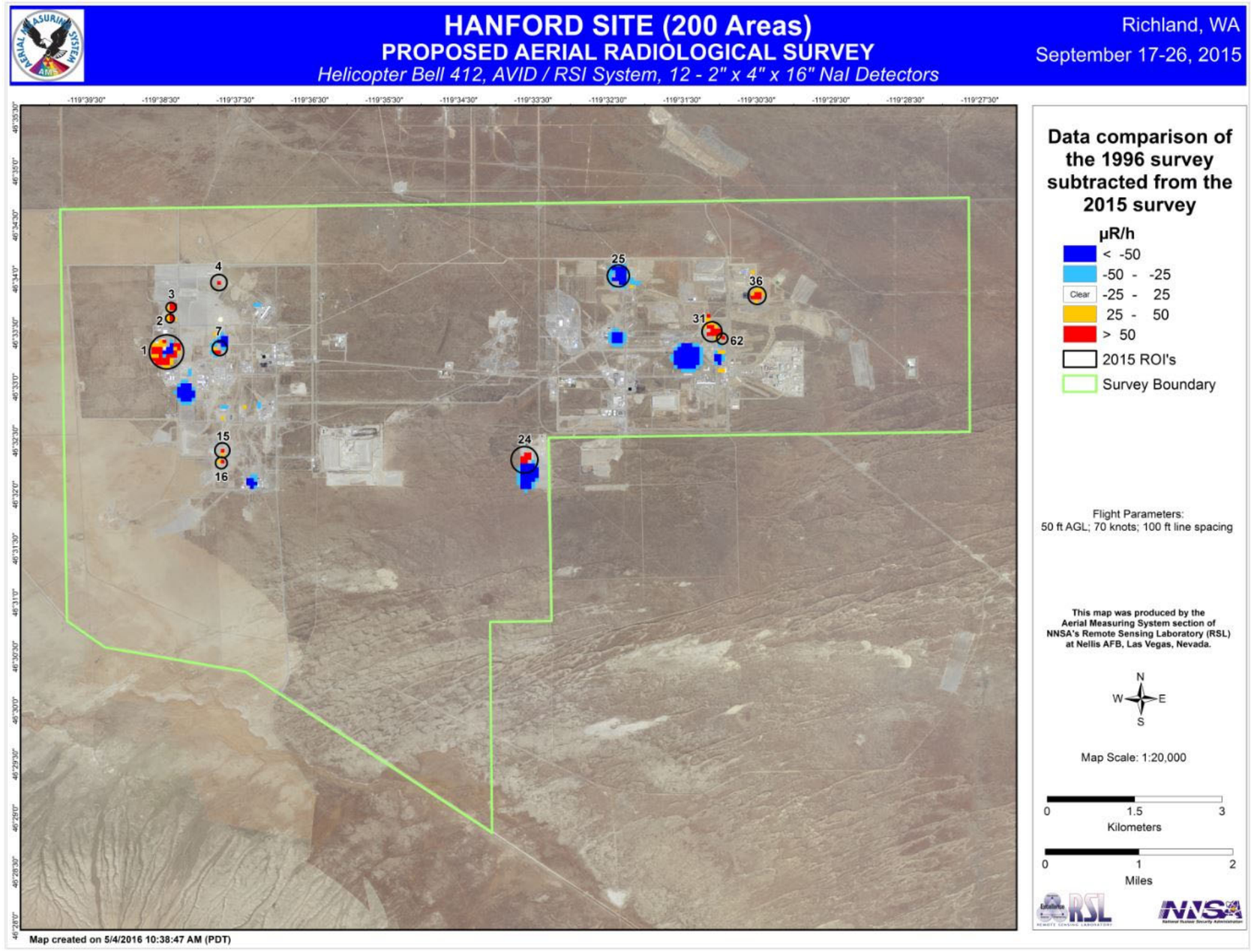

Figure 36. Comparison of data from the 2015 survey with data from the 1996 survey. Areas where exposure rates have decreased are in blue, and area which have increased are in yellow or red.

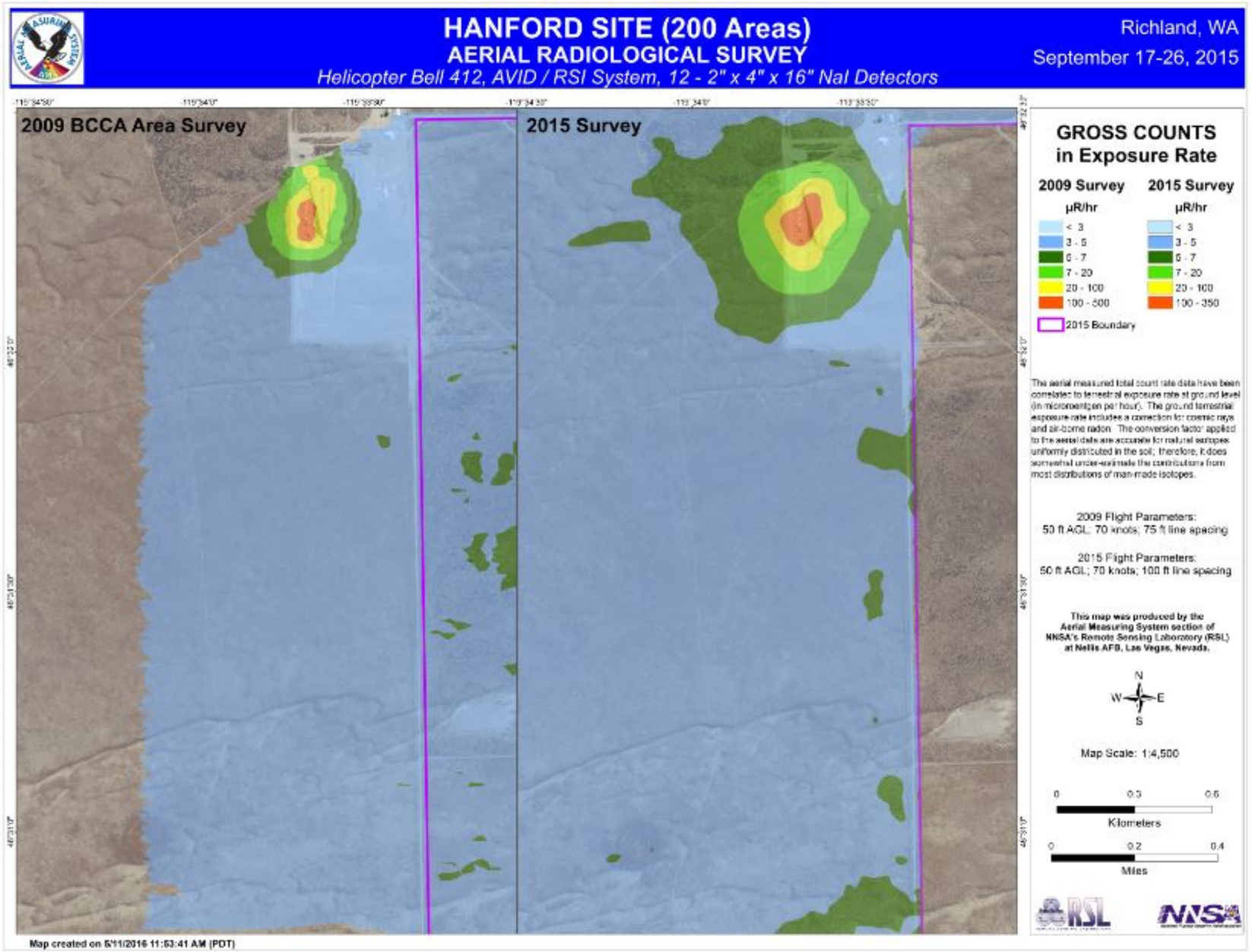

Figure 37. Comparison of the overlap area from the 2009 and 2015 surveys. Contours are color-coded by exposure rate. The highest exposure rate is over the US Ecology facility in both surveys. The spatial extent of the high exposure rate area is larger in 2015, but this may be a function of activities occurring at the facility on the days of the surveys.

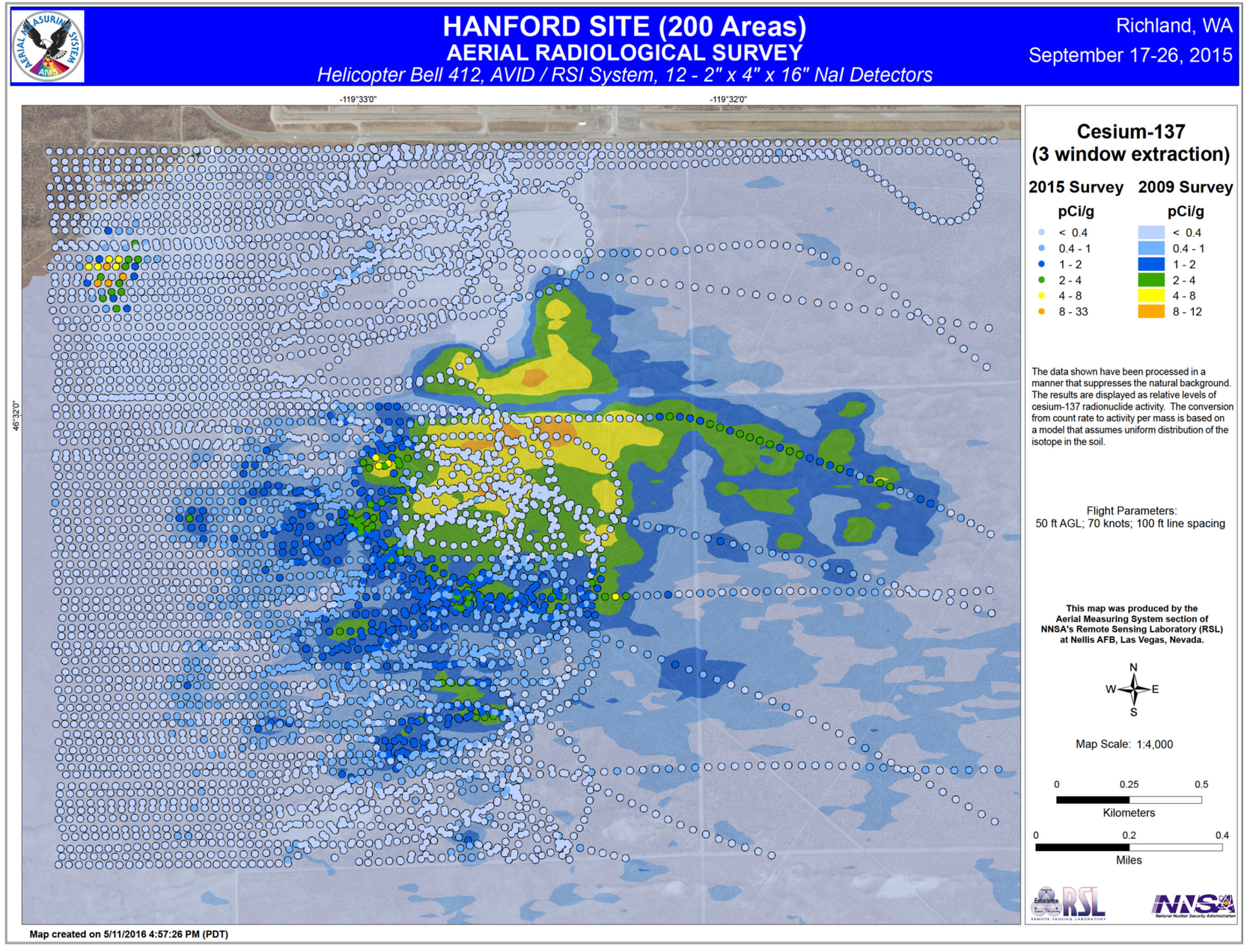

Figure 38. Comparison between the 2009 survey and 2015 survey over the 'coyote dens'. This was not a planned area for the 2015 survey, and data shown are from helicopter turns. Even allowing for the greater uncertainty in the result, a decrease in Cs-137 activity is noticeable in the 2015 survey.

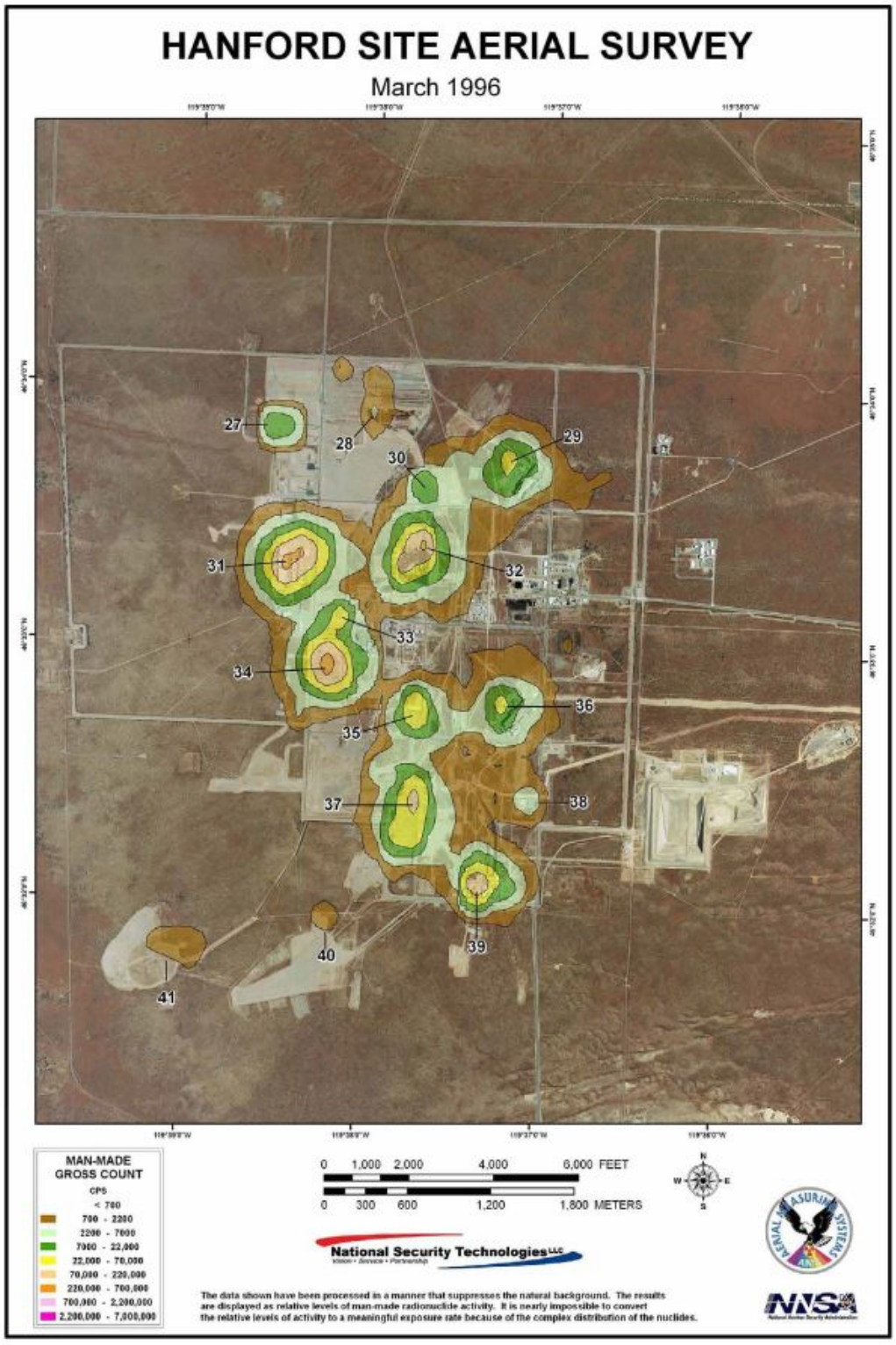

Figure 39. Anthropogenic count rates in the 200 West area from the 1996 survey.

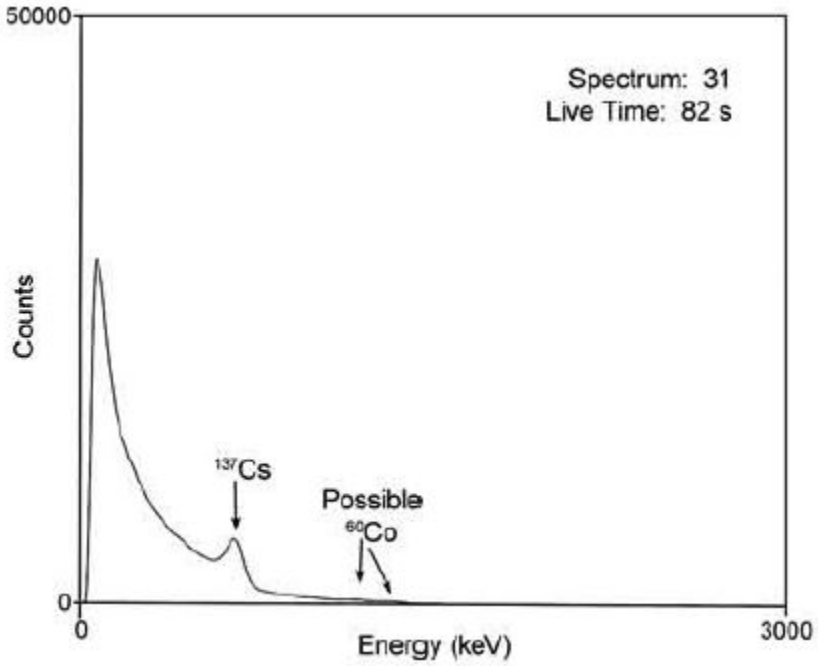

Figure 40. Spectrum 31 from the 1996 Hanford survey report.

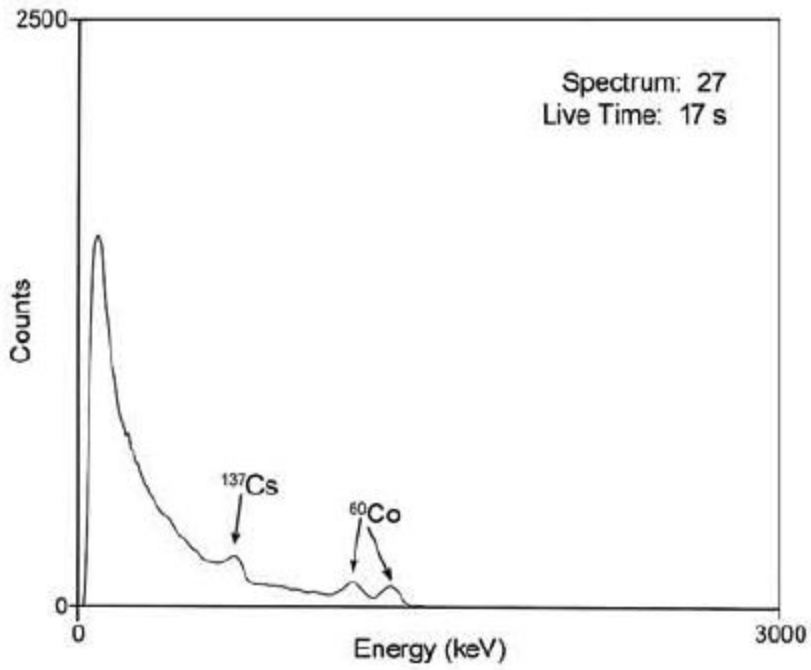

Figure 41. Spectrum 27 from the 1996 Hanford survey report.

11. References

Colton, D. P. (1996). An Aerial Radiological Survey of the Hanford Reservation. *No DOE Number*. Las Vegas, NV: National Security Technologies, LLC.

Colton, D. P., & Hendricks, T. J. (1999). *Radiological Characterization of the Lake Mohave Test Line.* DOE/NV/11718--024: Remote Sensing Laboratory.

Hendricks, T. J. (1983). Radiation and Environmental Data Analysis Computer (REDAC) Hardware, Software, and Analysis Procedures. In *Remote Sensing Technology, Proceedings of a Symposium on Remote Sensing Technology in Support of the United States Department of Energy* (Vols. EGG-10282-1057). Las Vegas, NV: EG&G.

Hendricks, T., & Riedhauser, S. (1999). An Aerial Radiological Survey of the Nevada Test Site. *DOE/NV/11718--127*. Las Vegas, NV: Bechtel Nevada.

IAEA. (2003). *Guidelines for Radioelement Mapping Using Gamma Ray Spectrometry Data.* IAEA-TECHDOC-1363: International Atomic Energy Agency.

Knoll, G. F. (2010). *Radiation Detection and Measurement* (4th ed.). John Wiley & Sons, Inc.

Lyons, C. L. (2009). An Aerial Radiological Survey of teh BC Controlled Area and West Lake Area. Las Vegas, NV: National Security Technologies, LLC.

Moon, N. (2007). An Aerial Radiological Survey of the Portsmouth Gaseous Diffusion Plant and Surrounding Area. *DOE/NV/25946-335, December 2007*. Las Vegas, NV: National Security Technologies, LLC.

Proctor, A. E. (1997). *Aerial Radiological Surveys DOE/NV/11718-127.* Washington DC: U. S. Department of Energy.

US Geological Survey. (2104, Oct 23). *Mineral Resources On-Likne Spatial Data.* Retrieved from mrdata.usgs.gov/general/map.html

Appendix A. Survey Parameters

Survey Site:	200 West and 200 East Areas
Survey Coverage:	67 Acres (271,082 m^2)
Survey Date:	September 2015
Survey Altitude:	50 ft (15.24 m)
Aircraft Speed:	70 knots (36 meters per second)
Line Spacing:	100 feet (30.5 meters)
Navigation System:	Trimble DGPS (WAAS corrections) differential
Line Direction:	West - East
Detector Configuration:	Twelve 2" × 4" × 16" NaI(Tl) detectors
	Vgd00 = 12 NaI detectors
	Vgd01 = 3 NaI detectors
	Vgd02 = 3 NaI detectors
	Vgd03 = 3 NaI detectors
	Vgd04 = 3 NaI detectors
Acquisition System:	AVID
Conversion Factors:	0.000331 μR/h per cps
Air Attenuation Coefficient:	0.00174 ft^{-1}
Vehicle:	Bell 412 N411DE
Project Management:	Karen McCall
Project Scientist:	Piotr Wasiolek
Data Scientist	Ashlee Dailey
Data Scientist:	Russell Malchow
Data Analyst:	Jez Stampahar
Electronic Technicians:	Tom Stampahar

Appendix B. Spectra From Regions of Interest

Spectra extracted from identified regions of interest (ROI) are presented in this appendix. Spectra are from the twelve-log NaI detector array carried by the RSL-N Bell 412 helicopter. The spectra were collected at an altitude of 50 ft AGL, and have not been corrected for air attenuation. One-second spectra collected over each region of interest have been summed to produce the spectra in this appendix. The total data collection time (i.e., live time) represented by each of the summed spectra are shown in the upper right-hand corner of the spectra. The locations of full-energy peaks from Am-241, Cs-137, Co-60, K-40, and Tl-208 are indicated all spectra whether or not the peaks are evident. K-40 and Tl-208 are naturally-occurring and present in all spectra.

ROI 1

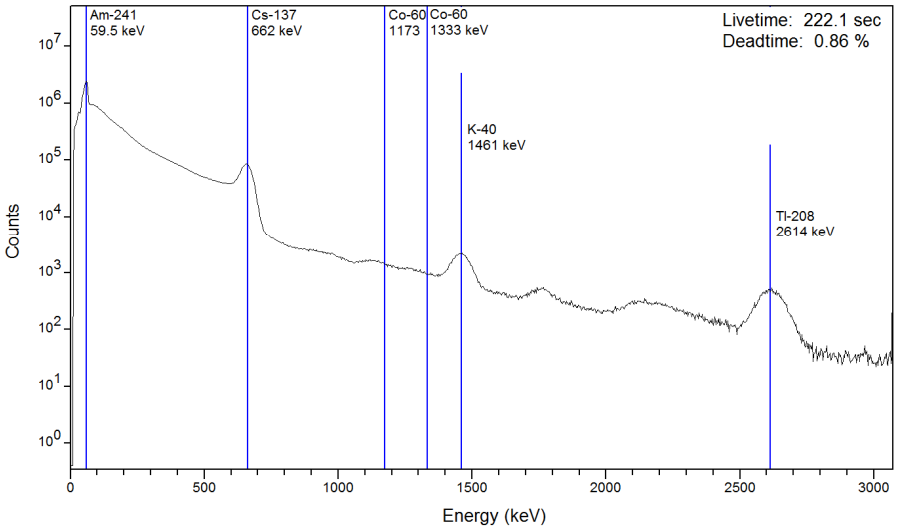

ROI 2

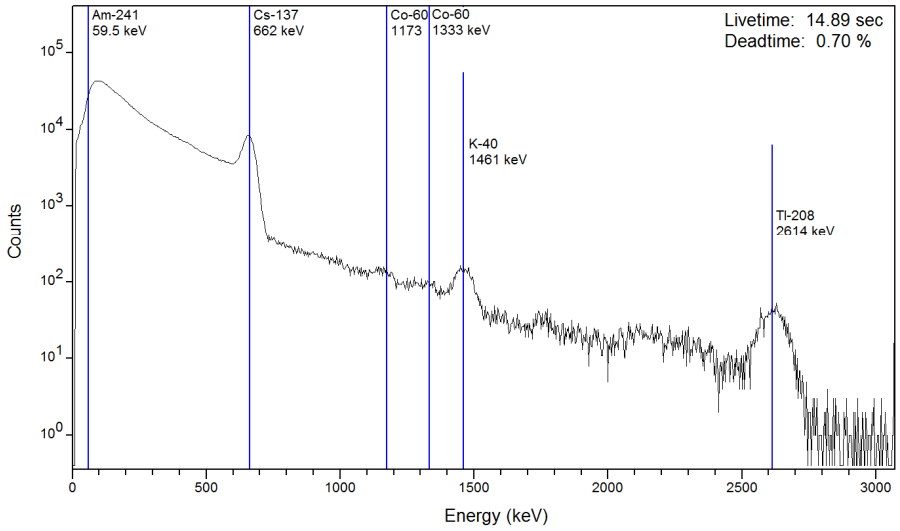

ROI 3

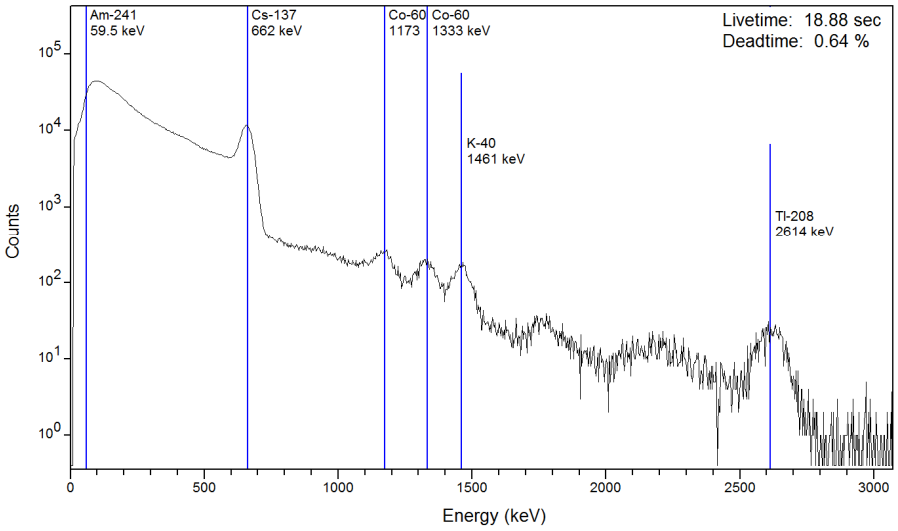

ROI 4

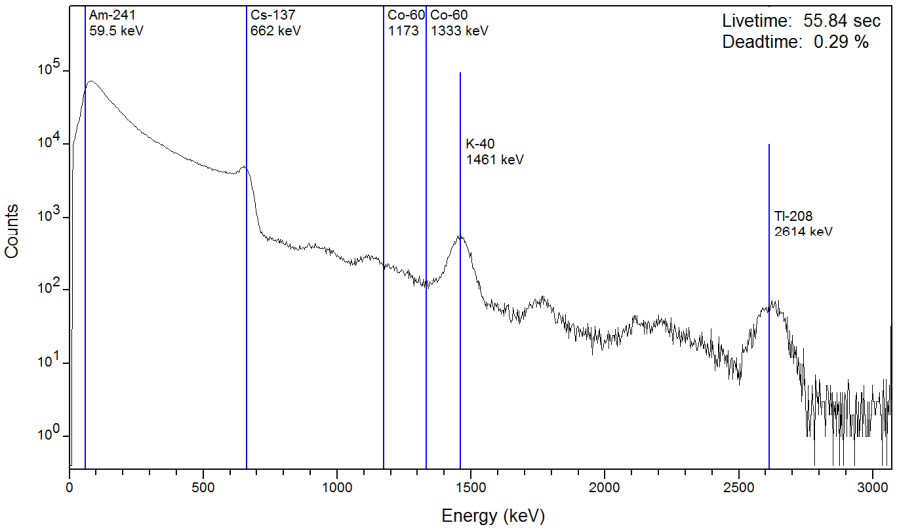

ROI 5

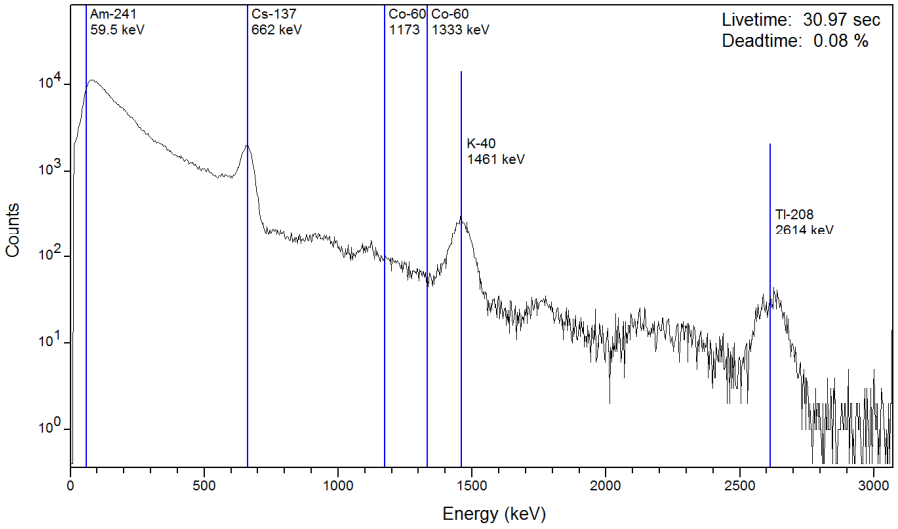

ROI 6

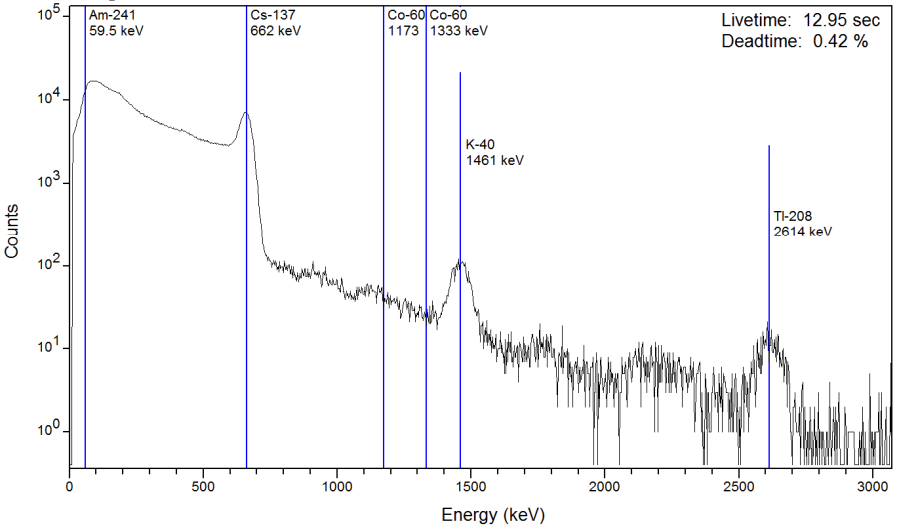

ROI 7

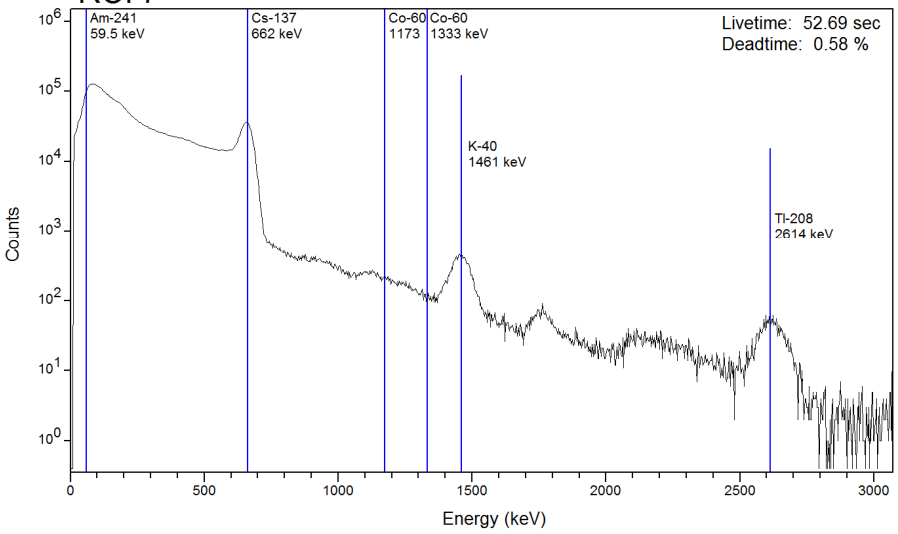

ROI 8

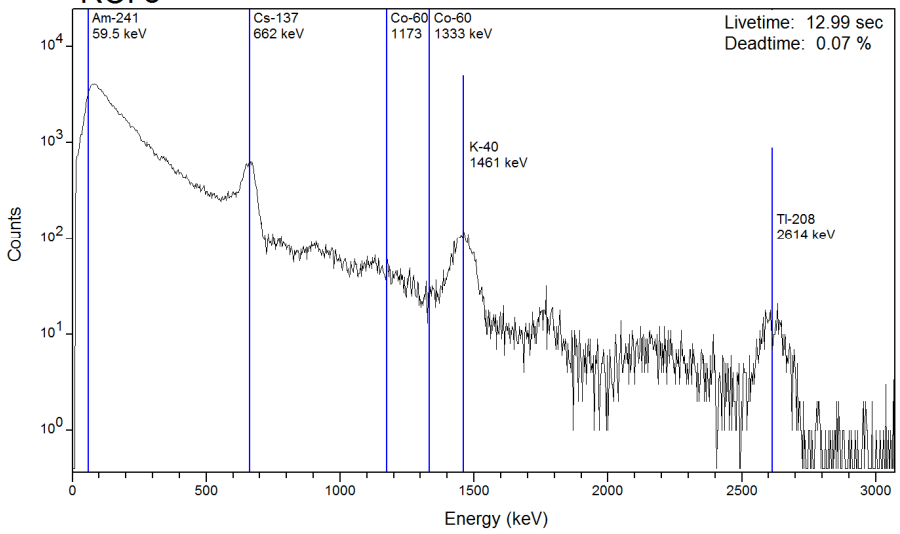

ROI 9

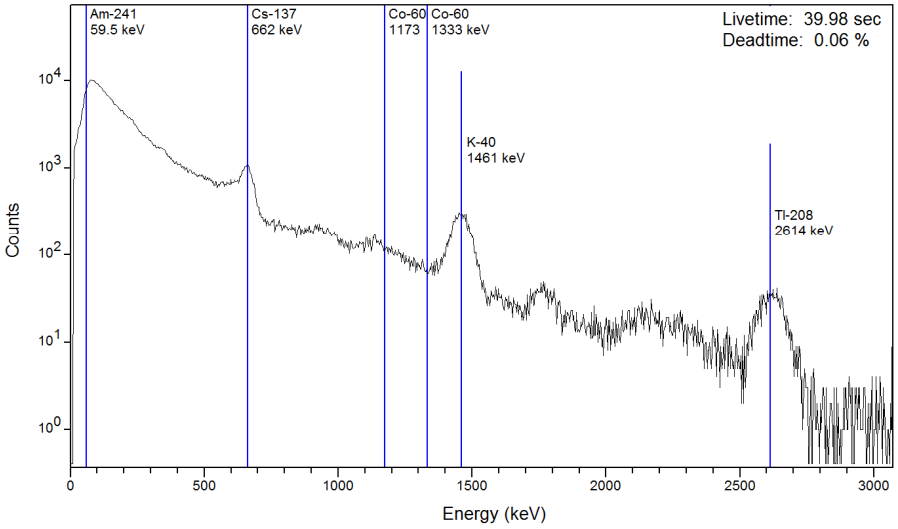

ROI 10

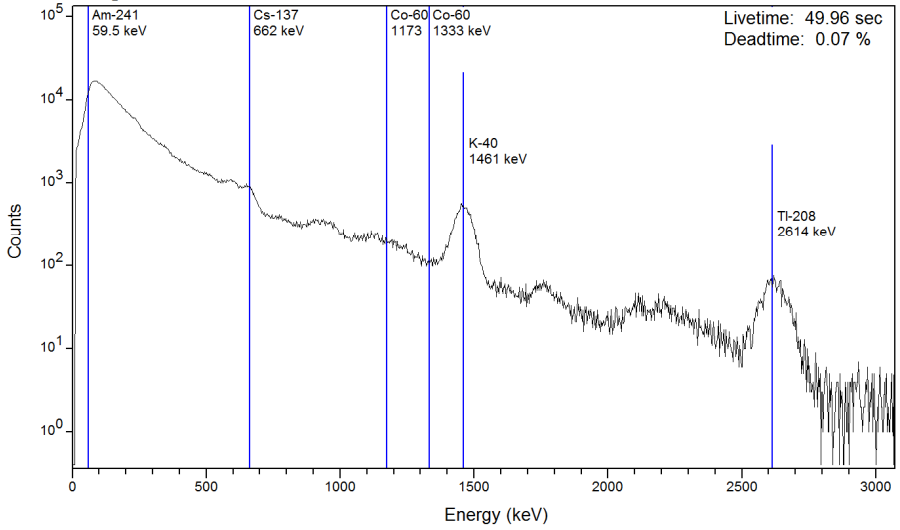

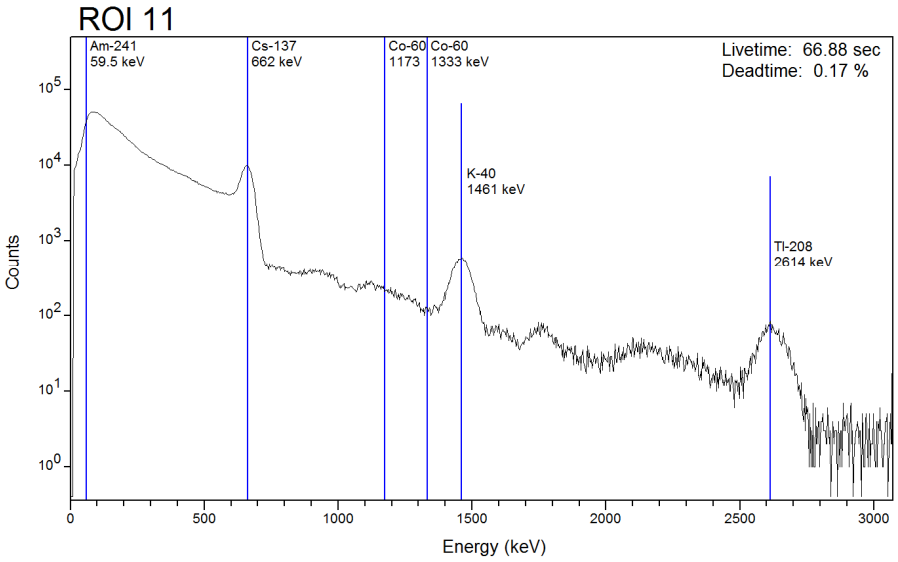
ROI 11
Am-241
59.5 keV
Cs-137
662 keV
Co-60
1173
Co-60
1333 keV
Livetime: 66.88 sec
Deadtime: 0.17 %
K-40
1461 keV
Tl-208
2614 keV
Counts
Energy (keV)

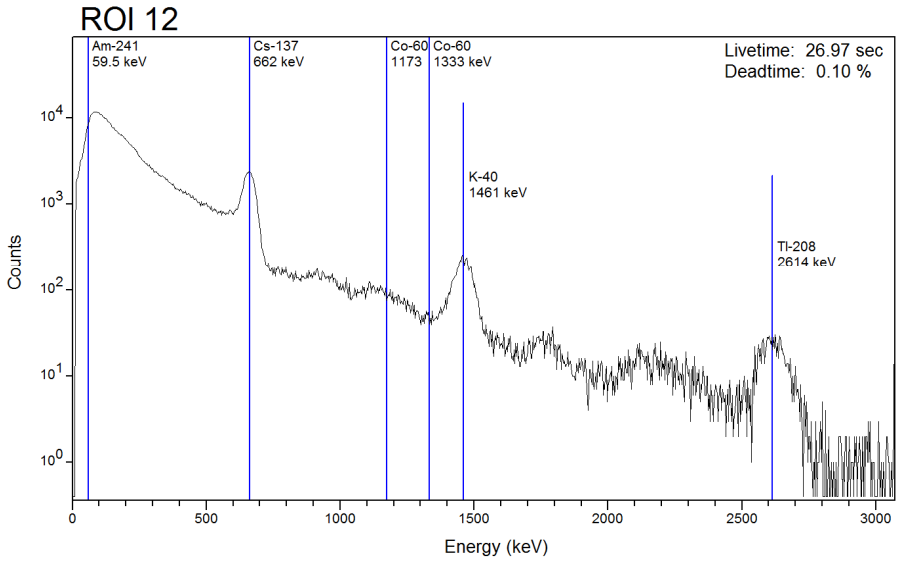
ROI 12
Am-241
59.5 keV
Cs-137
662 keV
Co-60
1173
Co-60
1333 keV
Livetime: 26.97 sec
Deadtime: 0.10 %
K-40
1461 keV
Tl-208
2614 keV
Counts
Energy (keV)

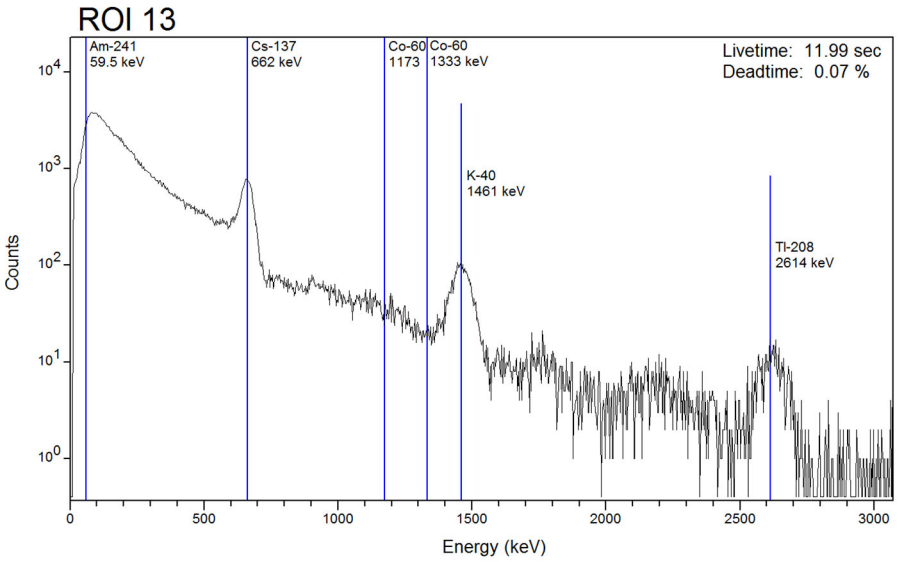
ROI 13
Am-241
59.5 keV
Cs-137
662 keV
Co-60
1173
Co-60
1333 keV
Livetime: 11.99 sec
Deadtime: 0.07 %
K-40
1461 keV
Tl-208
2614 keV
Counts
Energy (keV)

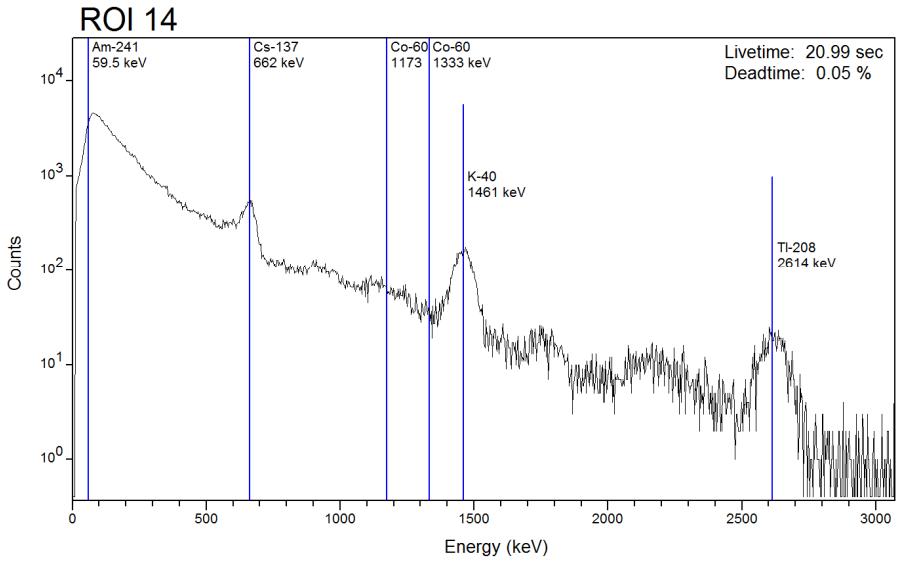
ROI 14
Am-241
59.5 keV
Cs-137
662 keV
Co-60
1173
Co-60
1333 keV
Livetime: 20.99 sec
Deadtime: 0.05 %
K-40
1461 keV
Tl-208
2614 keV
Counts
Energy (keV)

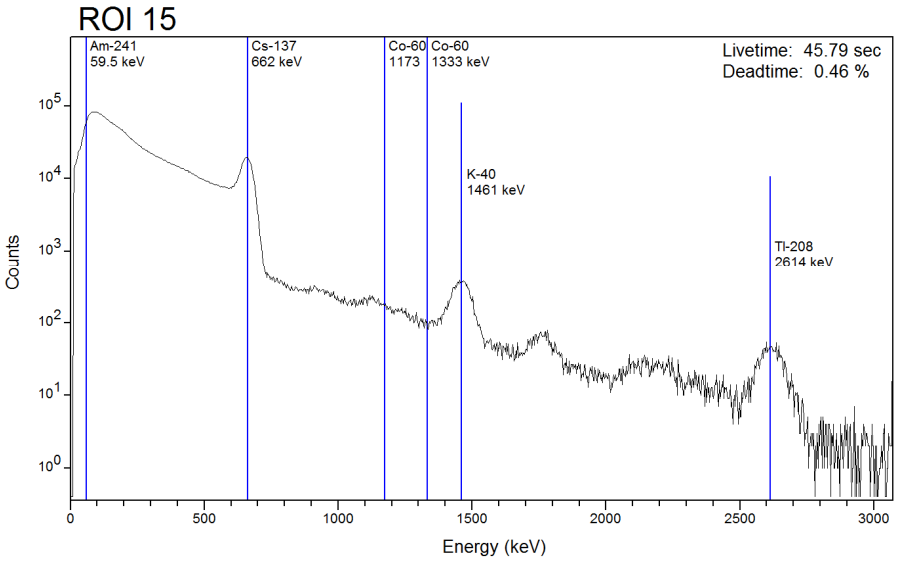
ROI 15
Am-241
59.5 keV
Cs-137
662 keV
Co-60
1173
Co-60
1333 keV
Livetime: 45.79 sec
Deadtime: 0.46 %
K-40
1461 keV
Tl-208
2614 keV
Counts
Energy (keV)

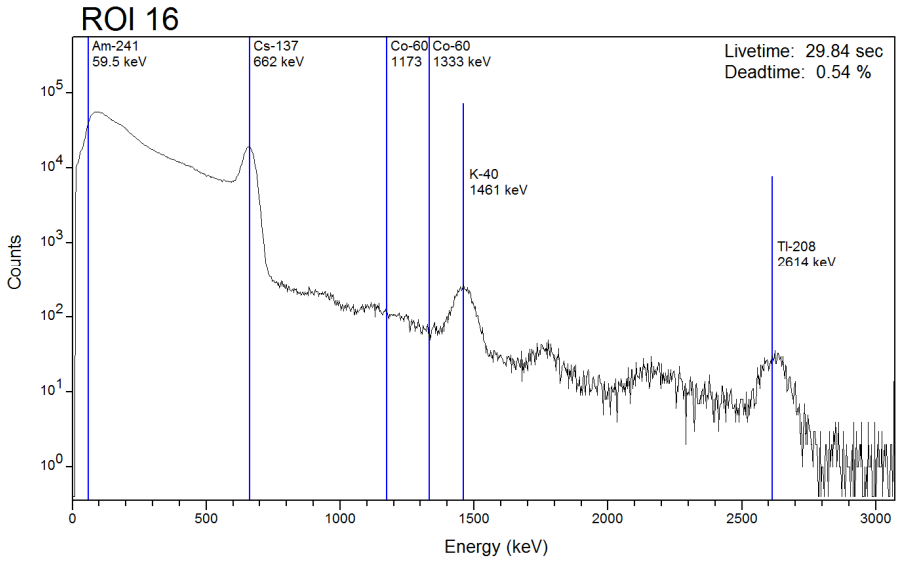
ROI 16
Am-241
59.5 keV
Cs-137
662 keV
Co-60
1173
Co-60
1333 keV
Livetime: 29.84 sec
Deadtime: 0.54 %
K-40
1461 keV
Tl-208
2614 keV
Counts
Energy (keV)

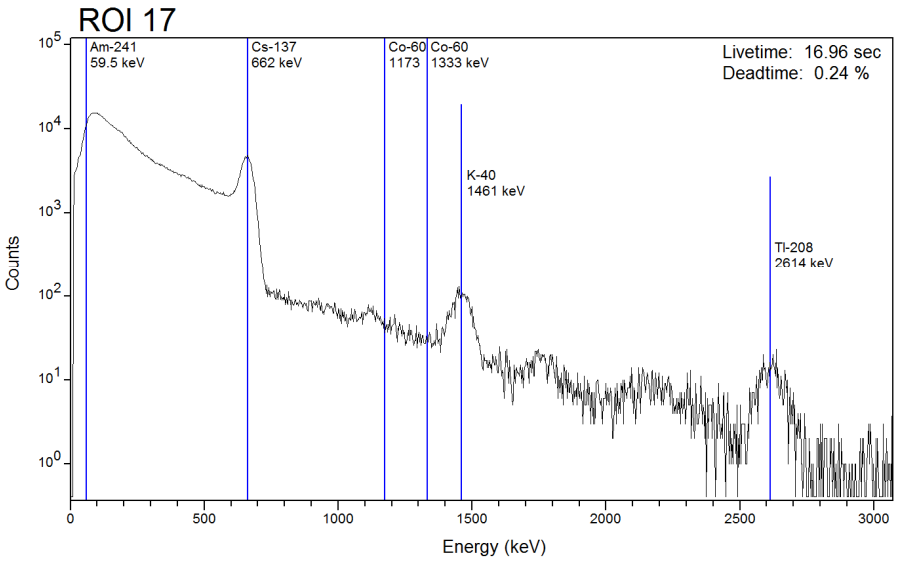
ROI 17
Am-241
59.5 keV
Cs-137
662 keV
Co-60
1173
Co-60
1333 keV
Livetime: 16.96 sec
Deadtime: 0.24 %
K-40
1461 keV
Tl-208
2614 keV
Counts
Energy (keV)

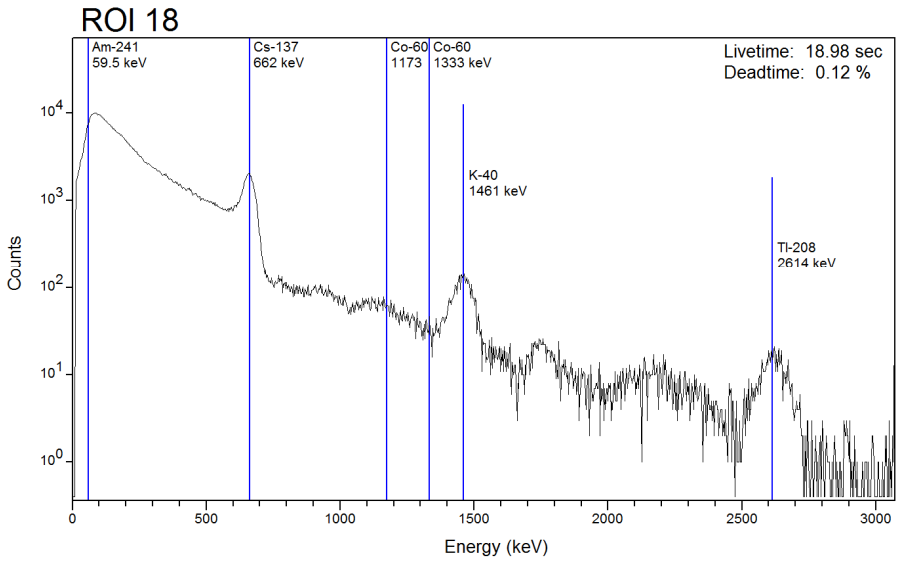
ROI 18
Am-241
59.5 keV
Cs-137
662 keV
Co-60
1173
Co-60
1333 keV
Livetime: 18.98 sec
Deadtime: 0.12 %
K-40
1461 keV
Tl-208
2614 keV
Counts
Energy (keV)

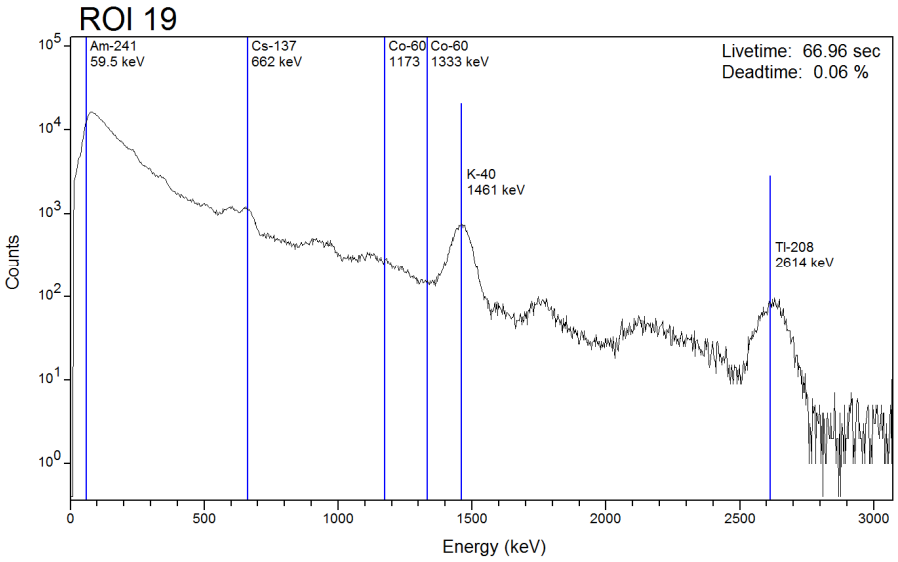
ROI 19
Am-241
59.5 keV
Cs-137
662 keV
Co-60
1173
Co-60
1333 keV
K-40
1461 keV
Tl-208
2614 keV
Livetime: 66.96 sec
Deadtime: 0.06 %
Counts
Energy (keV)

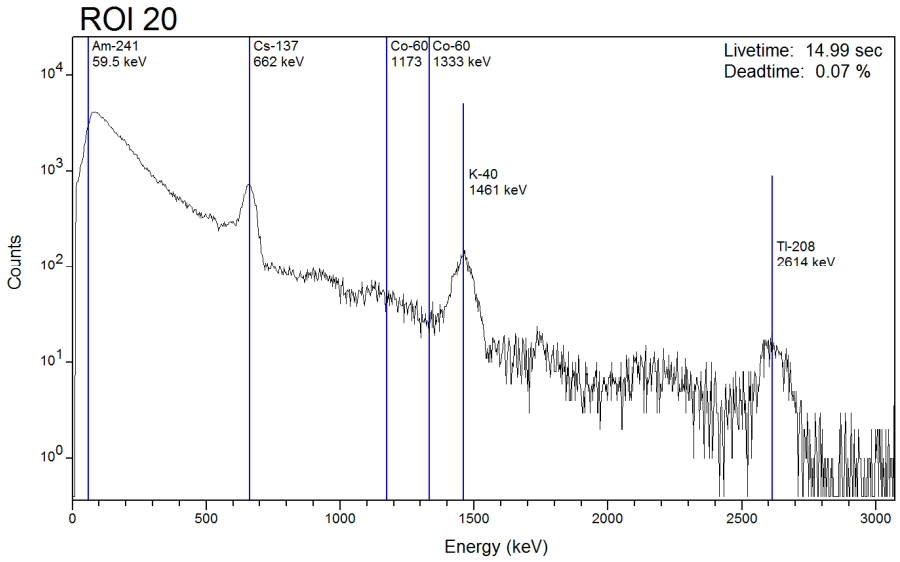
ROI 20
Am-241
59.5 keV
Cs-137
662 keV
Co-60
1173
Co-60
1333 keV
K-40
1461 keV
Tl-208
2614 keV
Livetime: 14.99 sec
Deadtime: 0.07 %
Counts
Energy (keV)

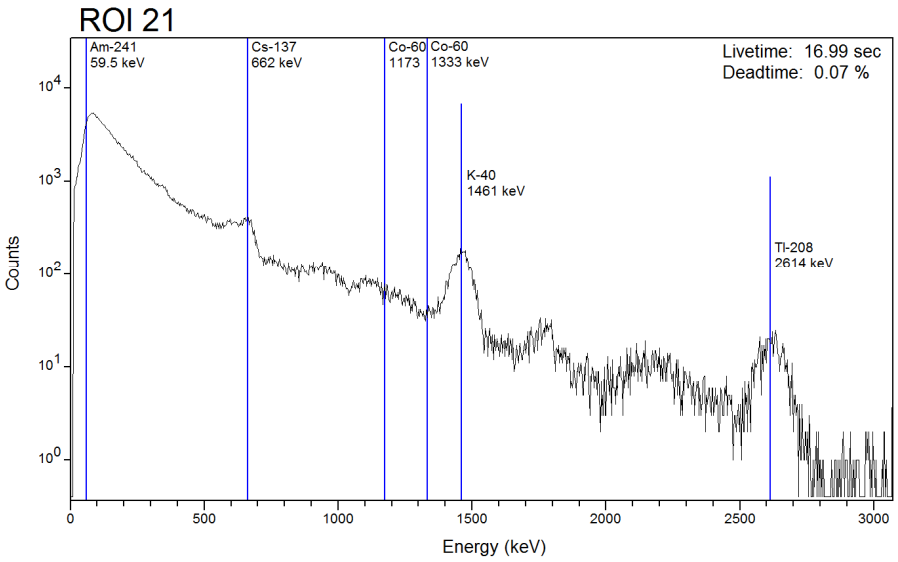
ROI 21
Am-241
59.5 keV
Cs-137
662 keV
Co-60
1173
Co-60
1333 keV
K-40
1461 keV
Tl-208
2614 keV
Livetime: 16.99 sec
Deadtime: 0.07 %
Counts
Energy (keV)

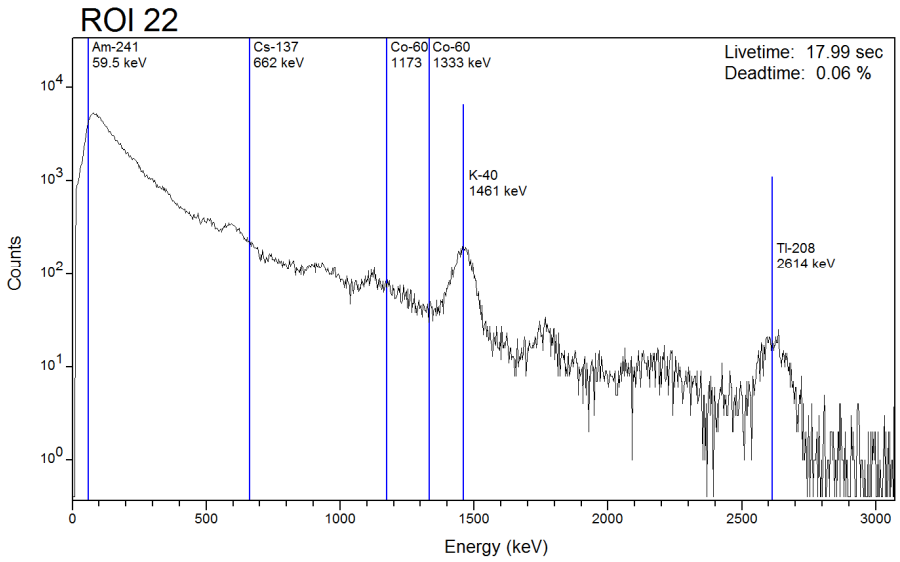
ROI 22
Am-241
59.5 keV
Cs-137
662 keV
Co-60
1173
Co-60
1333 keV
K-40
1461 keV
Tl-208
2614 keV
Livetime: 17.99 sec
Deadtime: 0.06 %
Counts
Energy (keV)

ROI 23

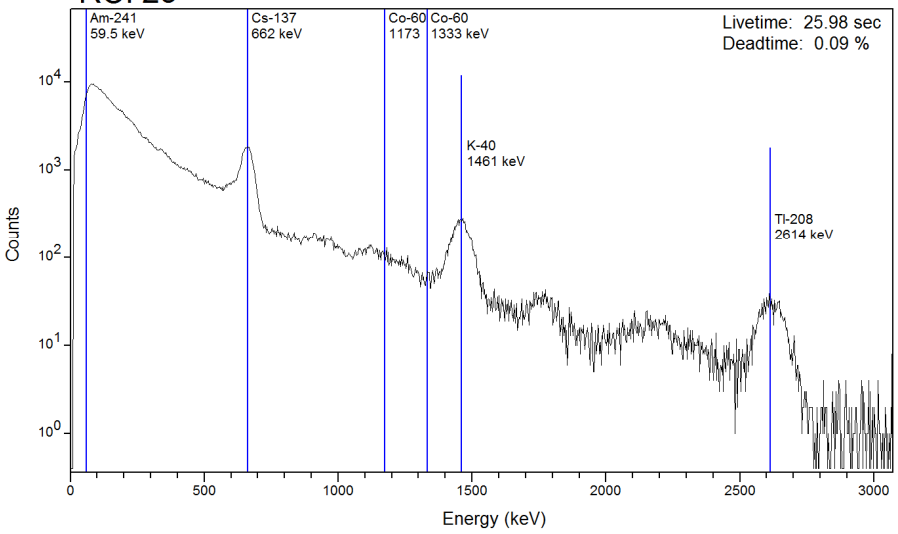

ROI 24

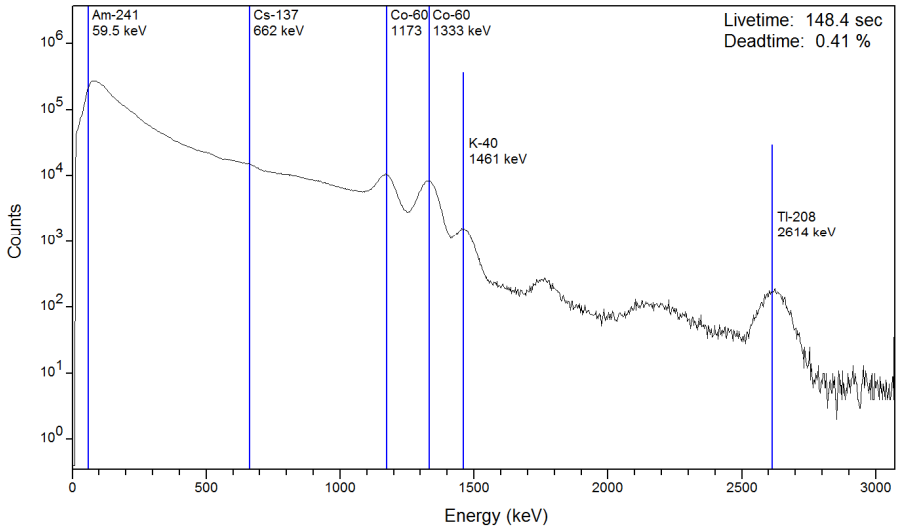

ROI 25

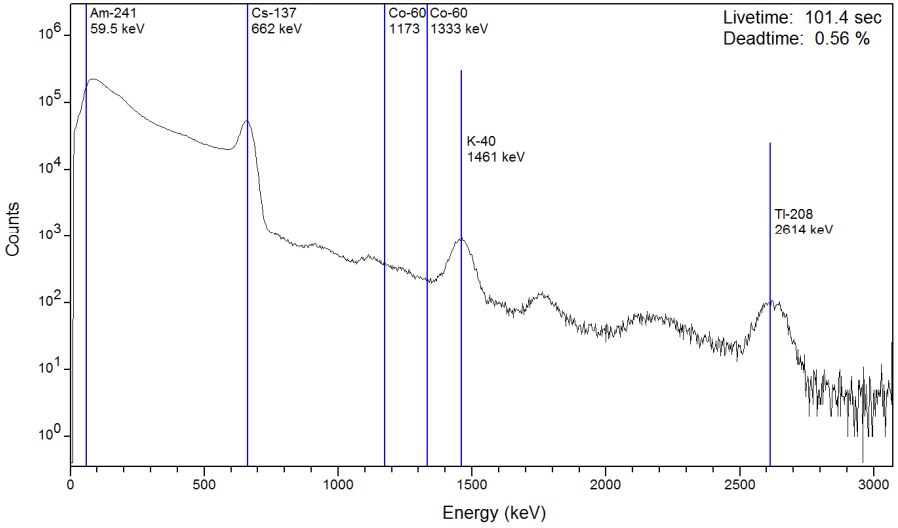

ROI 26

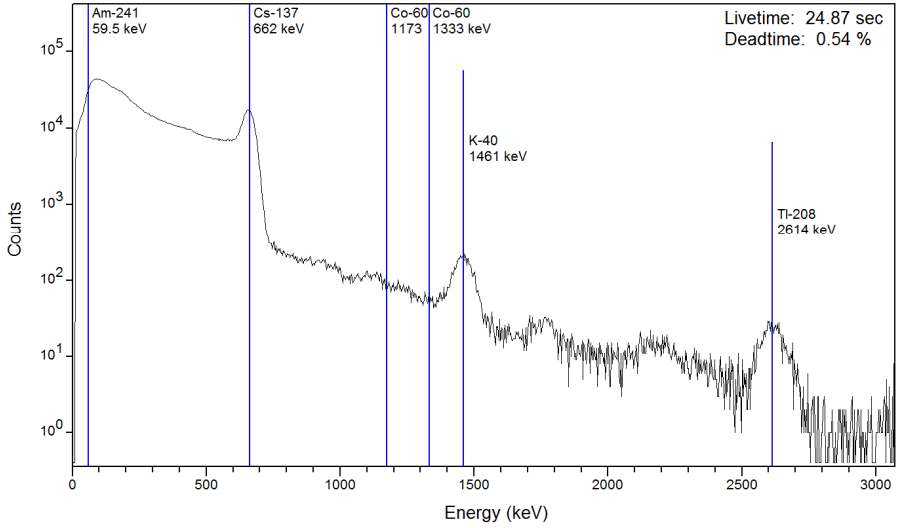

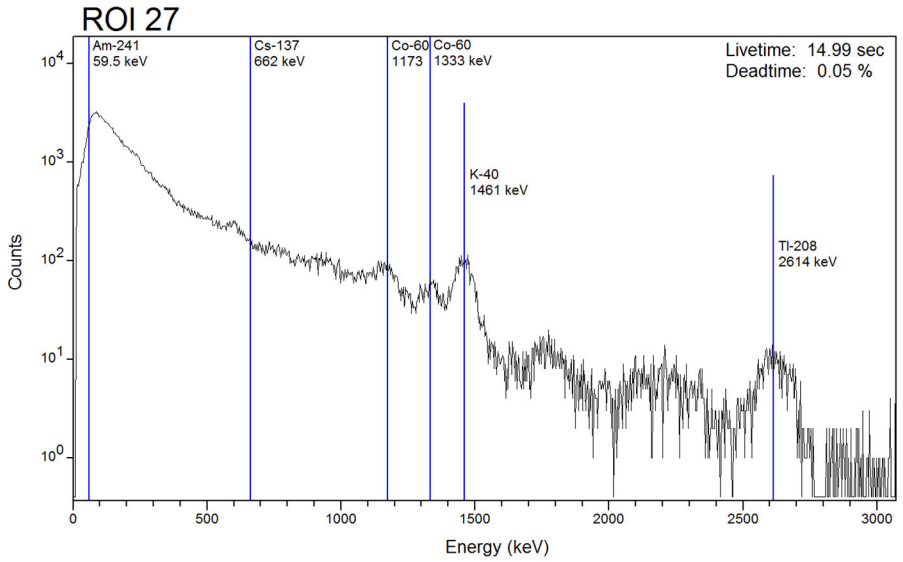
ROI 27
Am-241
59.5 keV
Cs-137
662 keV
Co-60
1173
Co-60
1333 keV
Livetime: 14.99 sec
Deadtime: 0.05 %
K-40
1461 keV
Tl-208
2614 keV
Counts
Energy (keV)

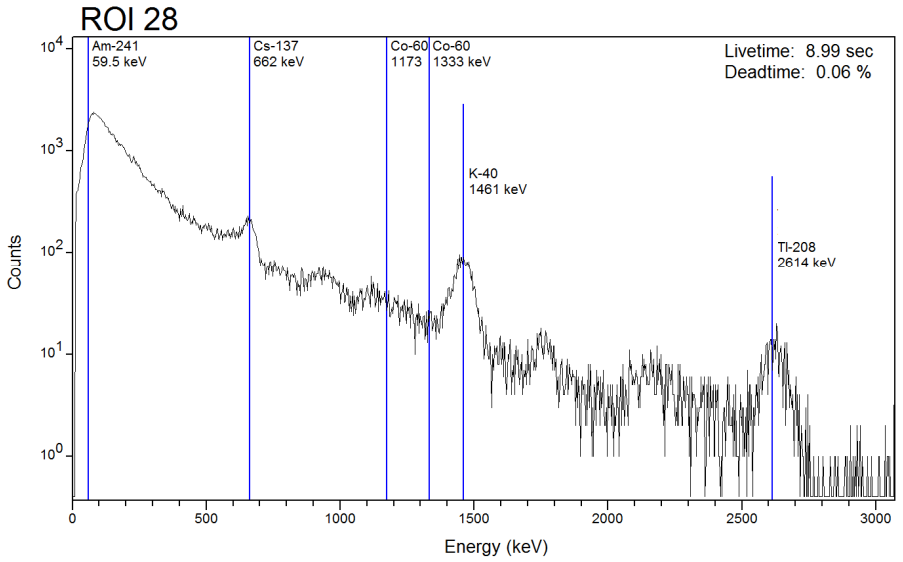
ROI 28
Am-241
59.5 keV
Cs-137
662 keV
Co-60
1173
Co-60
1333 keV
Livetime: 8.99 sec
Deadtime: 0.06 %
K-40
1461 keV
Tl-208
2614 keV
Counts
Energy (keV)

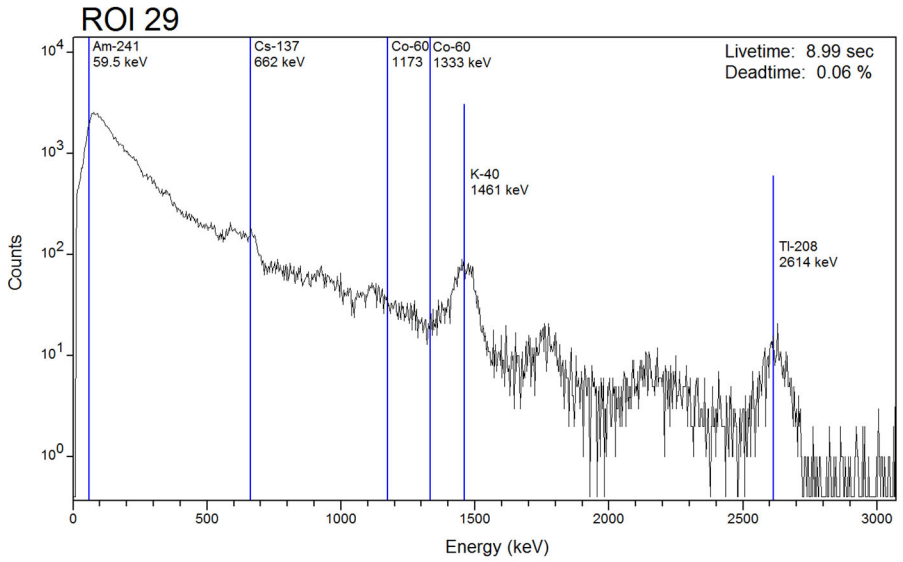
ROI 29
Am-241
59.5 keV
Cs-137
662 keV
Co-60
1173
Co-60
1333 keV
Livetime: 8.99 sec
Deadtime: 0.06 %
K-40
1461 keV
Tl-208
2614 keV
Counts
Energy (keV)

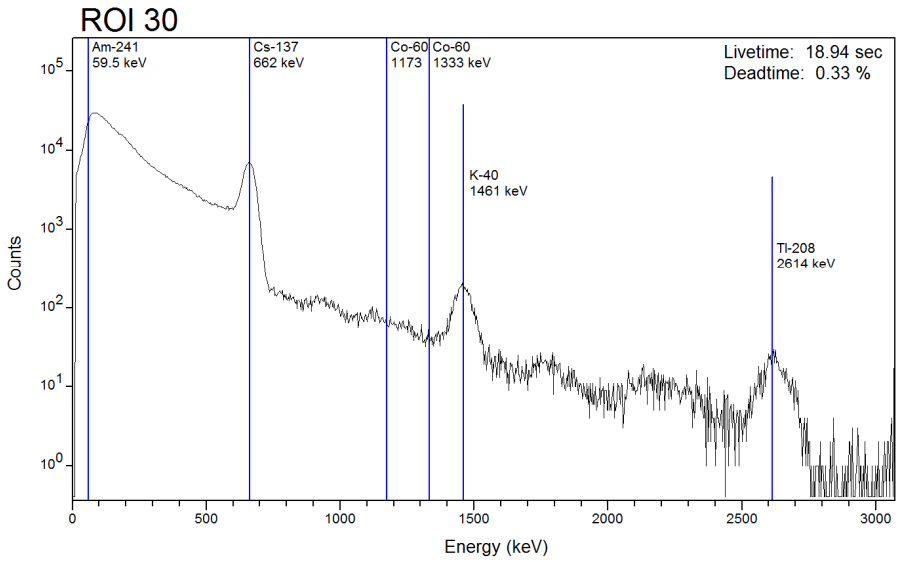
ROI 30
Am-241
59.5 keV
Cs-137
662 keV
Co-60
1173
Co-60
1333 keV
Livetime: 18.94 sec
Deadtime: 0.33 %
K-40
1461 keV
Tl-208
2614 keV
Counts
Energy (keV)

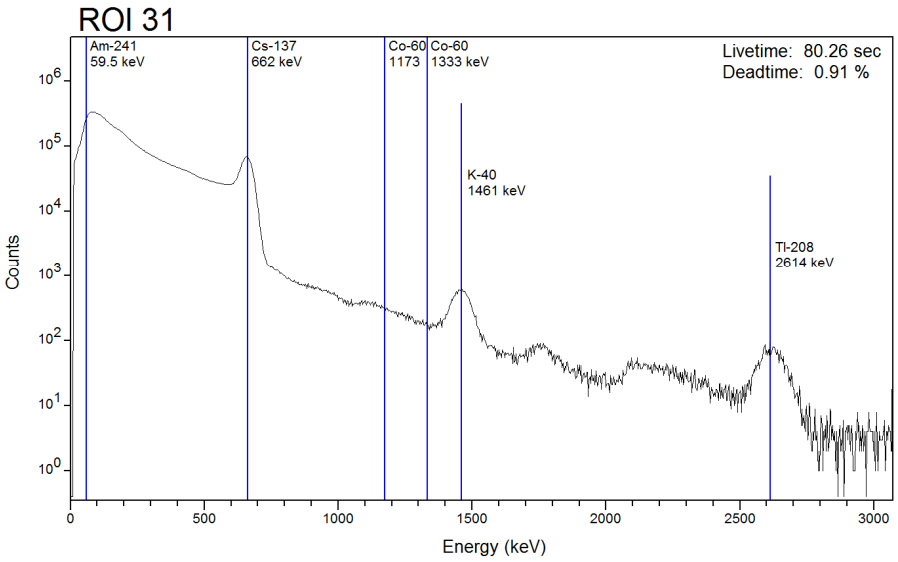
ROI 31
Am-241
59.5 keV
Cs-137
662 keV
Co-60
1173
Co-60
1333 keV
Livetime: 80.26 sec
Deadtime: 0.91 %
K-40
1461 keV
Tl-208
2614 keV
Counts
Energy (keV)

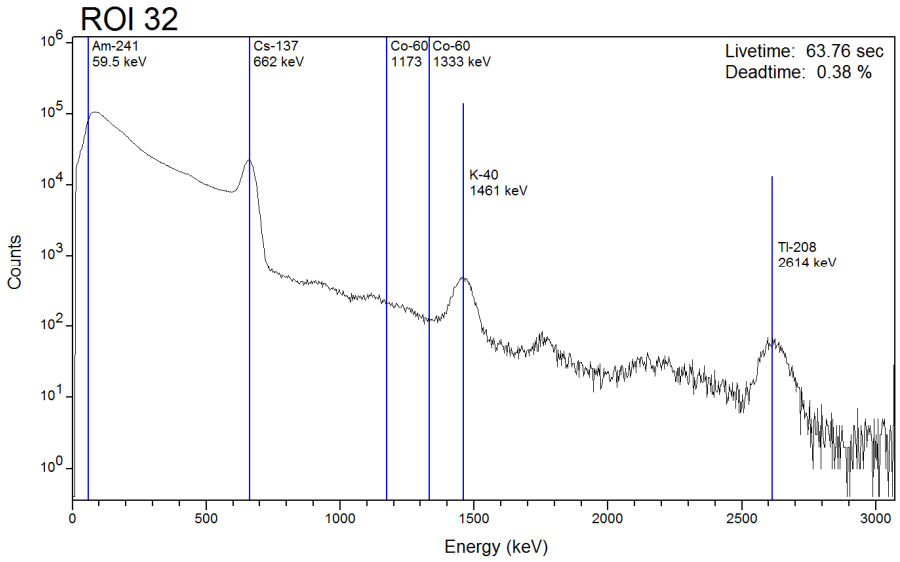
ROI 32
Am-241
59.5 keV
Cs-137
662 keV
Co-60
1173
Co-60
1333 keV
Livetime: 63.76 sec
Deadtime: 0.38 %
K-40
1461 keV
Tl-208
2614 keV
Counts
Energy (keV)

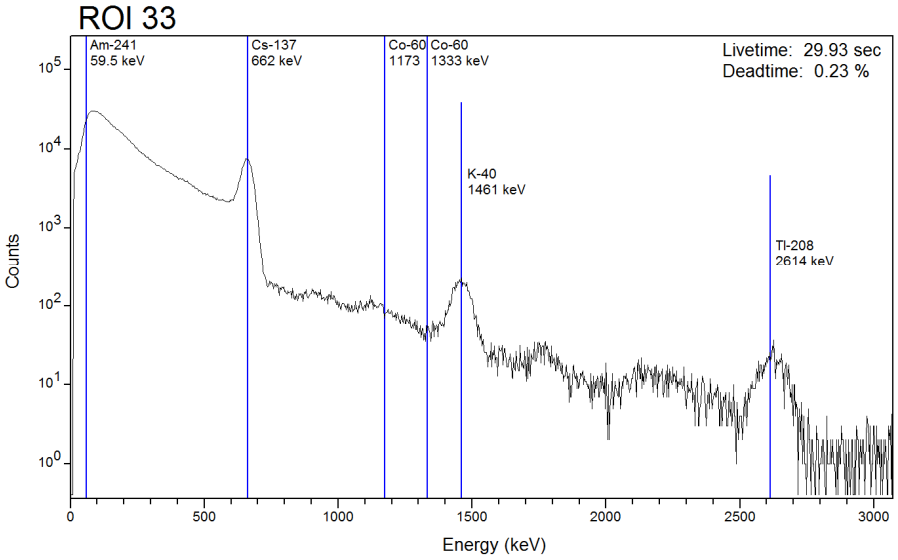
ROI 33
Am-241
59.5 keV
Cs-137
662 keV
Co-60
1173
Co-60
1333 keV
Livetime: 29.93 sec
Deadtime: 0.23 %
K-40
1461 keV
Tl-208
2614 keV
Counts
Energy (keV)

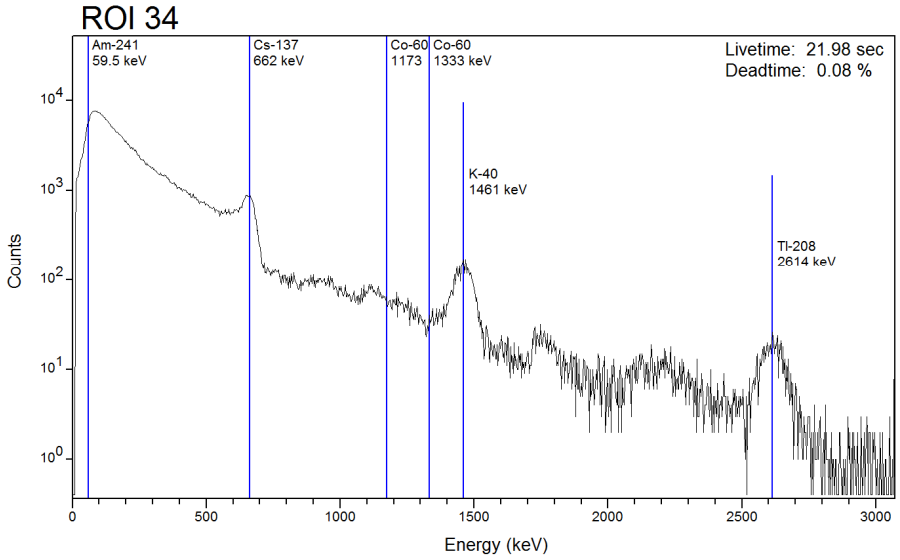
ROI 34
Am-241
59.5 keV
Cs-137
662 keV
Co-60
1173
Co-60
1333 keV
Livetime: 21.98 sec
Deadtime: 0.08 %
K-40
1461 keV
Tl-208
2614 keV
Counts
Energy (keV)

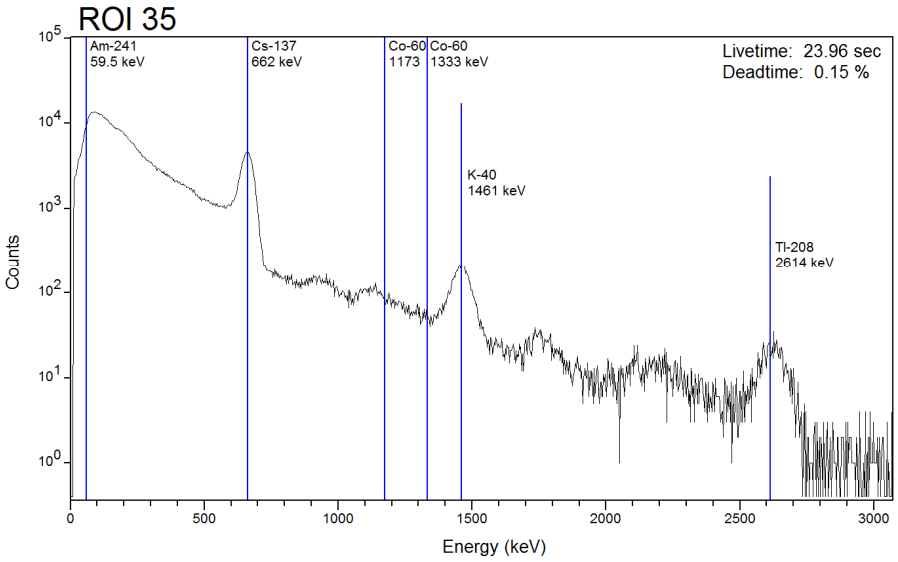
ROI 35
Am-241
59.5 keV
Cs-137
662 keV
Co-60
1173
Co-60
1333 keV
Livetime: 23.96 sec
Deadtime: 0.15 %
K-40
1461 keV
Tl-208
2614 keV
Counts
Energy (keV)

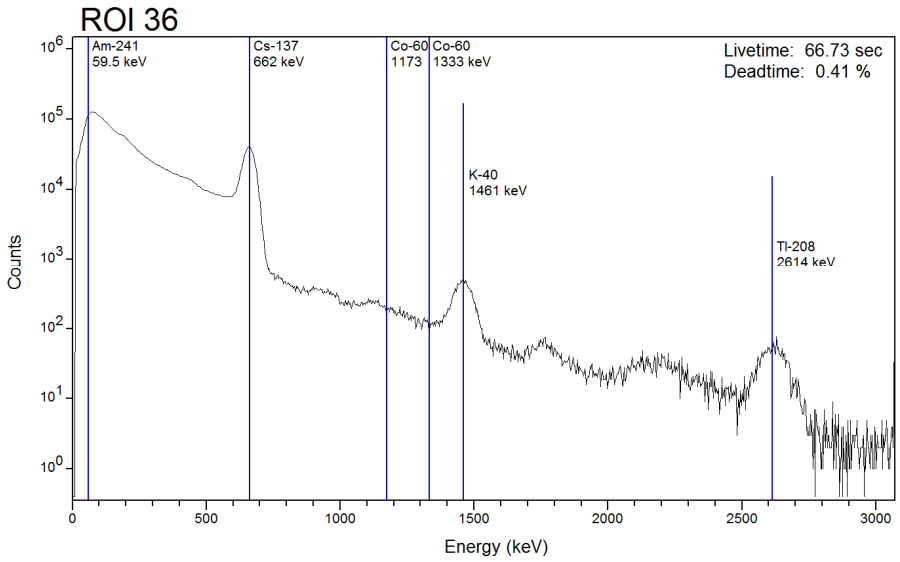
ROI 36
Am-241
59.5 keV
Cs-137
662 keV
Co-60
1173
Co-60
1333 keV
Livetime: 66.73 sec
Deadtime: 0.41 %
K-40
1461 keV
Tl-208
2614 keV
Counts
Energy (keV)

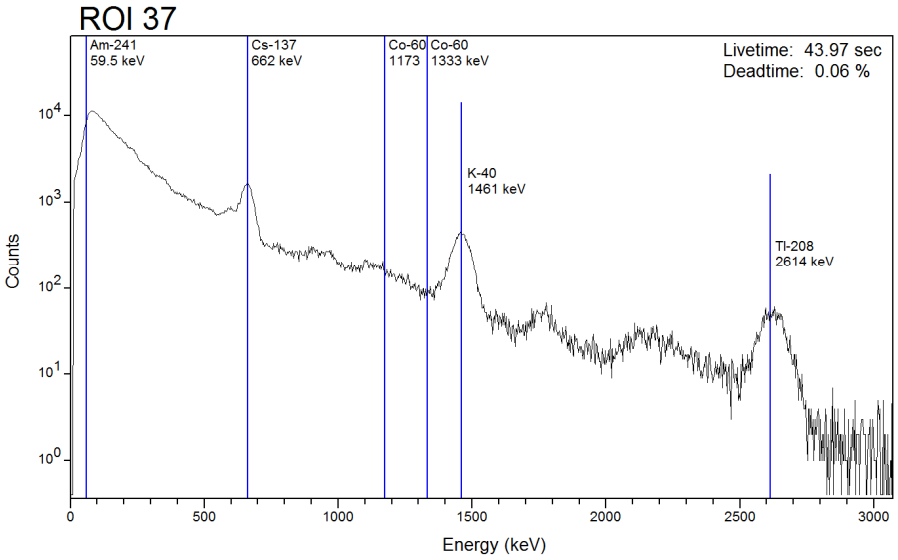
ROI 37
Am-241
59.5 keV
Cs-137
662 keV
Co-60
1173
Co-60
1333 keV
Livetime: 43.97 sec
Deadtime: 0.06 %
K-40
1461 keV
Tl-208
2614 keV
Counts
Energy (keV)

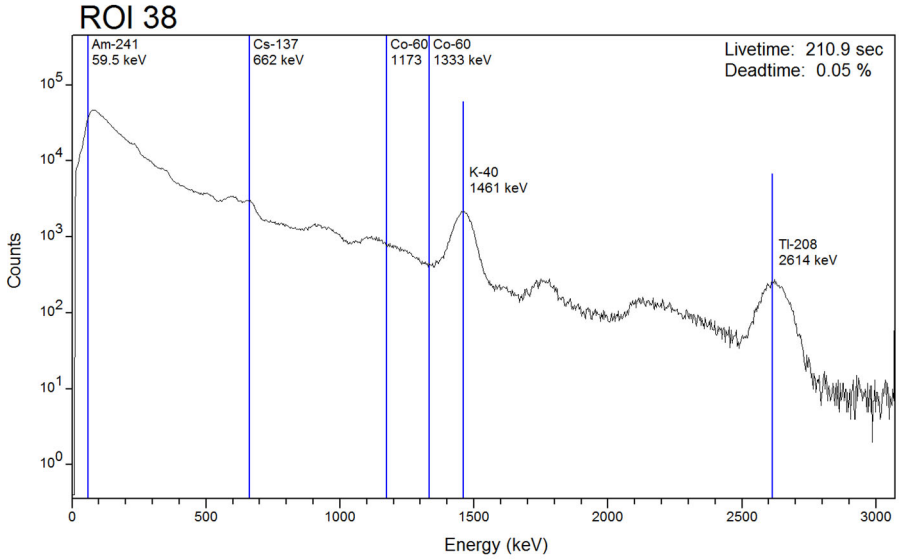
ROI 38
Am-241
59.5 keV
Cs-137
662 keV
Co-60
1173
Co-60
1333 keV
Livetime: 210.9 sec
Deadtime: 0.05 %
K-40
1461 keV
Tl-208
2614 keV
Counts
Energy (keV)

ROI 39

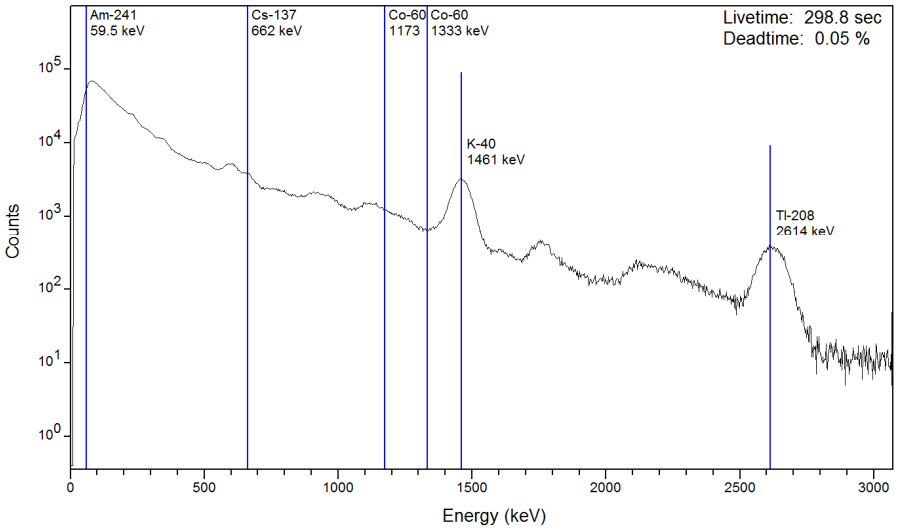

ROI 40

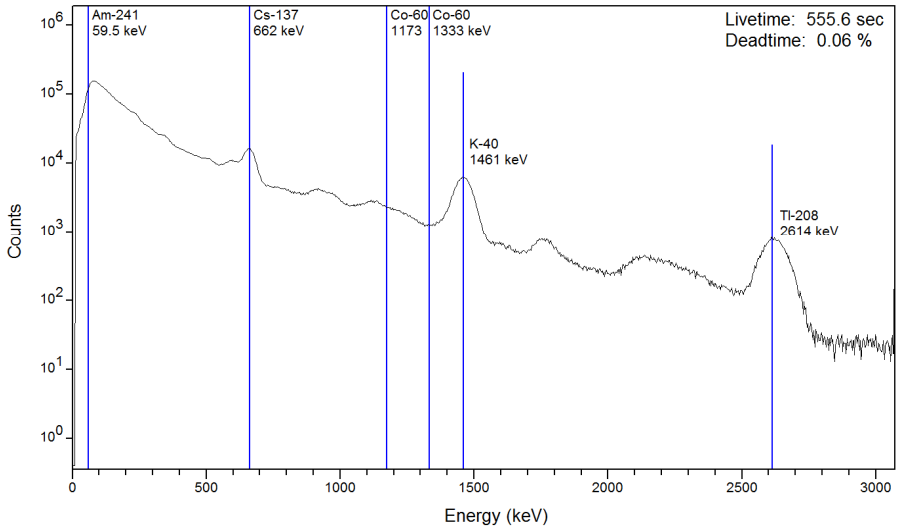

ROI 41

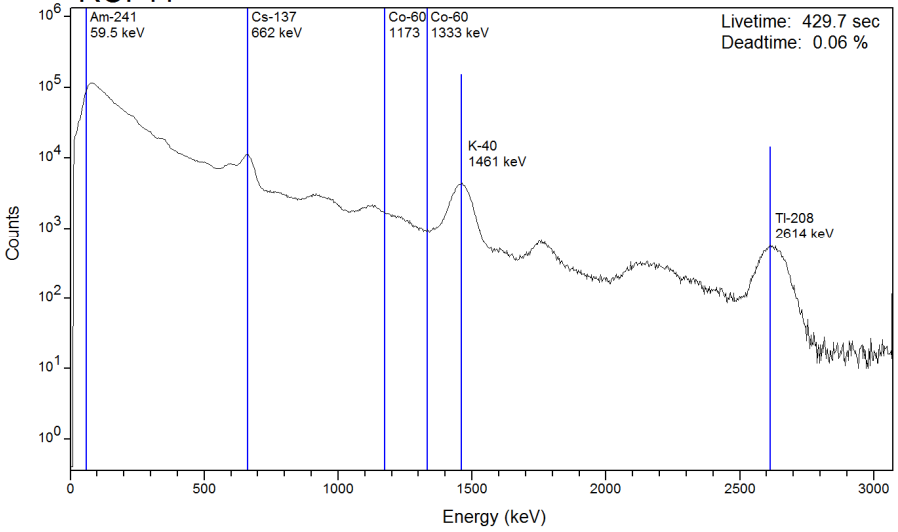

ROI 42

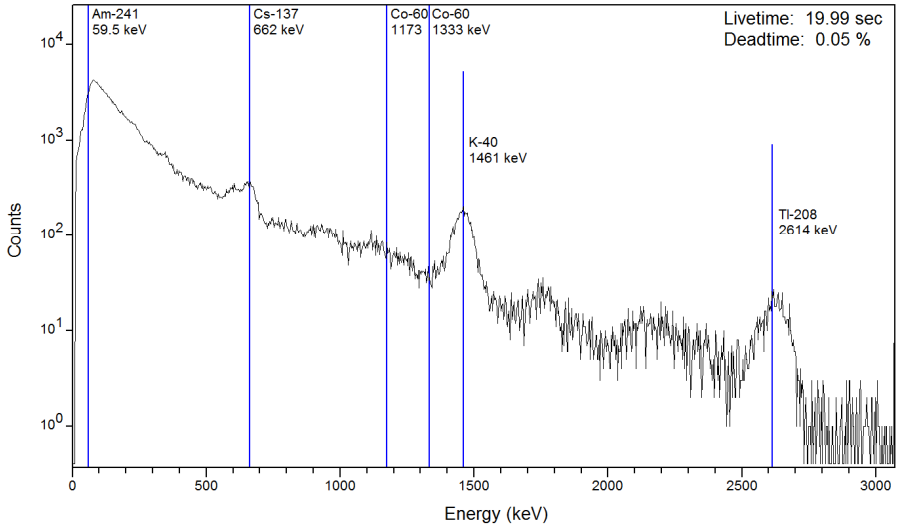

ROI 43

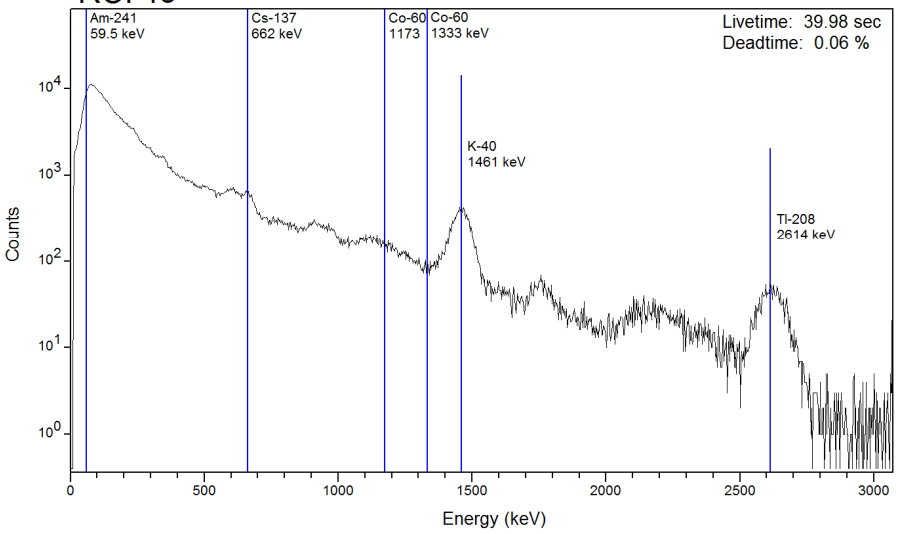

ROI 44

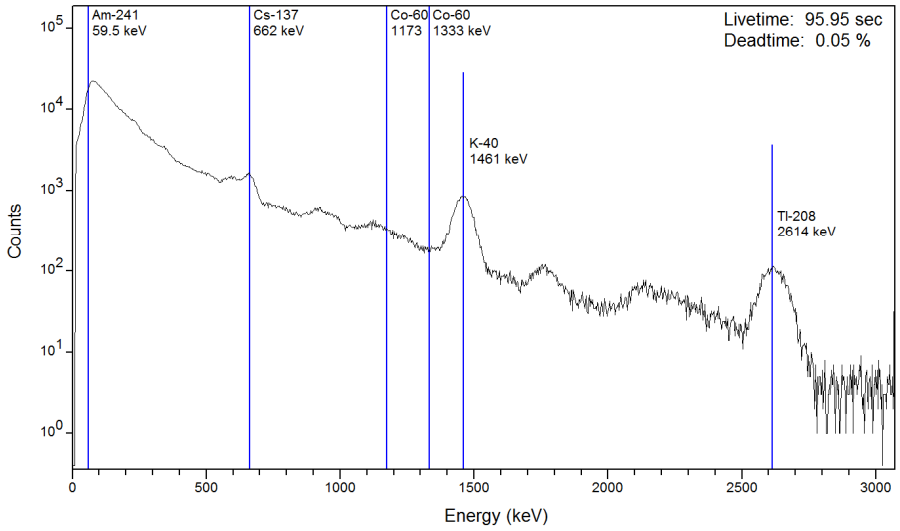

ROI 45

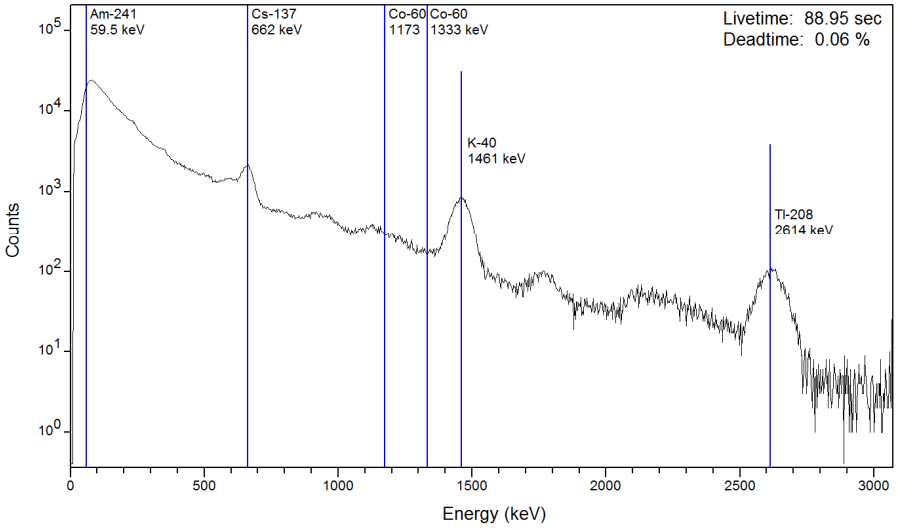

ROI 46

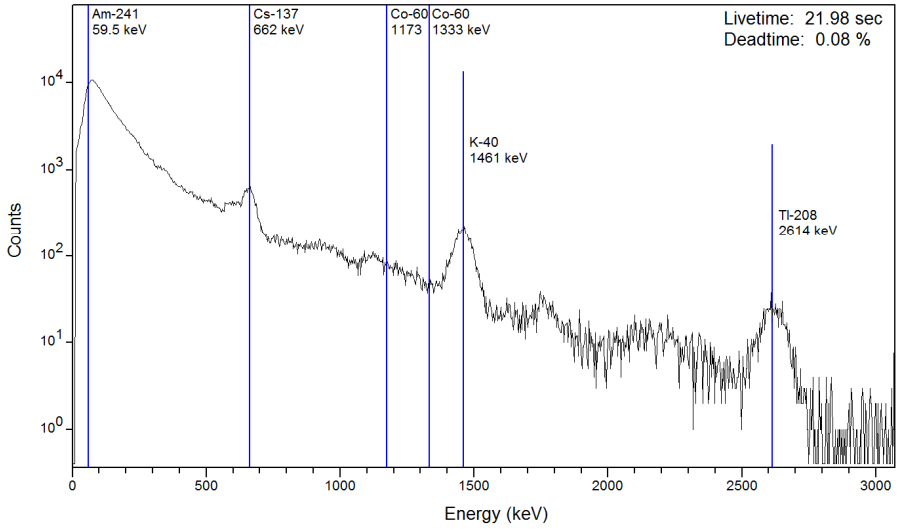

ROI 47

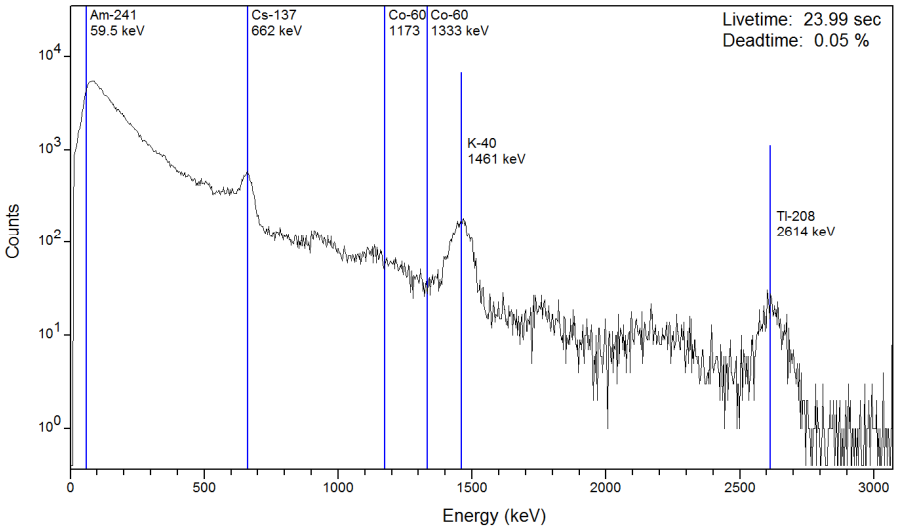

ROI 48

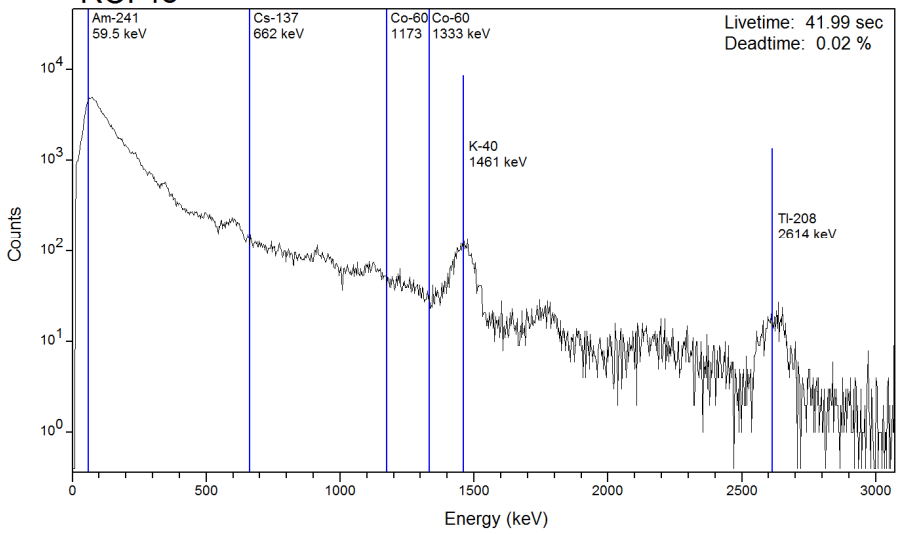

ROI 49

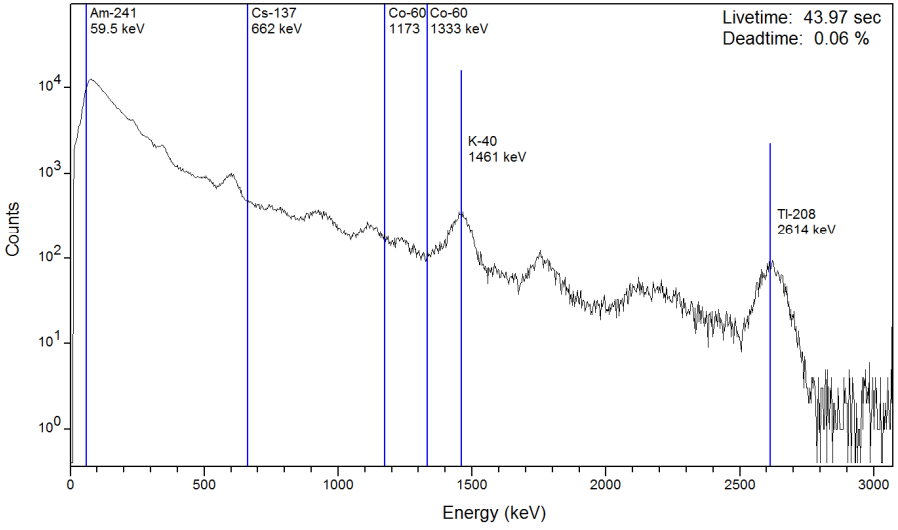

ROI 50

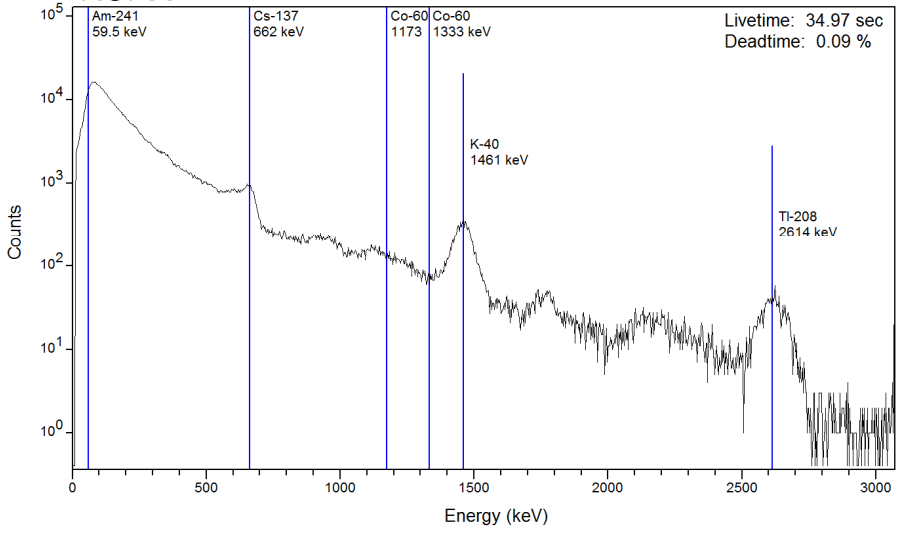

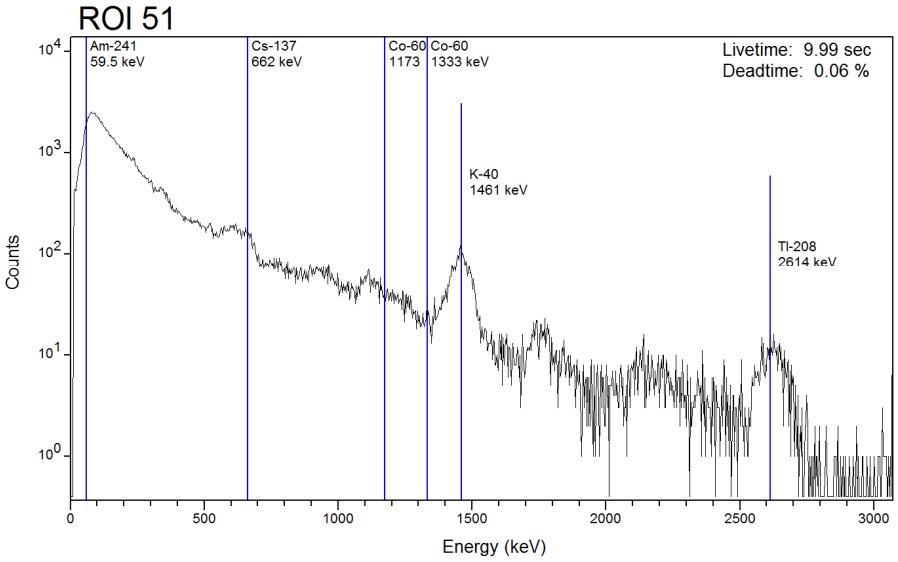
ROI 51
Am-241
59.5 keV
Cs-137
662 keV
Co-60
1173
Co-60
1333 keV
Livetime: 9.99 sec
Deadtime: 0.06 %
K-40
1461 keV
Tl-208
2614 keV
Counts
Energy (keV)

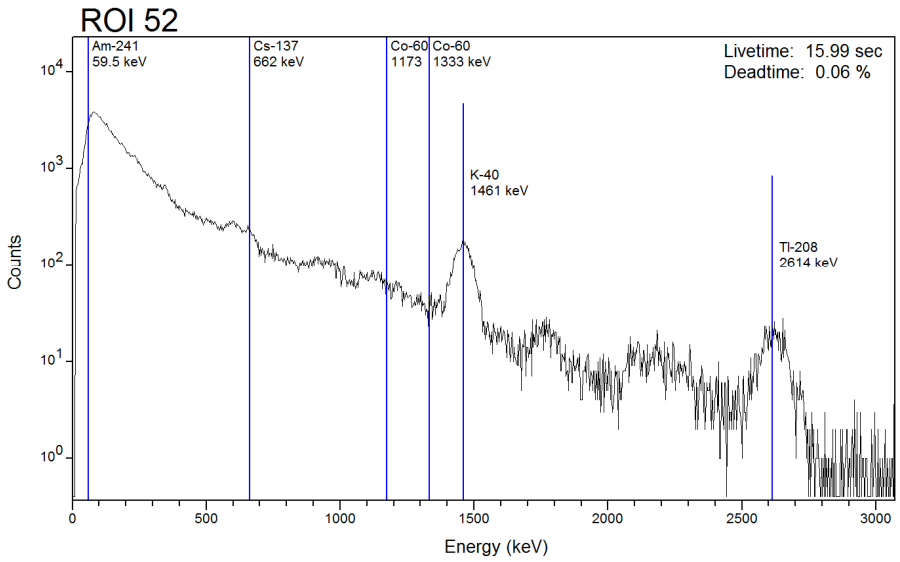
ROI 52
Am-241
59.5 keV
Cs-137
662 keV
Co-60
1173
Co-60
1333 keV
Livetime: 15.99 sec
Deadtime: 0.06 %
K-40
1461 keV
Tl-208
2614 keV
Counts
Energy (keV)

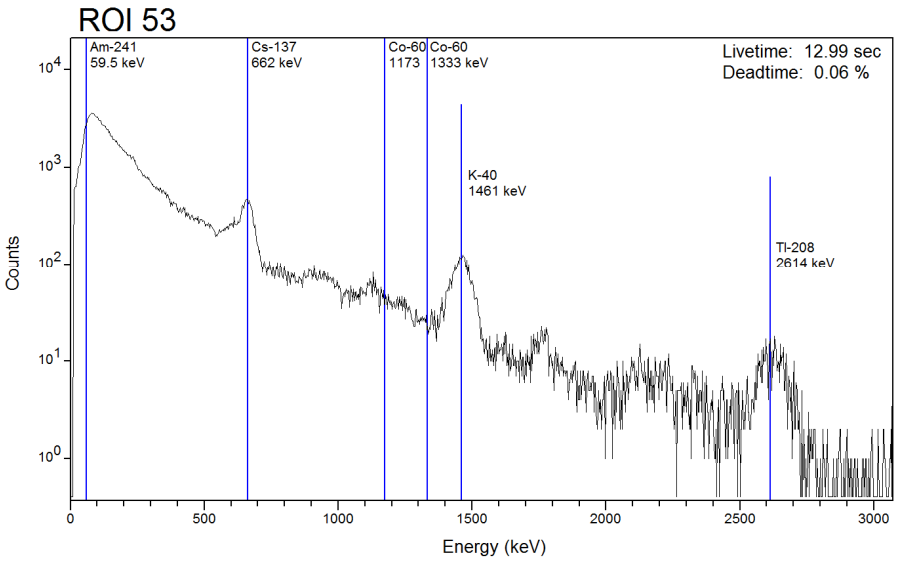
ROI 53
Am-241
59.5 keV
Cs-137
662 keV
Co-60
1173
Co-60
1333 keV
Livetime: 12.99 sec
Deadtime: 0.06 %
K-40
1461 keV
Tl-208
2614 keV
Counts
Energy (keV)

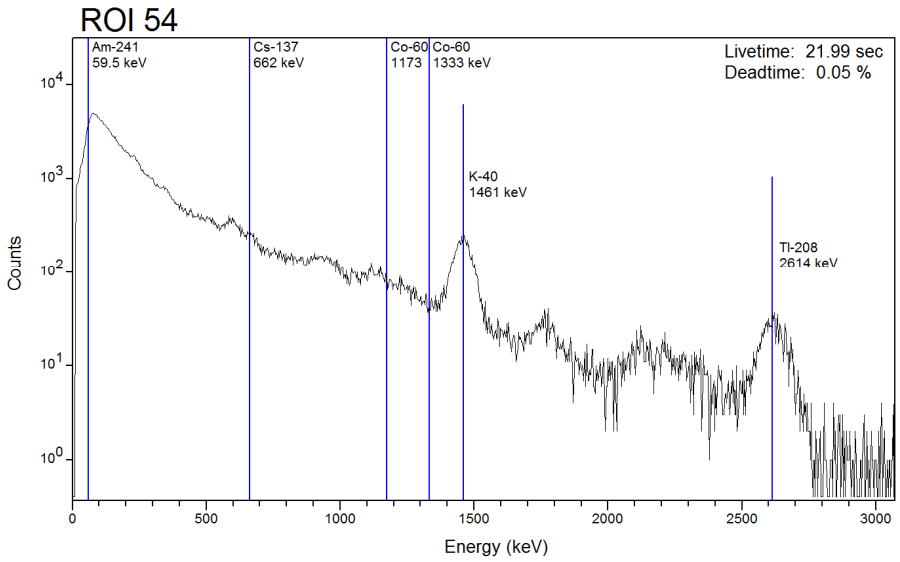
ROI 54
Am-241
59.5 keV
Cs-137
662 keV
Co-60
1173
Co-60
1333 keV
Livetime: 21.99 sec
Deadtime: 0.05 %
K-40
1461 keV
Tl-208
2614 keV
Counts
Energy (keV)

ROI 55

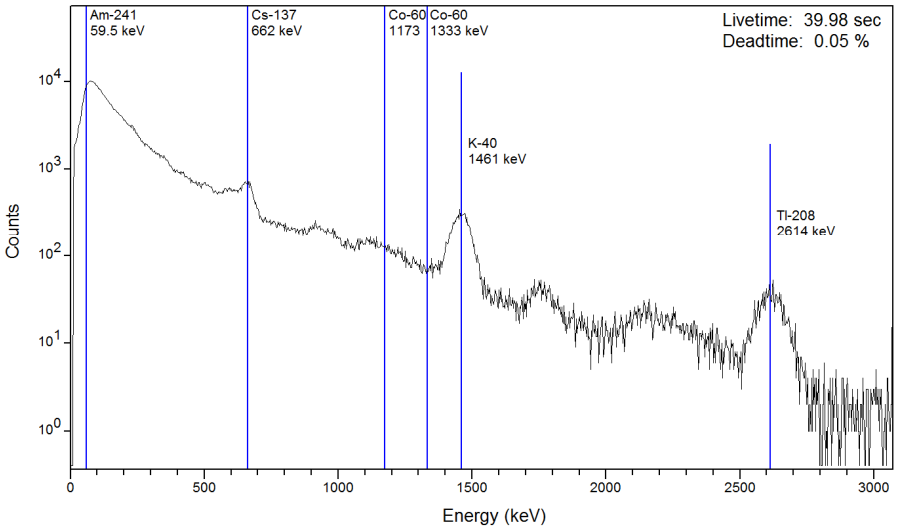

ROI 56

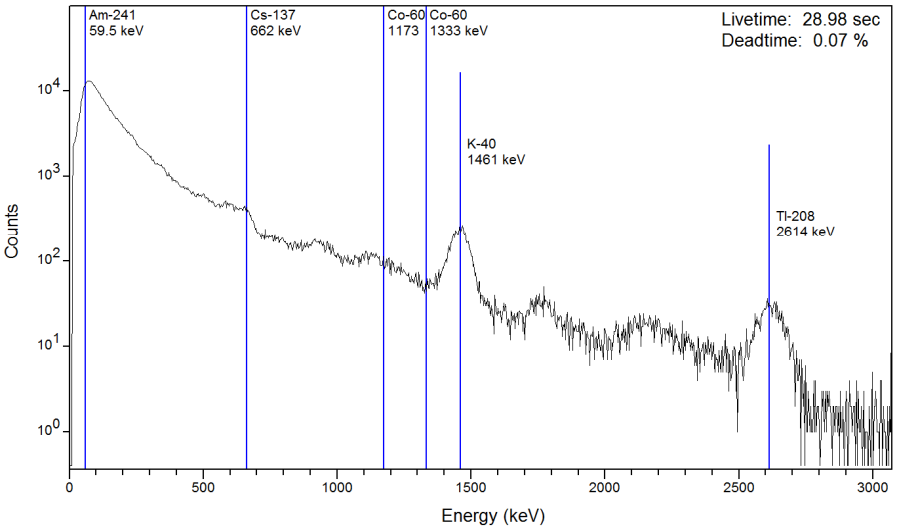

ROI 57

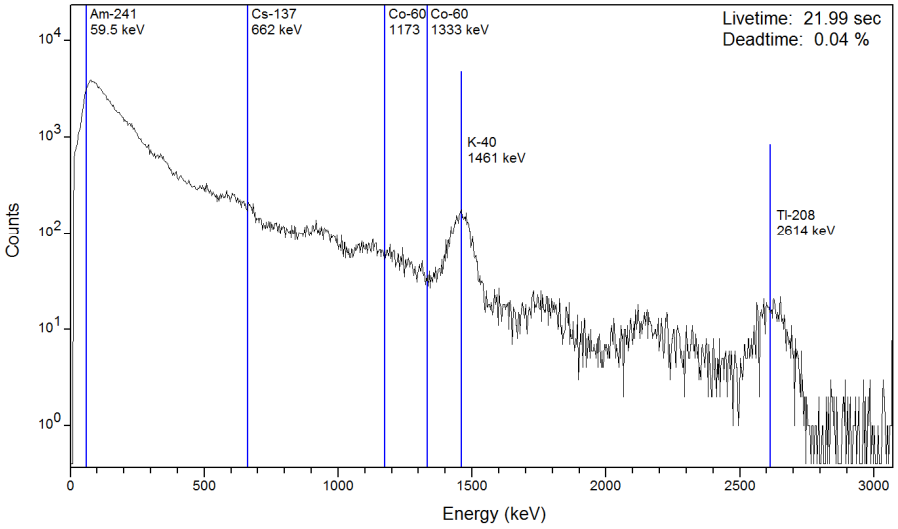

ROI 58

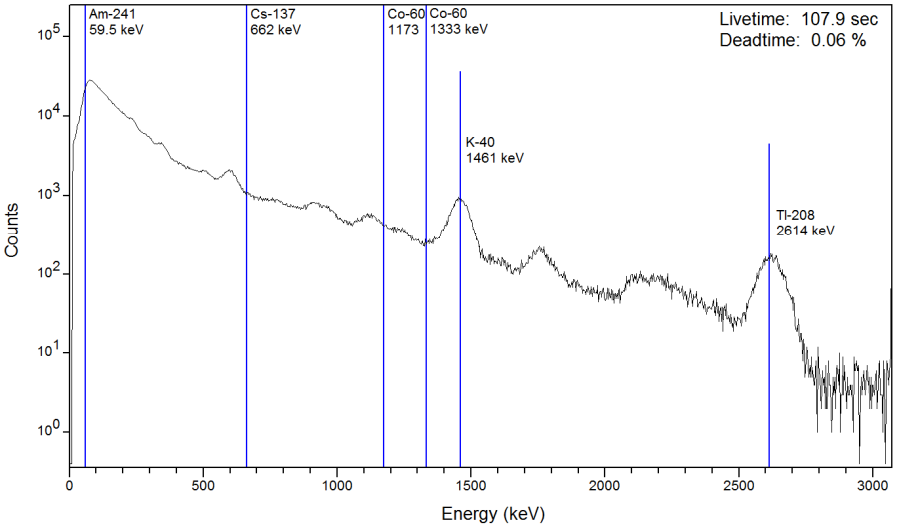

ROI 59

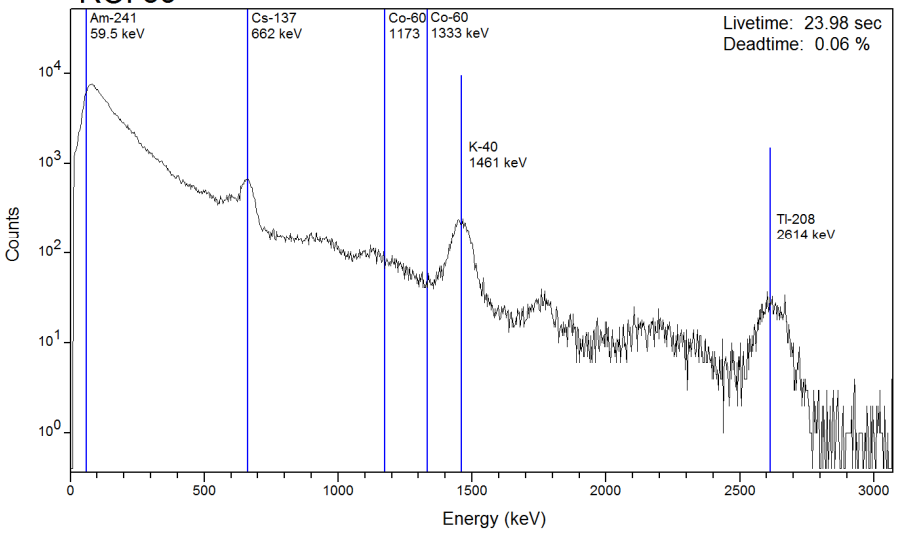

ROI 60

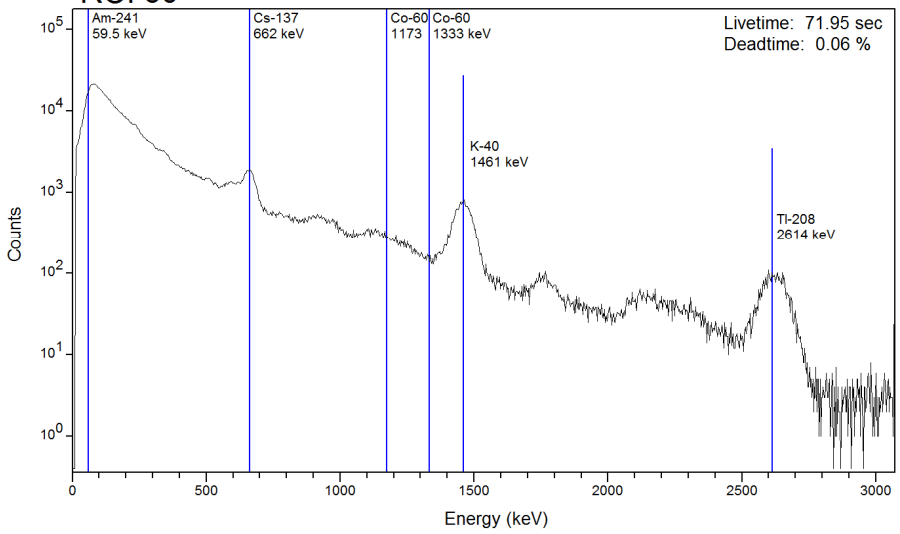

ROI 61

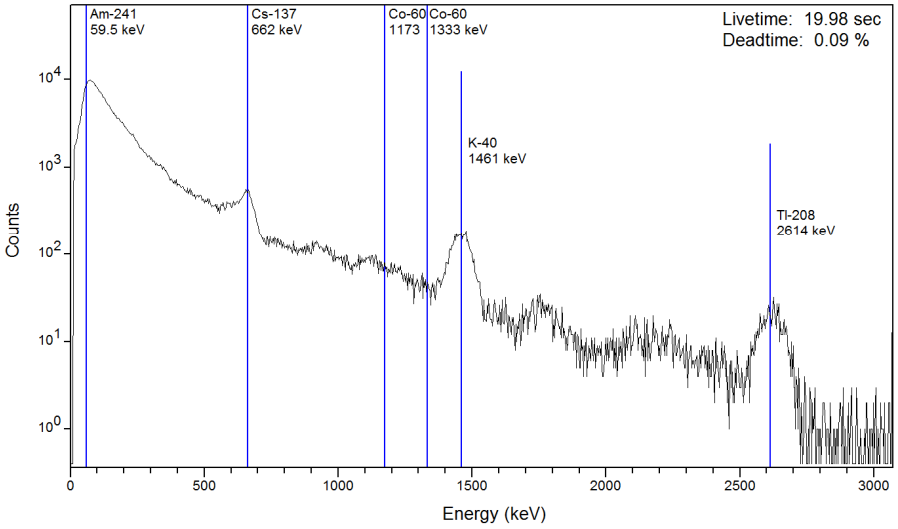

ROI 62

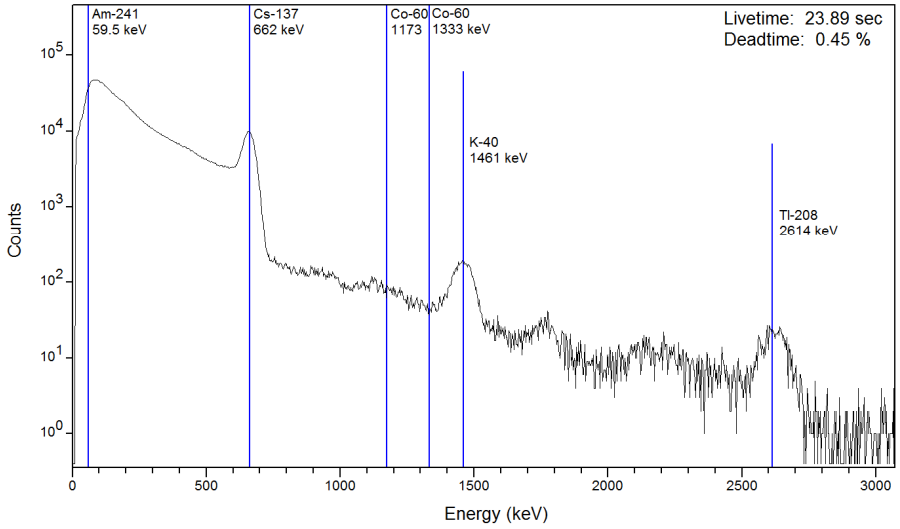

ROI 63

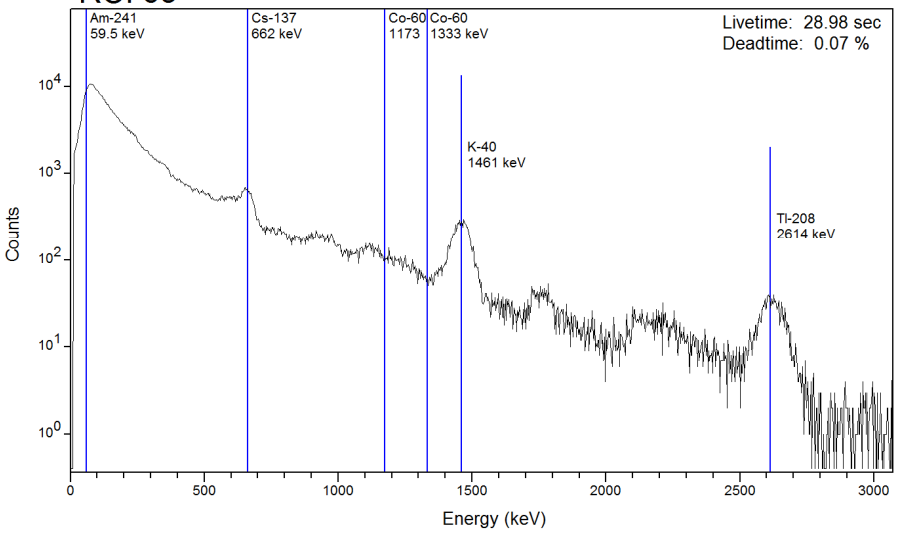

ROI 64

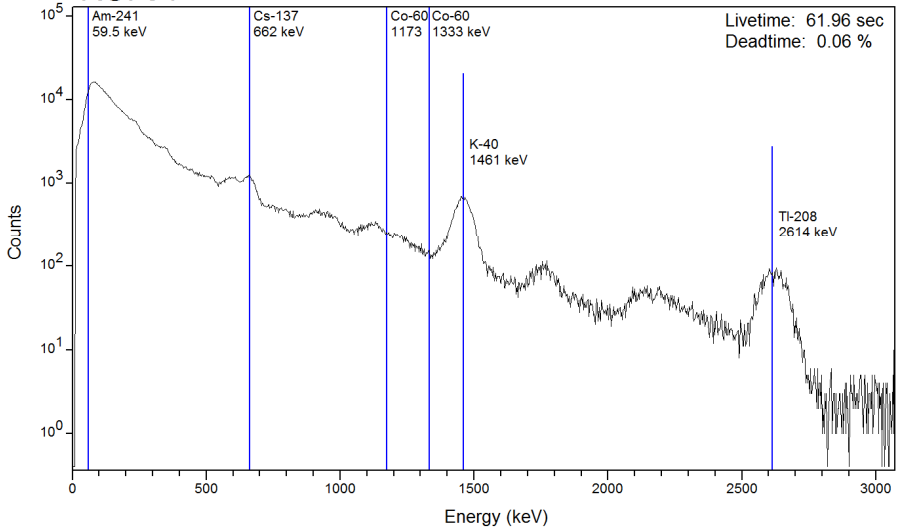

ROI 65

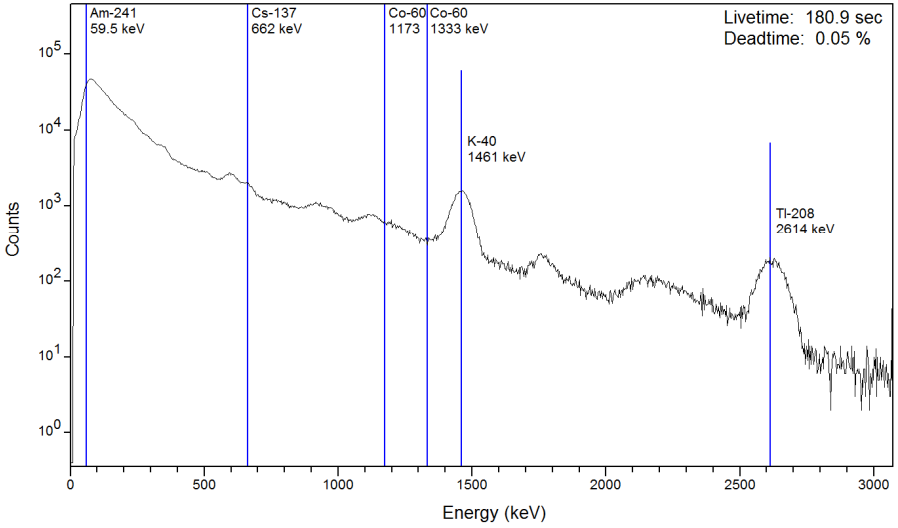

ROI 66

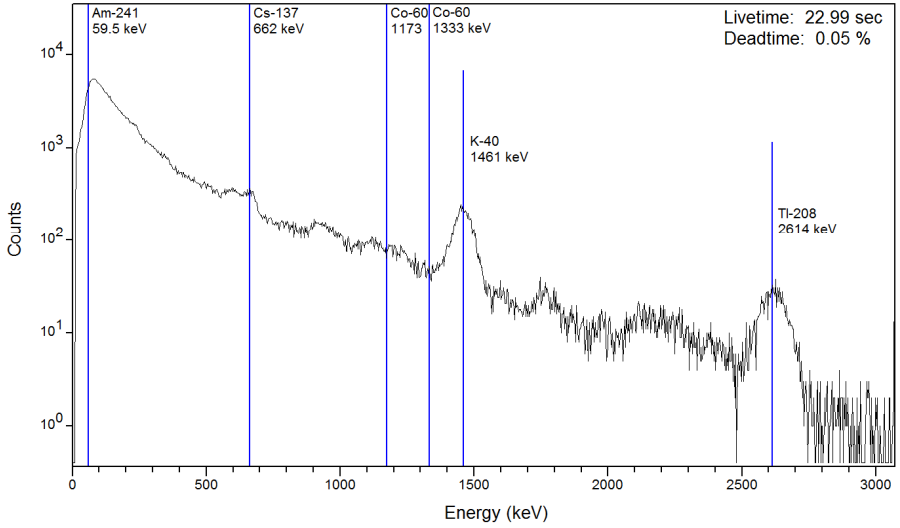

ROI 67

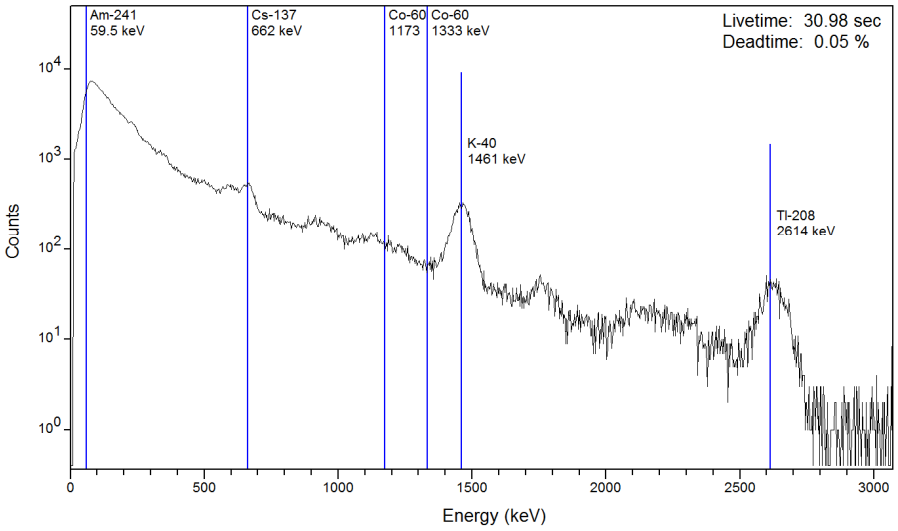
Am-241
59.5 keV
Cs-137
662 keV
Co-60
1173
Co-60
1333 keV
K-40
1461 keV
Tl-208
2614 keV
Livetime: 30.98 sec
Deadtime: 0.05 %
Counts
Energy (keV)

ROI 68

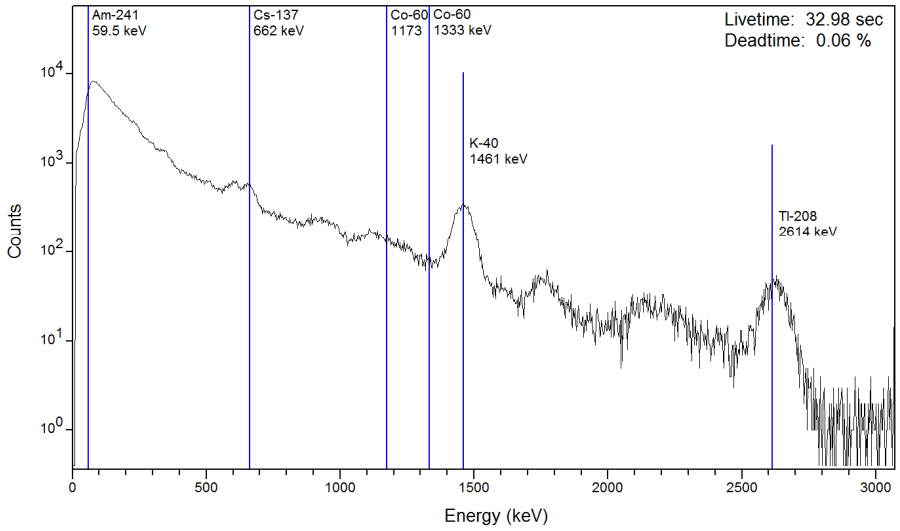
Am-241
59.5 keV
Cs-137
662 keV
Co-60
1173
Co-60
1333 keV
K-40
1461 keV
Tl-208
2614 keV
Livetime: 32.98 sec
Deadtime: 0.06 %
Counts
Energy (keV)